

# **Testing the importance of explicit glacier dynamics for future glacier evolution in the mountain regions**

MASTER'S THESIS

in Atmospheric Sciences

Submitted to the  
DEPARTMENT OF ATMOSPHERIC AND CRYOSPHERIC  
SCIENCES  
of the  
UNIVERSITY OF INNSBRUCK

in Partial Fulfillment of the Requirements for the Degree of  
MASTER OF SCIENCE

by  
MORITZ OBERRAUCH

Advisor  
Fabien Maussion, PhD

Innsbruck, February 2021



*To Sir Psycho*

*And all others who try to move their toes individually*

*And #savethewhales* 



# Abstract

Global glacier models are imperative to project future glacier ice mass loss and the accompanied sea level rise. Glaciers are controlled by their mass balance and the resulting ice flow. The scarcity of ice volume observations makes the calibration, and especially validation, of geometry models difficult. As a consequence, most global model use volume/area scaling relations instead of a dedicated ice physic model. Over the last years, the increasing accuracy and coverage of global data inventories, in combination with new and automated methods, as well as increased computing power allowed for the development of more sophisticated models. This study compares the global glacier model based on scaling relations by [Marzeion et al. \(2012\)](#) to the globally applicable flowline model based on the Shallow Ice Approximation by [Maussion et al. \(2019\)](#) under controlled boundary conditions.

The reimplemented volume/area scaling model is able to correctly simulate glacier changes in response to various climatic forcings. The results are conceptually correct and comparable to those of the flowline model. The 21st century projection for South Asia West (RGI region 14) forced by CMIP6 data estiamtes an ice loss relative to 2020 between  $-27 \pm 3\%$  under SSP1-2.6 and  $-37 \pm 4\%$  under SSP5-8.5 for the volume/area scaling model, and  $-26 \pm 8\%$  under SSP1-2.6 and  $-48 \pm 10\%$  under SSP5-8.5 for the flowline model. For Central Europe the projected ice loss is much higher with up to  $-84 \pm 5\%$  estimated by the volume/area scaling model and  $-98 \pm 2\%$  estimated by the flowline model for SSP5-8.5, and the differences between the models are larger. The differences between volume/area scaling model and flowline model are eventhe introduction of ice physics modules does not devalue more pronounced for idealized equilibrium experiments and can be attributed to a missing mass-balance-elevation feedback and the overestimation of model-internal time scales. Additionally, these too long time scales result in oscillating adjustments of glacier geometries to step changes in climate. Nevertheless, the volume/area scaling model performane is still competitive for global applications and the introduction of ice physics modules does not complete devalue the scaling approach.



# Contents

<b>Abstract</b>	<b>iii</b>
<b>Contents</b>	<b>v</b>
<b>1 Introduction</b>	<b>1</b>
1.1 Motivation . . . . .	1
1.2 A brief history of global glacier modeling . . . . .	2
1.3 State of Research . . . . .	7
1.4 Goals and Outline . . . . .	9
<b>2 Model implementation</b>	<b>11</b>
2.1 General concepts . . . . .	11
2.1.1 Glacier volume/area scaling . . . . .	11
2.1.2 Temperature index model . . . . .	16
2.1.3 Glacier evolution model . . . . .	19
2.2 Implementation . . . . .	22
2.2.1 Mass balance models . . . . .	22
2.2.2 Glacier evolution model . . . . .	24
<b>3 Results</b>	<b>27</b>
3.1 Single glacier test case . . . . .	27
3.1.1 Experimental setup . . . . .	28
3.1.2 Results . . . . .	29
3.2 Autocorrelation function and Power spectral density . . . . .	35
3.2.1 Theoretical background . . . . .	35
3.2.2 Experimental setup . . . . .	36
3.2.3 Power spectral density . . . . .	39
3.2.4 Autocorrelation function . . . . .	41
3.3 Regional runs with all Alpine glaciers . . . . .	45
3.3.1 Experimental setup . . . . .	46
3.3.2 Results . . . . .	46

3.4	Sensitivity experiments . . . . .	48
3.4.1	Experimental setup . . . . .	48
3.4.2	Sensitivity to model-internal time scales . . . . .	51
3.4.3	Sensitivity to scaling parameters . . . . .	52
3.5	Projections for the 21st century . . . . .	54
3.5.1	Experimental setup . . . . .	54
3.5.2	Results . . . . .	55
<b>4</b>	<b>Discussion</b>	<b>61</b>
4.1	Values of ice volume (change) . . . . .	61
4.2	Missing physical processes . . . . .	63
4.3	Mass balance calibration . . . . .	64
4.4	Initializing historic glacier states . . . . .	65
<b>5</b>	<b>Conclusions</b>	<b>67</b>
<b>A</b>	<b>Single glacier test cases</b>	<b>69</b>
<b>B</b>	<b>ARMA model order</b>	<b>75</b>
	<b>Bibliography</b>	<b>77</b>
	<b>Acknowledgments</b>	<b>91</b>

# Chapter 1

## Introduction

### 1.1 Motivation

According to the scientific consensus presented in the latest assessment report (AR5) of the Intergovernmental Panel on Climate Change ([IPCC 2013](#)), past and ongoing global warming is *virtually certain* and *unprecedented*. One of many effects of rising global air temperature is the increased melt of snow and ice in polar and high mountain regions. Glaciers and ice caps outside the major ice sheets in Greenland and Antarctica (hereafter simply referred to as *glaciers*) make up less than 1% of the global land ice mass (cf. [Farinotti et al. 2019](#); [Vaughan et al. 2013](#)). However, the direct and indirect effects of changes in mountain cryosphere are disproportional and reach from the mountain regions themselves over the surrounding plains all the way to the oceans ([IPCC 2019](#)): destabilization of slopes by retreating glaciers and thawing permafrost affects the frequency and severity of geohazards (e.g., [Richardson and Reynolds 2000](#); [Deline et al. 2015](#); [Haeberli et al. 2017](#)); changes in seasonal meltwater runoff impact water availability for consumption, agriculture and hydropower (e.g., [Farinotti et al. 2016](#); [Huss and Hock 2018](#); [Ali et al. 2018](#); [Immerzeel et al. 2020](#)); biodiversity and ecosystems are affected by changes in mountain habitats (e.g., [Milner et al. 2017](#)); tourism and mountain sports have to adapt to a decline in snow cover and glacier area (e.g., [Stewart et al. 2016](#); [Lemieux et al. 2018](#); [Mourey et al. 2019](#)). The most relevant effect on a global scale is, however, the contribution of melting glaciers to the sea level rise.

Glaciers have contributed significantly to the observed sea level rise over the 20th century, despite their small share ( $\approx 0.5\%$ ) in global land ice volume (e.g., [Marzeion et al. 2015](#); [Bamber et al. 2018](#)). Up to 30% of the current global sea level rise can be attributed to mass loss of glaciers, which is equivalent to the contribution of the Greenland ice sheet and even exceeds the contribution of the Antarctic ice sheet ([Zemp et al. 2019](#)). Thereby, the attribution to natural and anthropogenic

causes is still debated. [Marzeion et al. \(2014\)](#) attribute  $25\pm35\%$  of the global glacier mass loss over the industrial era to anthropogenic forcing, with a strong increase for the period between 1991 and 2010 to  $69\pm24\%$ . [Roe et al. \(2020\)](#) conclude that the entire mass loss can be attributed to anthropogenic forcing, following that the central estimate of anthropogenic contribution to the industrial era temperature rise is  $100\pm20\%$  ([Allen et al. 2018](#)). Projections of future mass loss show a continued significant contribution of glaciers over the entire 21st century, even though the absolute amount is highly dependent on the chosen emission scenario ([Hock et al. 2019](#); [Marzeion et al. 2020](#)).

As seen by their widespread effects, glaciers and their changes are integral parts of the climate system and therefore imperative to be observed and investigated. Estimations of past changes in global glacier ice mass are difficult due to the comparably scarce data availability. Numerical glacier models can improve the accuracy and precision of such estimates. But more importantly, glacier models are indispensable for global projections that go beyond simple extrapolations. Despite all that, there are currently only a handful of models capable of estimating future changes in global glacier ice mass as a response to climate input data. All except one were developed in the last ten years and most of them rely on volume/area scaling relations to represent glacier geometry changes (e.g., [Van De Wal and Wild 2001](#); [Marzeion et al. 2012](#); [Radić et al. 2014](#)). Only the Open Global Glacier Model (OGGM, [Maussion et al. 2019](#)) implements a flowline model based on the shallow ice approximation (SIA e.g., [Hutter 1983](#)). The following section provides an overview over the current state of research, including a brief history of global glacier modeling and the accompanied sea level rise projections.

## 1.2 A brief history of global glacier modeling

Computer models are widely used in all earth sciences, providing a valuable part to the scientific process and a viable addition to classical observations and experiments. In meteorology and climatology for example, general circulation models (GCM) date back to the 1960s (see [Williamson \(2007\)](#) for an overview), and are imperative for daily weather forecast as well as for century-scale climate projections (e.g., [Côté et al. 2015](#); [Lauritzen et al. 2011](#)). And while ice sheet models have a longstanding tradition in cryospheric research (e.g., [Pattyn et al. 2012](#); [Nowicki et al. 2016](#)), the most glacier models—especially on a global scale—have emerged only over the past few years. The following section provides a brief overview over the evolution of global glacier models over the last twenty years. Hereby, the focus is on the general complexity of the dynamic model core, the spatial and temporal resolution, the resolved, parametrized and neglected processes, and the data used for calibration and

validation. Additionally, the performance differences between temperature-index and energy balance mass balance models is noted, but not discussed in more depth. A good overview over all assessments of global glacier mass change (from in-situ observations over satellite gravimetry up to recent modeling approaches) can be found in [Radić and Hock \(2014\)](#).

Numerical models for single glaciers date back to the late 20th century (e.g., [Budd and Jenssen 1975](#); [Bindschadler 1982](#); [Oerlemans 1997](#)), while global applications were heavily hampered by a lack of observational data at the time (and to some degree they still are today). [Van De Wal and Wild \(2001\)](#) pioneered the usage of volume/area scaling models for global sea level rise projections. Their model resolves fifteen glacier size classes within one-hundred individual glaciated regions and is forced by GCM data. Building on the mass balance sensitivity parametrization of [Gregory and Oerlemans \(1998\)](#), yearly ice volume changes are computed for each size class within each region. Glacier area is then updated using the volume/area scaling relation for each region, depending on its characteristic size distribution. Incomplete inventories and a lack of observational data at the time of publication made assumptions and extrapolations necessary: the mass balance sensitivities to temperature and precipitation were based on observations of only twelve glaciers; the size distribution was known for and extrapolated from only forty-one of the one-hundred regions; In the end, only about 100 000 individual glaciers were explicitly considered. Despite that, the contribution of glaciers to projected sea level rise over a simulation period of 70 years could be corrected down by 19 % in comparison to prior estimates performed with constant glacier area and/or constant mass balance sensitivities.

A similar approach to estimate global glacier volume change and accompanied sea level rise over the 21st century was used by [Raper and Braithwaite \(2006\)](#), by combining a degree-day model ([Braithwaite et al. 2003](#)) and a geometric model based on scaling relations ([Raper et al. 2000](#)). While the model had a higher spatial resolution and ran on a  $1^\circ \times 1^\circ$  grid, the major problem at the time was still estimating the needed parameters for areas not sufficiently covered by inventories. The mass balance model could run only in seven regions who had sufficient data coverage. A multiple linear regression (with annual precipitation and summer temperatures as explanatory variables and mass balance gradient as dependent variable) was computed from the mass balance profiles of each single grid cell of these seven regions. This regression was then used to extrapolate the results to all other regions. Statistical glacier characteristics like volume and area distribution, area-elevation distribution and elevation range were also estimated from those seven regions and extrapolated into each grid cell. In addition to the aforementioned assumptions and extrapolations, the coarse grid creates multiple problems for the volume/area scaling

model. On one hand, multiple glaciers are combined in a single cell, i.e., treated as glacier complexes, and on the other hand, single glaciers are subdivided along grid cell boundaries. According to [Bahr et al. \(2015, Section 8.6\)](#), volume/area scaling should not be applied to glacier complexes, nor to fractional parts of glaciers.

The IPCC's fourth assessment report ([IPCC 2007](#)) estimated the sea level contribution of glaciers excluding any dynamic effects. The estimation was based on a consensus estimate by [Kaser et al. \(2006\)](#), who in turn summarized three different publications which all used the same data. The use of a constant mass balance sensitivity results in a complete melt of glaciers for any warming, since no new equilibrium condition can be established ([Raper and Braithwaite 2006; Pfeffer et al. 2008](#)). Frontal ablation of water-terminating glaciers was not considered, despite its considerably fast ice discharge of ice directly into the ocean, which was already known at the time ([Pfeffer et al. 2008](#)). Additionally, glaciers and ice caps on the periphery of the Greenland and Antarctic ice shield were still missing from inventories. Their respective sea level rise contribution was estimated by adding 20 % to the global estimate. The general reasoning was that the relevant processes were not yet well enough understood to allow for reliable model estimates. In response, some studies circumvented the problems of direct modeling by e.g., extrapolating observed mass loss rates and their acceleration over the last decades ([Meier et al. 2007](#)), predefining low and high sea level rise projections and investigate the plausibility of climatic scenarios needed to meet them ([Pfeffer et al. 2008](#)), or projecting observed accumulation-area ratios (AAR) and their rate of change into the future ([Bahr et al. 2009](#)).

Motivated by the discrepancies of the few 21st century projections of global mass loss of glaciers, [Radić and Hock \(2011\)](#) published projections from a new model, which resolves each glacier individually. However, the scarcity of usable mass balance observations still hampered the model performance. The proposed calibration of the elevation dependent surface mass balance model with monthly temperature reanalysis and precipitation climatologies relied on observations of seasonal mass balance profiles of only thirty-six glaciers. Transfer functions based on a multiple linear regression were used to extrapolate the resulting mass balance calibration parameters to all glaciers in the global inventory. At the time this meant only about 120 000 glaciers and 2600 ice caps, corresponding to about 40 % of the total global glacier area. Area-averaged mass balance estimates for forty-one glacier regions (based on observations from only over 300 glaciers) were used to tune the model by an iterative process, which impeded an independent model validation with 20th century observations. The same area-averaged mass balance estimates were then used for initialization. The calibrated and initialized model ran with downscaled monthly temperature and precipitation projections of ten different GCMs, based on

a mid-range emission scenario. Volume/area and volume/length scaling was used to update glacier geometries and allowed for a potential new equilibrium under a changed climate. While modeling each individual glacier was a step in the right direction there was still room for improvements, especially concerning the calibration and validation process.

[Marzeion et al. \(2012\)](#) described the construction, validation and application of another new global surface mass balance model. This model is implemented and discussed in detail in this study. The model includes a simple representation of glacier geometry change, based on a combination of volume/length, volume/area and response time scaling. It is able to simulate past and future glacier states using observed climate data, model based climate reconstruction and GCM projections. It is the first global glacier model that was independently validated, using a leave-one-glacier-out cross validation of all 255 globally available glaciers with sufficiently long mass balance records. Thanks to a new inventory of global glacier outlines—the first version of the Randolph Glacier Inventory (RGI [Arendt et al. 2012](#))—each individual glacier and ice cap outside Antarctica could be modeled. The problem arising from the undersampling of mass balance observation was circumvented by a new calibration process: it is assumed that neighboring glaciers are most likely in an equilibrium state around the same time, while mass balance sensitivities of neighboring glaciers can be drastically different (due to different aspect, slope, shading, etc.). This means that instead of directly interpolating the mass balance sensitivities, the *equilibrium years* are interpolated from the ten closest glaciers with mass balance observations (for details see Section 2.1.2). The benefits of this technique are reflected in a decreased mass balance error, estimated by a leave-one-glacier-out cross validation. The model is used to project global sea level contribution of all glaciers over the 21st century, and its result are incorporated in the subsequent IPCC report.

The latest IPCC assessment report ([Church et al. 2013](#), AR5, Chapter 13) discusses the following 21st century sea level rise projections for global glaciers under different emission scenarios: [Slangen and Van De Wal \(2011\)](#) use an updated version of the model by [Van De Wal and Wild \(2001\)](#) and provide additional uncertainty estimations for different sources; [Marzeion et al. \(2012\)](#) as presented above; [Giesen and Oerlemans \(2013\)](#) also use a volume/area scaling model to account for geometry changes but include a simplified energy balance model with hourly resolution. However, only 89 glaciers are modeled explicitly (again due to missing input data) and the results are then upscaled to all other glacier grater than  $0.1 \text{ km}^2$ ; [Radić et al. \(2014\)](#) use an updated version of the model by [Radić and Hock \(2011\)](#) calibrated and validated with new data and applied to each individual glacier. The globally complete inventory of glacier location, area and hypsometry provided by the RGI

drastically improved the projections made by all the above mentioned models. However, they all still rely on scaling relation to update glacier geometries and allow for new equilibrium states. Additionally, none of the models accounts for calving or other rapid dynamic responses.

The increasing number of large scale datasets for all global glaciers over the last years—e.g., a satellite-borne digital elevation model ([Jarvis et al. 2008](#)), a distributed ice thickness and volume estimate ([Huss and Farinotti 2012](#)), a consensus estimate of regionally distributed mass budget between 2003 and 2009 ([Gardner et al. 2013](#)), digital glacier outlines and areas (RGI v4.0, [Pfeffer et al. 2014](#))—allows for new and more sophisticated models. The Global Glacier Evolution Model (Glo-GEM, [Huss and Hock 2015](#)) computes each glacier’s surface mass balance (including refreezing) with a temperature-index model on 10 m elevation bands with monthly resolution, and frontal ablation of water-terminating glaciers with yearly resolution. The dynamic response of glacier geometry based on [Huss et al. \(2010\)](#) adjusts area, thickness and surface elevation of each elevation band. Thereby, a non-dimensional empirical function redistributes the total mass change to each individual band, assuming maximum ice thickness change at the glacier terminus and no thickness change at the glacier top. The parametrization of this so called  $\Delta h$  function depends on the glacier size class. Glacier advance is accounted for by adding bands, if the thickness change exceeds a threshold. If the ice thickness of the lowest elevation band shrinks to zero, the band gets removed and the glacier retreats. Additionally, the computed sea level equivalent accounts for ice volume already below sea level, which systematically reduces the contribution of glaciers by about 11–14 %.

The IPPC’s most recent Special Report on the Ocean and the Cryosphere in a Changing Climate (SROCC [IPCC 2019](#)) includes updates of previous studies using new inventories and/or climate projections ([Bliss et al. 2014](#); [Slanger et al. 2017](#); [Hock et al. 2019](#)). Additionally, the following two new models are included: Glo-GEM as described above, and HYOGA2 [Hirabayashi et al. \(2013\)](#). HYOGA2 uses a temperature-index mass balance model and relies on volume/length scaling to update glacier geometries (only the area at the lowest elevation band is updated). As all IPCC report, SROCC mainly summarizes established literature, but also provides an updated uncertainty analysis by adding new and updated models.

A recent addition to the global glacier models is the OGGM ([Maussion et al. 2019](#)). The implemented temperature-index model and mass balance calibration is adapted from [Marzeion et al. \(2012\)](#), an added calving parametrization accounts for frontal ablation of water-terminating glaciers. Individual glaciers are represented by a depth integrated flowline, with the possibility of tributaries. Ice flow is computed by an explicit ice dynamics module, which solves the SIA equations on a staggered grid without converting them into a diffusion equation ([Maussion et al. 2019](#)). By

doing so, the OGGM is the first and so far only globally applicable model using flowline representations of glaciers. But much more importantly, it is open source (see the GitHub repository <https://github.com/OGGM/oggm>) and hence by design modular. This allows to compare the performance of various parameterizations of e.g., the mass balance model or downscaling procedures as well as the implementation of additional features to resolve new processes like e.g., the effect of debris cover. It is also a basic prerequisite for this study, since it enables the implementation of the original Marzeion et al. (2012) model into the OGGM framework.

Research involving global glacier models has come a long way in the last twenty years. In analogy to the Coupled Model Intercomparison Project (CMIP, e.g., Eyring et al. 2016) for atmospheric models, recent coordinated efforts for glacier models have been made, e.g., the Ice Thickness Models Intercomparison eXperiment (Farinotti et al. 2017, 2020, <https://cryosphericosciences.org/activities/ice-thickness/>) and the Glacier Model Intercomparison Project (GlacierMIP, <https://climate-cryosphere.org/mips/glaciermip>). Two recent studies on global sea level rise projections of glaciers are published as part of GlacierMIP. Hock et al. (2019) provide a consensus estimate of glacier contribution to 21st century sea level rise projections. The results are based on the five global or nearly global (i.e., without Greenland and/or Antarctic periphery) models (Slangen et al. 2012; Marzeion et al. 2012; Giesen and Oerlemans 2013; Hirabayashi et al. 2013; Radić et al. 2014; Huss and Hock 2015) forced by multiple GMCS and emission scenarios. Marzeion et al. (2020) use four of those models and add the global model GLIMB (Sakai and Fujita 2017), the two nearly global models JULES (Shannon et al. 2019) and OGGM, and four regional models to the ensemble to provide an updated uncertainty analysis. The new additional feature of both GLIMB and JULES is the implementation of an energy balance model to compute the surface mass balance (refer to the original publications for details about the individual models not discussed here). Seven of these thirteen models rely on some form of scaling relation to update glacier geometries while the OGGM is the only global model using a flowline model. It shows that volume/area scaling based models were, and still are, the most broadly used type of models to estimate glacier geometry changes. Given their long tradition and broad application, several studies have investigated the performance, strength and weaknesses of scaling based models. An overview is given in the following section.

## 1.3 State of Research

Volume/area scaling is a simple power law relation  $V = c A^\gamma$ , based on the empirical relationship between glacier volume  $V$  and surface area  $A$ . The scaling constant  $c$  is

a random variable depending on glacier characteristics and needs calibration. The scaling exponent,  $\gamma_{\text{glacier}} = 1.375$  for glaciers and  $\gamma_{\text{ice cap}} = 1.25$  for ice caps, is a physically based constant and should not be changed (Bahr et al. 1997). It can be formally derived by a dimensional analysis of the relevant continuum equations. The derivation does not rely on any assumptions like steady state conditions, perfect plasticity, plain strain or shallow-ice approximation, which is why Bahr et al. (2015) insist on the validity and viability of volume/area and similar scaling relations. Additionally, volume/area scaling has inherent benefits in dealing with the non-uniqueness and instabilities arising from the ill-posed nature of ice thickness inversions (Bahr et al. 2014). However, dimensional analysis do—by definition—only provide characteristic results, which should not be misunderstood as specific results for any specific state of the system. Such misconceptions and the accompanied successful and unsuccessful application of glacier scaling relations have lead to some controversy in past publications (Bahr et al. 2015, see Table 1 for an overview).

Radić et al. (2007) used a set of thirty-seven synthetic glaciers created by a one-dimensional flowline model to compute and compare scaling exponents between steady state and transient conditions. Bahr et al. (2015) indicate potential pitfalls of this approach. The first of which is that the estimated range for  $\gamma$  is well outside any physically sensible bounds. Secondly, no assumption of steady state conditions is used for the derivation of the scaling relations. Volume/area scaling is fully valid for transient conditions, however it must be used in conjunction with an appropriate response time scaling. Thirdly, the scaling exponent is a physically based constant and its value does not change in time or space. And lastly, the used sample size is rather small. This undersampling problem is even more severe in Radić et al. (2008), where the performance of a volume/area scaling model for mass change projections of only six different real world glaciers is compared to a flowline model. Scaling relations are statistically relevant for a large enough population of glaciers, but do not apply to individual glaciers. Volume scaled from the area of a single glacier can only be treated as order of magnitude estimate, the relative volume error is directly proportional to the relative error in scaling constant  $c$  (Bahr et al. 2015). However, both publications endorse the use of volume/area scaling for glacier volume projections and sea level rise estimations. Results from volume/area scaling agree well with the flowline model, even though the ice loss is underestimated up to 47 %. While initial volume estimations are highly sensitive to the chosen scaling parameters, volume projections over a century timescale are not, especially when normalized with initial values (Radić et al. 2007, 2008). Slangen and Van De Wal (2011) came to the same conclusion, by varying only  $c$  and fixing  $\gamma$  at appropriate values. More important are uncertainties introduced by the mass balance sensitivity, glacier inventory and emission scenario.

[Adhikari and Marshall \(2012\)](#) performed a similar analysis, evaluating the volume/area scaling model with respect to a numerical model. Using an ensemble of 280 glaciers randomly generated by a three-dimensional Stokes model, they assessed the influence of different characteristics of topography, climate, glacier flow and disequilibrium with climate on the scaling relations. Most of the above mentioned points of criticism (wrongful steady state assumption, non-constant scaling exponent) also applies to this study. However, their estimated scaling exponents (for steady state and transient conditions) are much more in line with the theoretical values and past observations, most likely due to the bigger sample size. [Farinotti and Huss \(2013\)](#) show that in order to estimate the total ice volume of a population of more than thousand glaciers within 30 % of its true value, 280 pairs of volume and area measurements are needed to calibrate the scaling parameters. Hereby, reducing either the population size or the number of measurements for calibration decreases the estimation's accuracy. Uncertainties in ice volume measurements are negligible, if a systematic bias can be ruled out.

None of the above mentioned studies evaluated the performance of scaling models on the example of real world glaciers on a regional scale. The modular design of the OGGM allows the implementation of the original [Marzeion et al. \(2012\)](#) model in the same framework and facilitates a comparison under controlled boundary conditions.

## 1.4 Goals and Outline

As outlined above, volume/area scaling has a long academic tradition. It was, and still is used with great success in many global glacier models. Nowadays, new global inventories and improved data availability (e.g., glacier outlines, digital elevation models) as well as increased computational power allow for more sophisticated glacier models on a global scale. One of these models is the Open Global Glacier Model (OGGM, [Maussion et al. 2019](#)), which developed out of the volume/area scaling model ([Marzeion et al. 2012](#)) by adding a dedicated ice physics module to solve the shallow ice approximations for flowline glaciers. That raises the following questions, which are investigate in this work:

- What are the differences in dynamic response between the volume/area scaling model and the flowline model?
- How do those differences influence ice volume projections for the 21st century for mountain regions?

In order to compare both models, the volume/area scaling model is implemented in the OGGM framework. This allows to use the same mass balance model and

calibration as well as the same boundary conditions (like climate input data, glacier outlines and digital elevation models). Therefore, any differences in model output will arise from differences in the dynamic response.

Chapter 2 details the model implementation, which is—albeit necessary to answer the research questions—a central part of this work. The implementation of the volume/area scaling model into the OGGM framework highlights the possibilities arising from a modular, community based glacier model. The programming related implementation details provided here can be seen as a form of documentation. The chapter starts with the general theoretical concepts about the glacier volume/area scaling relations, the used temperature-index mass balance model, and the scaling glacier evolution model. Chapter 3 details the individual experiments and their outcome. It starts with single glacier test cases, including a time series analysis. Since volume/area scaling should only be applied to large populations of glaciers, the same experiment is rerun on a regional scale, by investigating the aggregate ice volume of all Alpine glaciers. The model’s sensitivity to its scaling parameters is investigated before the final experiment: a projection of glacier mass change in the Alps and High Mountain Asia over the 21st century based on different climate scenarios of general circulation models (GCM). Chapter 4 provides a discussion of the identified strength and weaknesses of each model, by relating the result to recently published literature. A final summary and an outlook on possible future work can be found in Chapter 5.

# Chapter 2

## Model implementation

This chapter describes the model implementation process, including the underlying theory. The first section explains the general concepts of glacier volume/area scaling relations as well as the theoretical basis for the implemented temperature-index mass balance model and glacier evolution model. Programming related implementation details are shown in the second section, including the description of relevant classes and methods, which serves as documentation. The third and final section of this chapter details the experimental setup for the following model evaluation.

### 2.1 General concepts

Before starting to write any code, a solid theoretical foundation has to be established. A summary of the extensive work on volume/area scaling ([Bahr 1997a,b; Bahr et al. 1997, 2015](#)) is provided, including a discussion about the ill-posed nature of ice volume inversions ([Bahr et al. 2014](#)). The description of the implemented mass balance model and glacier evolution model follows [Marzeion et al. \(2012\)](#).

#### 2.1.1 Glacier volume/area scaling

Ice volume is one of the most fundamental geometric glacier properties and yet unknown for the vast majority of all of the world's glaciers and ice caps. Direct measurements of ice volume and ice thickness (or any other internal property such subsurface topography, internal velocities, sliding rates, etc.) are difficult to obtain, incident to time and cost extensive fieldwork. Hence, glacier internal properties are often inferred from surface properties, a process called inversion ([Bahr et al. 2014](#)). Volume/area scaling has been, and still is, one of the most commonly used ice volume inversion methods.

A glacier's ice volume  $V$  can be estimated from its surface area  $A$  using the power law  $V = c A^\gamma$ . Hereby, the scaling constant  $c$  is a random variable, changing from

### Take Home Message: Glacier volume/area scaling

- Volume/area scaling relates a glacier's ice volume  $V$  to its surface area  $A$  via the power law  $V = cA^\gamma$ . It has a solid physical basis, the derivation does not rely on any simplifications.
- Two separate derivations and three different choices of a single closure condition all result in the same value for the scaling exponent  $\gamma_{\text{glacier}} = 1.375$ , which implies self consistency. The scaling constant  $c$  is a random variable that varies from glacier to glacier.
- Response time scaling should be used in conjunction with volume/area scaling to simulate transient glaciers.
- Scaling relations are determined, validated and should therefore be applied solely to large samples of glaciers spanning a large range of sizes, and not on single glaciers, parts or individual branches of glaciers, or glacier complexes spanning over flow divides.

glacier to glacier. The scaling exponent  $\gamma$  is a constant for a given geometric class of glaciers: it is distinguished between valley glaciers  $\gamma_{\text{glacier}} = 1.375$ , and radially symmetric ice caps  $\gamma_{\text{ice cap}} = 1.25$ <sup>1</sup>. The scaling parameters were initially determined empirically by computing a linear regression between  $V$  and  $A$  measurements in log-log space (e.g., [Chen and Ohmura 1990](#)). The underlying theoretical principles were established later by [Bahr \(1997a\)](#); [Bahr et al. \(1997\)](#). The following basic derivation relies on simple geometric observations, following [Bahr et al. \(1997, 2015\)](#).

### Basic derivation

Glacier volume can be scaled with a number of quantities (e.g., area, thickness, length and velocity), of which surface area is the most easily measurable one. To obtain a volume quantity  $V$  of dimension  $L^3$  (hereby  $L$  represent the fundamental dimension of length), an area  $A$  of dimension  $L^2$  must be multiplied by one additional quantity of dimension  $L$ . In the specific case of glacier ice volume and glacier surface area, the average ice thickness  $\bar{h}$  is an obvious choice. Thereby,  $\bar{h}$  can be estimated as the centerline thickness  $h$  corrected by shape factor, to account for lateral drag

---

<sup>1</sup>The following section focuses on mountain glaciers, however the general concepts hold also true for ice caps with The different values for scaling exponent and scaling constant result from different closure conditions (e.g., radial symmetric shape). A detailed derivation can be found in [Bahr et al. \(2015, Section 7.2\)](#).

and non U-shaped bed cross sections. This shape factor  $F$  scales as ratio of width to thickness  $F \propto w/h$ . The surface area is a product of average length  $\bar{l}$  and average width  $\bar{w}$ . Observations suggest that  $w \propto l^q$ , with  $q \approx 0.6$  for valley glaciers. It is sensible to use the average values as characteristic values. By bringing all those relations together, it can be shown that glacier volume scales with surface area as

$$\begin{aligned} V &\propto A \cdot \bar{h} = A \cdot Fh \\ &\propto \bar{w}\bar{l} \cdot \frac{\bar{w}}{h}h = \bar{w}^2\bar{l} \\ &\propto \bar{l}^{2q+1} \\ &\propto A^{\frac{2q+1}{q+1}} = A^\gamma = A^{1.375} \end{aligned} \tag{2.1}$$

The scaling relations for  $F$  and the  $w$  are necessary to fully express  $V$  as a function of  $l$  and consequentially of  $A$ . Those so called closure conditions are hypothesized but backed by observational data, and the *universal* nature of the scaling exponent stands and falls with them. However, the same volume/area scaling relation can be derived via two independent and mathematically consistent pathways. The following section gives a brief overview over the derivation from a dimensional analysis and the physical reasoning behind glacier scaling relations, following [Bahr et al. \(2015, Section 4 - 7\)](#).

## Formal derivation

Glacier volume/area scaling can be derived from a dimensional analysis of the full set of continuum equations ([Bahr et al. 1997, 2015](#)). The set of continuum equations describing the ice flow of glaciers accounts for mass balance and mass conservation via the continuity equation, and force balance and momentum conservation via the equation of motion. Both equations are linked by the constitutive equation, relating force to deformation, or more precisely stresses to strain rates (e.g., [Cuffey and Paterson 2010](#)). The values of variables like glacier geometries, surface mass balance, sliding velocity, and others are defined by boundary conditions. Since those boundary conditions affect only the values but not the dimensions of the relevant variables, they have no effect on the dimensional analysis. Similarly, the inclusion of an energy conservation equation only adds additional non-dimensional parameters. This does not alter other scaling relations and is therefore omitted ([Bahr et al. 2015](#)). The full set of continuum equations consist of eighteen fundamental variables, which span over the three fundamental dimensions length L, mass M, and time T. According to the Buckingham Pi theorem (e.g., [Evans 1972; Yarin 2012](#)) this yields a set of fifteen dimensionless  $\Pi$ -groups. The  $\Pi$ -groups relevant for volume/area scaling

are listed below, taken from [Bahr et al. \(2015\)](#), Section 4.1, Eq. 26, 28 & 33):

$$\Pi_2 = \frac{x}{z}, \quad \Pi_4 = \frac{u_x}{u_z}, \quad \Pi_9 = \frac{A\rho^n g_x^n z^{n+1}}{u_x}. \quad (2.2)$$

Hereby,  $x$  and  $z$  represent length and height (or more formally, distance in longitudinal and vertical direction),  $u_x$  and  $u_z$  velocities in  $x$  and  $z$  direction,  $\rho$  the ice density,  $g_x$  the gravitational acceleration in  $x$  direction, and  $n$  the exponent of Glen's flow law (e.g., [Cuffey and Paterson 2010](#), Chapter 3.4.4). The number indices are arbitrary. The same set of dimensionless parameters can be computed from a stretching analysis, with the added benefit of knowing the respective physical origin and removing potential mathematical ambiguities ([Bahr et al. 2015](#), Section 5). The stretching analysis shows that the geometric similarity  $\Pi_2$  and the kinematic similarity  $\Pi_4$  follow from the constitutive equation, while the velocity relationship  $\Pi_9$  follows from a combination of the constitutive equation and the equation of motion ([Bahr et al. 2015](#), Section 6).

Choosing and combining the  $\Pi$ -groups most relevant to the problem influences the form of the scaling constant  $c$ . The dimensionless parameters may vary from glacier to glacier, and so does  $c$ . However, variations in  $c$  are several orders of magnitude smaller than variations in  $A$  and  $V$ . This explains the strong power law relation between  $A$  and  $V$ , undeterred by variations in  $c$ , and allowed the empirical estimation in the first place ([Bahr et al. 2015](#)). Combining the above shown  $\Pi$ -groups yields

$$\frac{\Pi_4 \Pi_9}{\Pi_2} = \frac{A\rho^n g_x^n z^{n+2}}{u_z x}. \quad (2.3)$$

The characteristic values cancel when solving for area and volume, which is why their exact choice is of secondary importance. However, the choice will influence the scaling exponent  $\gamma$ . Some choices make intuitive sense, like using glacier length as characteristic length  $l \equiv x$ , average thickness as characteristic thickness  $h \equiv z$  and average width as characteristic width  $w \equiv y$ . Other choices are motivated by known closure conditions, like using the mass balance at the glacier terminus as characteristic vertical velocity  $b \equiv u_z$  ([Bahr et al. 2015](#)). Closure conditions are additional scaling relations backed by observations. They are necessary to express the ice thickness purely as function of glacier length. The following closure conditions are used:

- The volume/area scaling relation encapsulates the erosive power of a glacier by relating the “superficial” glacier size to its geometry. Similarly, a glacier's width relates to its length. Observational data suggests that the average glacier width scales with glacier length as  $w = c_q l^q$  with  $q \approx 0.6$  for valley glaciers. Hereby,  $c_q$  is a variable scaling constant ([Bahr 1997b](#); [Bahr et al. 2015](#)).

- Longer glaciers tend to span over a wider range of elevations and reach further into the ablation zone. The magnitude of the (point) mass balance is higher at lower—and thereby warmer—elevations. Hence, the mass balance scales with glacier length as  $\dot{b} = c_m l^m$ . Hereby observations suggest  $m \approx 2$  for valley glaciers, while  $c_m$  is a variable scaling constant (Bahr et al. 1997, 2015).

Substituting characteristic values and the mass balance closure into Equation 2.3, and solving for  $h$  yields

$$h = \left( \frac{\Pi_4 \Pi_9 c_m}{\Pi_2 A \rho^n g_x^n} \right)^{\frac{1}{n+2}} l^{\frac{m+1}{n+2}}. \quad (2.4)$$

Using  $V = lwh$  and  $S = lw$ , substituting Equation 2.4 and the width closure, and combining the two yields

$$V = c_A S^{1 + \frac{m+1}{(n+2)(q+1)}} \quad (2.5)$$

$$= c_A S^\gamma. \quad (2.6)$$

While the scaling constant  $c_A$  depends on a bunch of dimensionless parameters and other constants (not shown), the scaling exponent depends only the mass balance scaling exponent  $m$ , the exponent of Glen's flow law  $n$  and the width scaling exponent  $q$ . With the values suggested above this results in

$$\gamma = 1 + \frac{m+1}{(n+2)(q+1)} \quad (2.7)$$

$$= 1 + \frac{2+1}{(3+2)(0.6+1)} \quad (2.8)$$

$$= 1.375. \quad (2.9)$$

It can be shown that the used closure conditions are not independent of each other and only one closure condition is strictly necessary. Additionally, using independent observational data for all three closure conditions results in the same value for  $\gamma$ .

## Usage and best practice

Besides showing an improved and more detailed derivation, Bahr et al. (2015) review the usage of volume/area scaling in thirty-three papers published between 2006 and 2014. While all studies provide new insights, certain misconceptions in the validity and applicability of volume/area scaling led to a few unsuccessful applications. Bahr et al. (2015, Section 8) address all particular characteristics of volume/area scaling that have been ground for misunderstandings. The suggested guidelines for practical applications are summarized below:

- Fix the scaling exponent  $\gamma$  to its physically based value, and let the scaling constant  $c$  vary as necessary in time, space and others.

- Apply volume/area scaling to large populations of glaciers, whereby the aggregate volume gives the most accurate estimate. Avoid applying volume/area scaling to single glaciers and treat the result as order of magnitude estimate if you do.
- Avoid applying volume/area scaling to fractional parts of glaciers and glacier complexes that span over flow divides.
- Use response time scaling in conjunction with volume/area scaling to account for transient glacier states.

### 2.1.2 Temperature index model

A glacier's annual specific surface mass balance  $B$  is the area-averaged difference between accumulation and ablation over the course of a year. Hereby, accumulation refers to mass gain via snowfall, avalanches, snow drift, etc., while ablation refers to mass loss via ice melt, sublimation, calving, etc. The temperature index mass balance model explained and implemented hereafter relies solely on two input parameters: the area-averaged monthly solid precipitation onto the glacier surface  $P_i^{\text{solid}}$  and the monthly mean air temperature at the glacier's terminus elevation  $T_i^{\text{terminus}}$ . Hereby, the index  $i$  denotes the month of the year. The mass balance equation described by [Marzeion et al. \(2012\)](#) reads

$$B = \left[ \sum_{i=1}^{12} [P_i^{\text{solid}} - \mu^* \cdot \max(T_i^{\text{terminus}} - T_{\text{melt}}, 0)] \right] - \beta^*. \quad (2.10)$$

The terminus temperature  $T_i^{\text{terminus}}$  is computed by scaling the monthly mean air temperature  $T_i$  from the climate date reference elevation  $z_{\text{ref}}$  to the glacier's terminus elevation  $z_{\text{min}}$  using the temperature lapse rate  $\gamma_{\text{temp}}$ .

$$T_i^{\text{terminus}} = T_i \cdot \gamma_{\text{temp}} (z_{\text{min}} - z_{\text{ref}}) \quad (2.11)$$

The temperature at the maximum glacier elevation  $T_i^{\text{max}}$  is computed analogously  $T_i^{\text{max}} = T_i \cdot \gamma_{\text{temp}} (z_{\text{max}} - z_{\text{ref}})$ , whereby  $z_{\text{max}}$  represent the maximum glacier surface elevation. The positive melting temperature is computed as the difference between  $T_i^{\text{terminus}}$  and temperature threshold for ice melt  $T_{\text{melt}}$ , with an obvious lower bound of 0 °C. The glacier's temperature sensitivity  $\mu^*$  relates the positive melting temperature to the actual ice loss and needs to be calibrated for each glacier (as does the mass balance residual  $\beta^*$ ). The [calibration process](#) of these mass balance parameters is described below.

The area-average monthly solid precipitation onto the glacier surface  $P_i^{\text{solid}}$  is computed from the total precipitation of the climate data  $P_i$  as

$$P_i^{\text{solid}} = P_i \cdot f_{\text{solid}} \cdot (1 + \gamma_{\text{precip}} \cdot (z_{\text{mean}} - z_{\text{ref}})). \quad (2.12)$$

Hereby,  $P_i$  is scaled from  $z_{\text{ref}}$  to the average glacier surface elevation  $z_{\text{mean}}$  using the precipitation lapse rate  $\gamma_{\text{precip}}$  (given in units of percentage of precipitation per meters of elevation change [% m<sup>-1</sup>]). The fraction of solid precipitation  $f_{\text{solid}}$  depends on the relation of  $T_i^{\text{terminus}}$  and  $T_i^{\text{max}}$  to the temperature thresholds for solid and liquid precipitation,  $T^{\text{solid}}$  and  $T^{\text{liquid}}$ , respectively. The fraction of solid precipitation is linearly interpolated ( $f_{\text{solid}} = 1 + \frac{T_i^{\text{terminus}} - T^{\text{solid}}}{\gamma_{\text{temp}} \cdot (z_{\text{max}} - z_{\text{min}})}$ ) between the two extreme cases of only solid ( $T_i^{\text{terminus}} < T^{\text{solid}} \Rightarrow f_{\text{solid}} = 1$ ) and only liquid precipitation ( $T_i^{\text{max}} > T^{\text{liquid}} \Rightarrow f_{\text{solid}} = 0$ ). Values for the temperature thresholds are discussed below.

The downscaling of GCM data for the use with glacier mass balance models requires one additional step. The monthly precipitation amount is scaled by an additional factor  $a$ , since precipitation in mountainous regions is generally under-estimated. While this scaling factor is implemented in the mass balance models (as `prcp_scaling_factor`), it is not a physical component of the mass balance equation and therefore omitted in Equation 2.12. Values of  $a$  are discussed below.

The values of the above mentioned hyper parameters, like temperature thresholds, lapse rates, and scaling factors, can and should be calibrated depending on the region and the used baseline climate. The OGGM ships with default global values based on climate data provided by the Climate Research Unit (CRU, [Harris et al. 2014](#)) and default Alpine values based on the Historical Instrumental Climatological Surface Time Series Of The Greater Alpine Region (HISTALP, [Auer and Böhm 2007](#)). These default values result from a leave-one-glacier-out cross validation between all reference glaciers. Thereby, individual hyper parameters are iteratively changed within a given range, as originally proposed by [Marzeion et al. \(2012\)](#) and refined for regional use by [Dusch \(2018\)](#). An analogous cross validation is performed for the volume/area scaling model using HISTALP data as baseline climate. The following parameters are chosen based on a simple scoring function of the computed statistical measures and used for all runs on Alpine glaciers:  $a = 2.5$ ,  $T^{\text{melt}} = -0.5^\circ\text{C}$ ,  $T^{\text{solid precip}} = 2.0^\circ\text{C}$ . The flowline mode uses the default OGGM HISTALP parameters ( $a = 1.75$ ,  $T^{\text{melt}} = -1.75^\circ\text{C}$ ,  $T^{\text{solid precip}} = 2.0^\circ\text{C}$ , [Dusch \(2018\)](#)) for the same runs. The 21st century projections are based on CRU climate data and the latest data from the Coupled Model Intercomparison Project (CMIP6, [Eyring et al. 2016](#)). Hence the volume/area scaling model uses updated global parameters taken from [Malles and Marzeion \(2020\)](#) for those runs, while the flowline model falls back to the OGGM default values. However, differences between those values are of minor importance, since the temperature sensitivity  $\mu^*$  compensates for most systematic biases in the climate input data ([Maussion et al. 2019](#), Appendix A).

## Calibration of the mass balance parameters

A complete and thorough description of the mass balance calibration process for this particular temperature index model can be found in [Marzeion et al. \(2012, Section 2.1.9-10\)](#) and [Maussion et al. \(2019, Section 3.3\)](#). The following summary is included here for completeness.

The first step is to estimate the so called  $\mu(t)$  *candidates* for all glaciers with available mass balance records (254 glaciers globally, see [World Glacier Monitoring Service, Zürich, Switzerland \(2017\)](#)). This is done by requiring the average mass balance  $\bar{B}(t)$  over the 31-year period centered around the year  $t$  to be zero and solving for  $\mu(t)$ .

$$\mu(t) = \frac{P_{\text{clim}}^{\text{solid}}(t)}{\max(T_{\text{clim}}^{\text{terminus}(t)} - T_{\text{melt}} 0)}, \quad (2.13)$$

whereby  $P_{\text{clim}}^{\text{solid}}(t)$  and  $T_{\text{clim}}^{\text{terminus}}(t)$  are the average yearly solid precipitation amount and average yearly air temperature at the glacier's terminus during the climatological period centered around the year  $t$ , respectively. The next step is to solve the mass balance equation (Equation 2.10) for each  $\mu(t)$  candidate and compare the results to the mass balance observations. The computed difference  $\beta(t)$  is a measure of how good the temperature sensitivity candidate approximates the *real* value, denoted as  $\mu^*$ . Hence,  $\mu^*$  is chosen as the candidate  $\mu(t = t^*)$  for which the absolute bias is minimal  $\beta^* := \beta(t = t^*) \approx 0$ —which in the best case is around zero. Hereby, the *equilibrium year*  $t^*$  represents the center of the 31-year climatic period where the given glacier geometry would stay in equilibrium. However, this is more of a model parameter and should not be overinterpreted as a real world value. The same is true for the corresponding temperature sensitivity  $\mu^*$  and mass balance residual  $\beta^*$ .

For all glaciers without mass balance records,  $t^*$  and  $\beta^*$  are interpolated from the ten closest glaciers, inversely weighted with distance. The temperature sensitivity is computed by requiring the mass balance to be zero ( $\bar{B}(t^*) = 0$ ) and solving for  $\mu^*$ . The temperature sensitivity  $\mu^*$  depends highly on glacier specific factors, such as avalanches from surrounding terrain, topographical shading, etc. Therefore,  $\mu^*$  can vary drastically from one glacier to another, even between neighboring glaciers. By contrast, it is intuitively more likely for a glacier to be in equilibrium if its surrounding glaciers are in equilibrium as well. This is one major factor, why the interpolation of  $t^*$  instead of  $\mu^*$  reduces the mass balance error in a leave-one-out cross validation (cf. [Marzeion et al. 2012](#); [Maussion et al. 2019](#)).

## Implementation note

The results of the calibration steps outlined above depend on the glacier outlines, the climate data, and the mass balance hyper parameters (i.e., the temperature

thresholds, lapse rates and the precipitation scaling factor). The equilibrium year  $t^*$  and mass balance residual  $\beta^*$  computed for each reference glacier are stored in the `ref_tstars.csv` file. Hence, for a given combination of RGI version, baseline climate and hyper parameters the calibration for the reference glaciers has to be done only once. Afterwards, the results can be read directly from the corresponding file. The OGGM comes with reference tables for combinations of RGI version 5 and 6, and CRU version 4 and HISTALP. The volume/area scaling model provides its own reference tables, for CRU version 4 and HISTALP data but only for RGI version 6, using the hyper parameters detailed in Section 2.1.2.

### Differences in mass balance model between the scaling and flowline model

The volume/area scaling mass balance model computes an average mass balance value for the entire glacier. The mass balance model requires only the minimal and maximal glacier elevation as additional input parameters ( $z_{\min}$ ,  $z_{\max}$ ), to compute the monthly terminus temperature  $T_i^{\text{terminus}}$  and the area averaged monthly amount of solid precipitation  $P_i^{\text{solid}}$ . The flowline model requires a mass balance value for each grid point of the flowline (i.e., for each elevation band). Therefore, the mass balance is computed as a function of elevation  $B(z)$ . Hence, the elevation of the grid points must be supplied as input parameters. Solid precipitation and air temperature are then computed for the given points of elevation, resulting in a point mass balance estimate.

### 2.1.3 Glacier evolution model

The volume/area scaling relation is derived from the complete set of continuum equations, without any assumptions of plane strain, shallow ice, perfect plasticity, or steady state conditions. This derivation from the fully time dependent equation of motion allows the volume  $V$ , area  $A$  and scaling constant  $c_A$  to change with time. Especially the scaling constant  $c_A$  can incorporate transient behavior, since it depends on closing conditions which show an explicit time dependency. However, to explicitly include a temporal component, volume/area scaling has to be used in conjunction with proper response time scaling. Response time scaling is a separate but equally valid scaling relation, based in the same dimensionless analysis. Hence, these two scaling relations cannot be separated and have to be applied together, in order to successfully model glacier evolution (Bahr et al. 2015).

The volume/area scaling model starts with the initial glacier surface area  $A_0$  as input. The initial glacier volume  $V_0$  and the initial glacier length  $L_0$  are computed using the volume/area scaling relation and the inverted volume/length scaling

relation, respectively (cf. Section 2.1.1):

$$V_0 = c_A \cdot A_0^\gamma, \quad L_0 = \left( \frac{V_0}{c_L} \right)^{\frac{1}{\gamma}}. \quad (2.14)$$

Only the mass balance model and the initial minimal  $z_{\min, 0}$  and maximal glacier surface elevation  $z_{\max}$  are additionally required.

The volume/area scaling model runs with a yearly time resolution ( $\Delta t = 1$  yr). Each time step from year  $t$  to year  $t + 1$  includes the following computational steps:

1. Compute the time scale of the glacier's length change response to volume change  $\tau_L$  and the time scale of the glacier's surface area change response to volume change  $\tau_A$  as

$$\tau_L(t) = \frac{V(t)}{P_{\text{clim}}^{\text{solid}}(t^*) \cdot A(t)} \quad \tau_A(t) = \tau_L(t) \frac{A(t)}{L(t)^2} \quad (2.15)$$

The equation for  $\tau_L$  is based on [Jóhannesson et al. \(1989\)](#). It implies that larger glaciers (indicated by  $V$ ) react slower, while glaciers with a higher mass turnover (indicated by  $P_{\text{clim}}^{\text{solid}}(t^*)$ , the average solid precipitation during the 31-year period centered around  $t^*$ ) react faster. Assuming that volume changes are directly translated into changes of width,  $\tau_A$  is a function of  $\tau_L$  following geometric reasoning. For more details see [Marzeion et al. \(2012\)](#). The implementation includes lower bounds for both time scales as well as the climatological turnover, for details see Section 2.2.2.

2. Get the specific mass balance  $B(t)$  from the mass balance model, by solving Equation 2.10. For implementation details see Section 2.2.1
3. Compute the volume change  $\Delta V(t) = \frac{1}{\rho_{\text{ice}}} A(t) \cdot B(t)$  as product of specific mass balance and glacier surface area. The volume change happens instantaneously, i.e., over one time step, hence the updated volume equals the sum of current volume and volume change  $V(t + 1) = V(t) + \Delta V(t)$ .
4. The (hypothetical) equilibrium surface area can be computed by inverting the volume/area scaling relation  $(V(t + 1)/c_A)^{1/\gamma}$ . However, the surface area does not change instantaneously, and proper response time scaling must be applied. Hence, the area change is computed as

$$\Delta A(t) = \frac{1}{\tau_A} \left( \left( \frac{V(t + 1)}{c_A} \right)^{\frac{1}{\gamma}} - A(t) \right). \quad (2.16)$$

The updated area then equals the sum of current area and area change  $A(t + 1) = A(t) + \Delta A(t)$ .

5. The updated glacier length and length change are computed analogously to the glacier surface elevation.  $L(t + 1) = L(t) + \Delta L(t)$ , with

$$\Delta L(t) = \frac{1}{\tau_L} \left( \left( \frac{V(t+1)}{c_L} \right)^{\frac{1}{q}} - L(t) \right). \quad (2.17)$$

6. The terminus elevation  $z_{\min}$  is adjusted by assuming a linear elevation change with changing glacier length (i.e., constant slope):

$$z_{\min}(t + 1) = z_{\max} + \frac{L(t)}{L_0} (z_{\min,0} - z_{\max}) \quad (2.18)$$

The maximum glacier elevation stays constant during the entire model run ( $z_{\max} = \text{const.}$ )

A schematic of the computational steps and the dependency of the different variables from each other is shown in Figure 2.1.

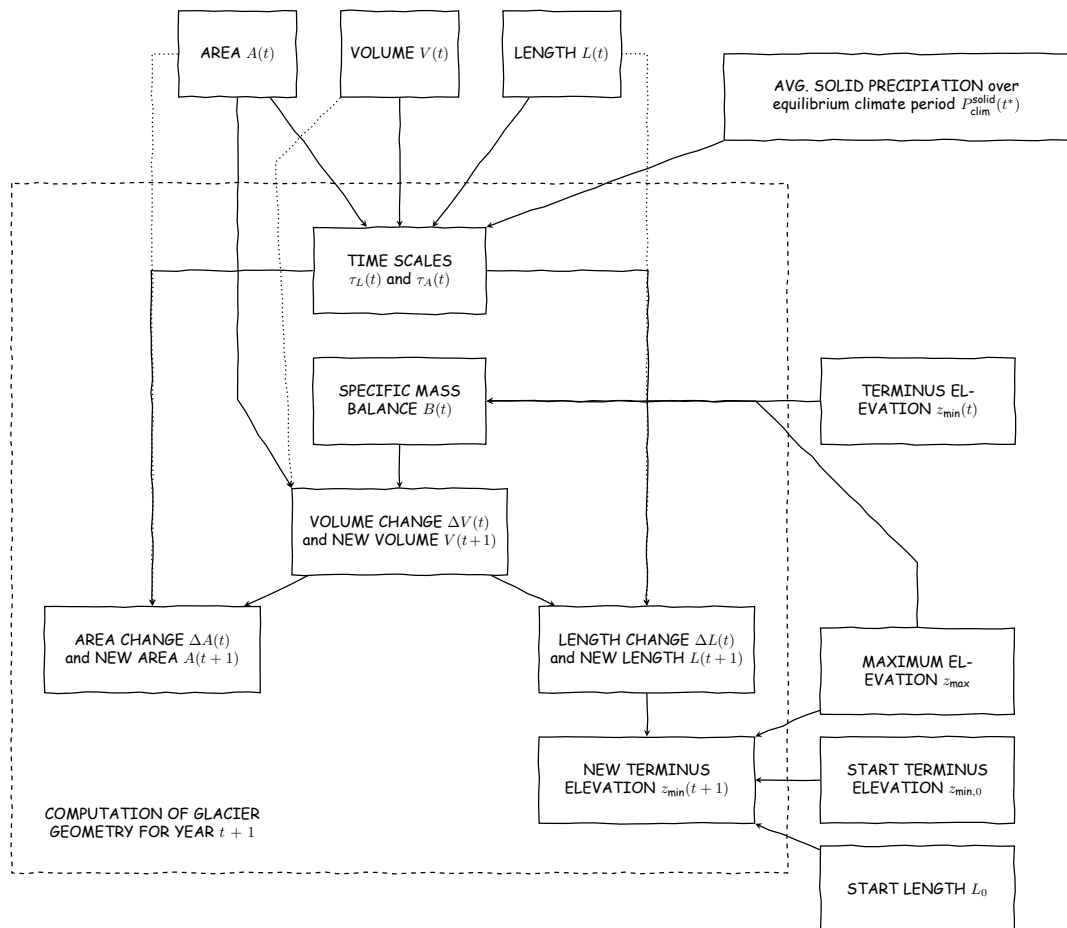


**Figure 2.1:** Schematic of the glacier evolution model's time stepping.

## 2.2 Implementation

The volume/area scaling model is implemented in [Python 3](#), following the code structure of the OGGM ([Maussion et al. 2019](#)). This compatibility is imperative, since the volume/area scaling model is no standalone project and relies on the OGGM for data downloads, preprocessing, post processing, and also the same boundary conditions. The mass balance models and the glacier evolution model are implemented as classes with their respective methods. Functions outside these classes can be characterized either as entity tasks, which are applied on individual glaciers, or as global tasks, which run on a population of glaciers that need to share information between each other (mostly for calibration and validation). The entire code can be found on GitHub <https://github.com/OGGM/oggm-vas> under an open source license, the following section can be seen as documentation.

### 2.2.1 Mass balance models

Following the OGGM, the mass balance models are implemented as classes. The `VAScalingMassBalance` model handles past or future climate data, while the `ConstantVASMassBalance` model and the `RandomVASMassBalance` model simulate a constant climate with and without inter-annual variability, respectively.

#### Volume/area scaling mass balance model

The `VAScalingMassBalance` model is the implementation of the original mass balance model by [Marzeion et al. \(2012\)](#). The model computes the mass balance of a glacier using historic or projected climate data provided by the climate input file. The general concept is fairly similar to the `oggm.core.massbalance.PastMassBalance` model. The main difference is, that the volume/area scaling mass balance model returns only one average value of glacier-wide mass balance, instead of point mass balance values for the different elevation bands.

The mass balance model is initialized for a single glacier, denoted by the OGGM specific glacier directory `gdir`. Per default, the model will use the calibrated mass balance parameters  $\mu^*$  and  $\beta^*$  and read temperature and precipitation records from the preprocessed climate file `climate_historical`. An alternative climate file can be used, by supplying either the filename and/or its suffix via the parameters `filename` and `input_filesuffix`, respectively. It is possible to specify the start year and end year of the climate period (`ys` and `ye`), if not all available data should be used. The parameter `repeat` controls whether the climate period given by `[ys, ye]` should be repeated indefinitely in a circular way.

The volume/area scaling mass balance model inherits the following methods from the `oggm.core.massbalance.MassBalanceModel` super class:

- `get_annual_climate()` and `get_monthly_climate()` compute and return the mass balance relevant climate information, i.e. positive air temperature at the terminus elevation in [°C] and solid precipitation amount in [ $\text{kg m}^{-2}$ ], for the given year and month/year combination, respectively.
- `get_annual_mb()` and `get_monthly_mb()` compute and return the glacier wide average mass balance in [ $\text{m s}^{-1}$ ], for the given year and month/year combination, respectively. A possible mass balance residual  $\beta^*$  is applied.
- `get_specific_mb()` and `get_monthly_specific_mb()` compute and return the glacier-wide average specific mass balance in [ $\text{mmw e /yr}$ ], for the given year and month/year combination, respectively. A possible mass balance residual  $\beta^*$  is applied.

All methods need the glacier terminus elevation `min_hgt` and the maximal glacier surface elevation `max_hgt` as input parameters. The date is supplied via the `year` parameter, using the hydrological float year convention. Given that the scaling mass balance model computes the glacier-wide average mass balance, it is not possible to estimate the equilibrium line altitude. Hence, the method `get_ela()` is not implemented, in contrast to the `PastMassBalance` model.

### Constant climate scenario

The `ConstantVASMassBalance` model simulates a constant climate based on the observations averaged over a 31-year period centered on a given year `y0`. Hence, the specific mass balance does not change from year to year. The task `run_constant_climate(gdir, ...)` initializes a `ConstantMassBalance` for the given glacier `gdir` and runs for a given number of years `nyears`. The task takes an additional temperature bias as parameters `temp_bias`, to alter the observed climate records.

The same idea of a constant climate is used during the mass balance calibration, solving the mass balance equation (Equation 2.10) for the temperature sensitivity  $\mu^*$ . So per definition,  $\mu^*$  is the temperature sensitivity to keep the glacier in equilibrium over the 31-year climate period centered around the *equilibrium year*  $t^*$ , while neglecting a potential mass balance residual  $\beta^*$ . Consequentially, a `ConstantMassBalance` model with  $y0 = t^*$  and  $\beta^* = 0$  keeps the glacier in equilibrium.

## Random climate scenario

Similar to the `ConstantVASMassBalance` model, the `RandomVASMassBalance` model is based on a 31-year period centered on a given year `y0`. However, the mass balance years are randomly shuffled within that period. More precisely, for each simulated year the model computes the specific mass balance using temperature and precipitation records from a randomly selected year within the given period. Hence, the model runs on a synthetic random climate scenario based on actual observations. A seed `seed` for the random generator can be supplied as parameter, to allow for reproducibility. Additionally, it is possible to choose between draws with and without replacement via the `unique_sample` parameter.

The task `run_random_climate(gdir, ...)` works analogously to the task `run_constant_climate(gdir, ...)`, using an instance of `RandomMassBalance` model instead of the `ConstantMassBalance` model. Hence, using the climatological period centered around  $y0 = t^*$ , the model glacier should stay in an equilibrium state while underlying minor fluctuations. Supplying a positive or negative temperature bias will result in a retreating or advancing model glacier, respectively, before reaching a new equilibrium after some years.

### 2.2.2 Glacier evolution model

The `oggm—vas.VAScalingModel` is the implementation of the above describe glacier evolution model (see Section 2.1.3, cf. [Marzeion et al. \(2012\)](#)) into the OGGM framework.

An instance of the `oggm—vas.VAScalingModel` class is initialized with the initial area `area_m2_0`, the initial glacier terminus elevation `min_hgt` and maximum glacier surface elevation `max_hgt` and an instance of a mass balance model. Additionally, the start year of the simulation `year_0` must be defined. Those initial values are stored as instance variables, since they are needed for later computations. Other than that, the `oggm—vas.VAScalingModel` object stores all model parameters as instance variables for the year it is in. This includes glacier geometries ( $V$ ,  $A$ ,  $L$ ,  $z_{\min}$ ,  $z_{\max}$ ) and their changes ( $\Delta V$ ,  $\Delta A$ ,  $\Delta L$ ), time scales ( $\tau_A$ ,  $\tau_L$ ), the mass balance model and the specific mass balance  $B$ , but also constants like the scaling parameters ( $c_A$ ,  $\gamma$ ,  $c_L$ ,  $q$ ) and ice density  $\rho_{\text{ice}}$ .

To advance the glacier model, there are three different methods. The `step()` method advances the model by one year, following the above described steps (see Section 2.1.3). The method `run_until(year_end)` runs the model until the specified year and returns the geometric glacier parameters at the end of the model evolution (year, length, area, volume, terminus elevation and specific mass balance). Thereby, the model starts from whatever year it currently is in. It is possible to start the model

run from `year_0` with the flag `reset`. The method `run_until_and_store()` works analogous to the previous one, with the difference that all parameters are stored for each time step (i.e., for each year). The resulting data set is returned and possibly stored to file, if a file path is give. The method `run_until_equilibrium()` tries to run the glacier model until an equilibrium state is reached. The model runs for a fixed number of iterations `max_ite`, the total elapsed time changes with the chosen time step `ystep`. The iteration breaks, either if the glacier volume is below  $1\text{ m}^3$  or an equilibrium is reached. An equilibrium state is reached, if the volume change rate  $|V(t) - V(t + \Delta t)|/V(t)$  falls below a given value `rate`. Therefore, the method should only be used with a [constant climate scenario](#) (see Section 2.2.1).



# Chapter 3

## Results

This chapter details all performed experiments and presents their results. All experiments run the implemented volume/area scaling model in a variety of setting and compare it to the flowline model. The focus is on the intrinsic model behavior and its comparison to the flowline model, and with the exception of the final projection experiment less on absolute ice volume estimations. The experiments start with a test run performed on six different single glacier (Section 3.1), including time series analysis investigating autocorrelation functions and power spectral density (Section 3.2). The same equilibrium runs are repeated on a regional scale (Section 3.3), before looking into the model’s sensitivities to its scaling parameters (Section 3.4). The final experiment runs projections over the 21st century for Central Europe and High Mountain Asia (Section 3.5).

### 3.1 Single glacier test case

The first qualitative look at the performance of the volume/area scaling model uses the Hintereisferner (RGI60-11.00897) as a test case. This test case is intended to get a feel for the model and set the stage for the following experiments, by comparing two evolution models and the two mass balance models. It has to be noted, that applying volume/area scaling to a single glacier gives only an order of magnitude estimate. The scaling constant  $c$  is a globally averaged value, and the relative error in scaling constant is directly proportional to the error in estimated ice volume (Bahr et al. 2015). However, a qualitative comparison between the volume/area scaling model and the flowline model is more practicable and meaningful for a single glacier. The model’s sensitivity to its scaling parameters is investigated in Section 3.4. Additionally, the same experiment is repeated for five more glaciers with similar results shown in Appendix A.

### Take Home Message: Single glacier test case

- Both evolution models produce the same qualitative results, advancing under colder climates and shrinking under warmer climates. The temporal correlation between both models under a random climate is satisfying.
- The volume/area scaling model estimates much smaller changes in glacier geometry compared to the flowline model (up to four times). For example, the relative volume changes for the run with positive mass balance bias amount to +17% for the volume/area scaling model and +71% for the flowline model.
- The volume/area scaling does not account for the mass-balance-elevation feedback and therefore produces highly symmetrical results between the positive and negative step change in air temperature. This symmetry can also be seen in the e-folding response times.
- The e-folding response times are much shorter for the volume/area scaling model. For example, the volume response times for the run with positive mass balance bias amount to 39 yr for the volume/area scaling model and 139 yr for the flowline model.
- The volume/area scaling model does not show an asymptotic adjustment but behaves more like a damped harmonic oscillator, whereby the model-internal time scale acts as damping factor.

#### 3.1.1 Experimental setup

For this first experiment, both evolution models run with the `ConstantMassBalance` model and the `RandomMassBalance` model, for 1000 years each. Both mass balance models emulate an equilibrium climate to keep the glacier in its initial equilibrium state. Therefore, the mass balance models must be initialized with the climatic period centered around the equilibrium year, i.e.,  $y_0 = t^*$ . As explained above, the mass balance calibration depends among other parameters on  $t^*$  (Section 2.1.2, see [Calibration of the mass balance parameters](#)). Hence, to run both evolution models with the identical climatic forcing,  $t^*$  must be equal for both. This is done by using the same  $t^*$  reference table (`oggm_ref_tstars_rgi6_histalp.csv`, corresponding to the flowline model) to compute the temperature sensitivity  $\mu^*$  for both models. Additionally, the mass balance residual must be omitted during the model run ( $\beta^* = 0$ , as by the definition of  $\mu^*$ , see Section 2.1.2). Each mass balance model runs three

different climate scenarios defined by respective the temperature bias of  $0\text{ }^{\circ}\text{C}$ ,  $-0.5\text{ }^{\circ}\text{C}$  and  $+0.5\text{ }^{\circ}\text{C}$ . This results in a equilibrium run, a run with positive mass balance perturbation and a run with negative mass balance perturbation, respectively.

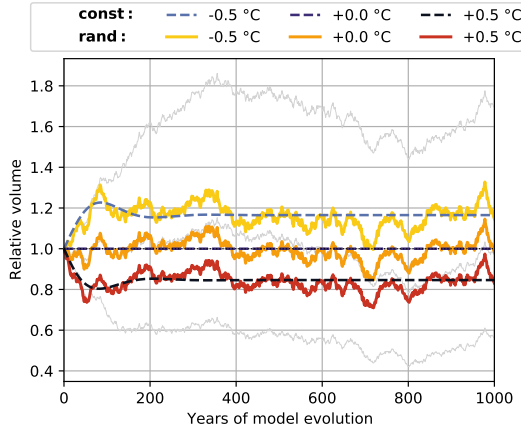
### 3.1.2 Results

Figure 3.1 shows the temporal evolution of relative ice volume, surface area and glacier length for Hintereisferner, comparing both mass balance models (solid vs. dashed lines) and both evolution models (left vs. right panels). The volume/area scaling model behaves as expected and produces the same qualitative results as the flowline model. The model glacier stays in an approximate equilibrium using the climate around  $t^*$ , and decreases and increases in size for a positive and negative temperature bias of  $\pm 0.5\text{ }^{\circ}\text{C}$ , respectively. However, the volume/area scaling model shows much lower changes in geometry compared to the flowline model. This is true for both the constant and random climate scenario, whereby the **RandomMassBalance** model, with its year-to-year variations, produces more short term variability.

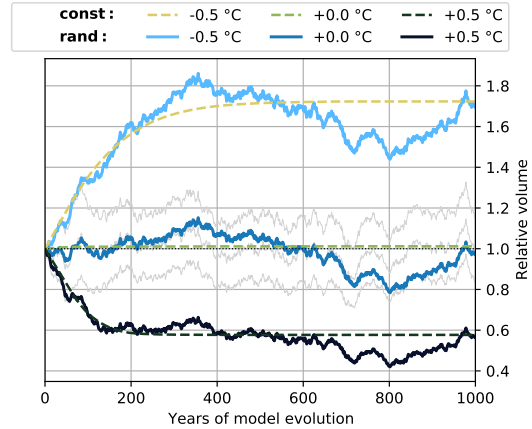
The modeled glacier advances and retreats forced by the random climate scenarios show a weak but highly significant correlation between the two evolution models (with correlation coefficients  $0.34 \leq r \leq 0.58$  and p-values of  $p \ll 0.01$ ). Given that the implementations of the mass balance models are almost identical between the volume/area scaling model and the flowline model, this is the first indication that the differences must arise from the geometry models. For both models, the ice volume exhibits the highest year-to-year variability, since volume changes happen instantaneously, i.e., over a single time step. The changes in surface area and glacier length are smoother, accounting for the glacier's response time. However, the flowline model shows generally less short term variabilities but stronger long term variabilities than the volume/area scaling model, indicating longer response times. This assumption is backed by the model behavior under the constant climate scenarios. Qualitatively speaking, the flowline model takes longer to reach a new equilibrium (about 400 years) than the volume/area scaling model (about 200 years). A quantitative analysis of the response times follows after the evaluation of the equilibrium values.

For the following discussion about the new equilibrium values, only the constant climate scenarios are considered (if not stated otherwise). It is assumed that the model glacier has reached a new equilibrium 1000 years after the climate perturbation. Hence, the equilibrium values are taken as the final values at year  $t = 1000$ . This assumption seems valid, given that the fluctuation of volume, area and length

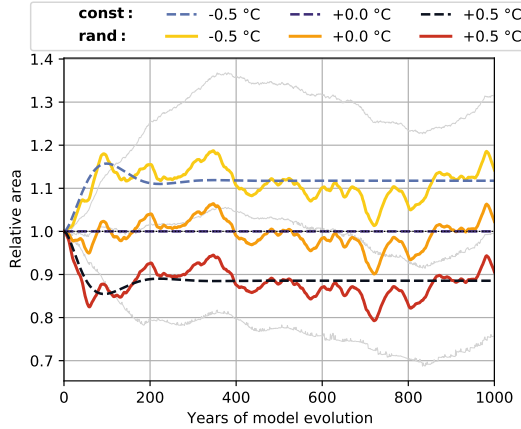
(a) Volume/area scaling model, relative ice volume



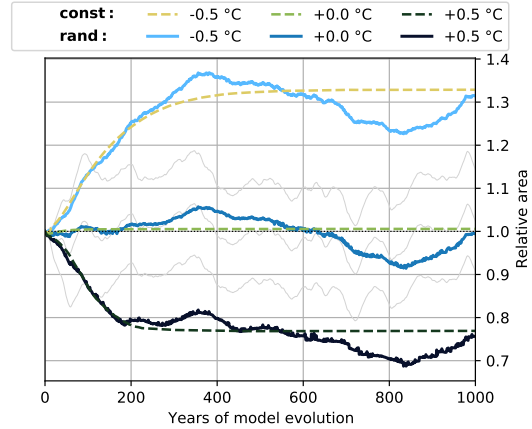
(b) Flowline model, relative ice volume



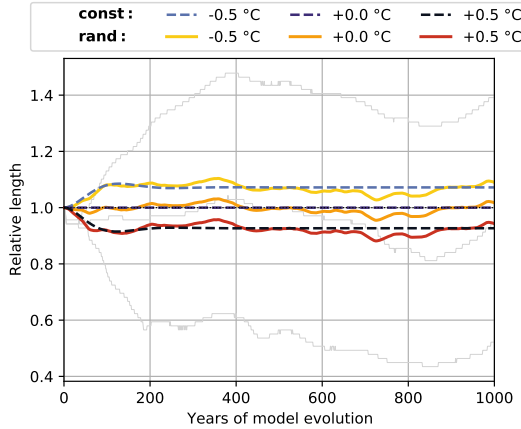
(c) Volume/area scaling model, relative surface area



(d) Flowline model, relative surface area



(e) Volume/area scaling model, relative glacier length



(f) Flowline model, relative glacier length

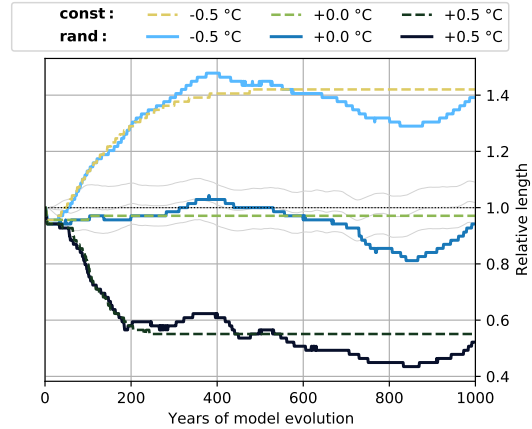


**Figure 3.1:** Temporal evolution of ice volume in (a) and (b), surface area in (c) and (d) and glacier length in (e) and (f) for Hintereisferner (RGI60-11.00897). The shown values are normalized with their respective initial values. The left panels show the result of the volume/area scaling model, the right panels show the results of the flowline model. Solid lines represent the random climate scenarios, while dashed lines represent the constant climate scenarios. All climate scenarios are based on an equilibrium climate. The applied temperature biases of  $-0.5^{\circ}\text{C}$ ,  $0^{\circ}\text{C}$  and  $+0.5^{\circ}\text{C}$  are color coded, see legend for details. The dotted line indicates the initial volume. The light gray lines represent the volume evolutions of the other model, to facilitate comparisons.

**Table 3.1:** Hintereisferner (RGI60-11.00897) equilibrium values after 1000 years of model evolution in response to a step change in climate of  $\Delta T = \pm 0.5^\circ\text{C}$  relative to the average climate between 1912 and 1942. Percentage values in parenthesis indicate normalized changes in respective to their initial values.

	Length [km]	Area [km <sup>2</sup> ]	Volume [km <sup>3</sup> ]
<b>Initial values</b>			
V/A scaling	4.89	8.04	0.60
Flowline	6.90	8.04	0.80
<b><math>\Delta T = -0.5^\circ\text{C}</math></b>			
V/A scaling	5.25 (+7 %)	8.98 (+12 %)	0.70 (+17 %)
Flowline	9.80 (+42 %)	10.64 (+33 %)	1.38 (+72 %)
<b><math>\Delta T = +0.5^\circ\text{C}</math></b>			
V/A scaling	4.54 (-7 %)	7.12 (-11 %)	0.50 (-15 %)
Flowline	3.80 (-45 %)	6.16 (-23 %)	0.46 (-42 %)

are in the order of only 0.01%<sup>1</sup> over the last 200 years of the simulations. Table 3.1 shows all new equilibrium values in response to the positive and negative step changes in climate. Percentage values refer to the normalized glacier geometries to their respective initial values, which facilitates the comparison.

The most apparent result is that the estimated changes in glacier geometry by the volume/area scaling are much lower when compared to the flowline model. While the volume/area scaling model estimates a volume change of +17% and -15%, the flowline estimates +72% and -42%, for the negative and positive temperature perturbation, respectively. In other words, the flowline model glacier grows more than four times larger and shrinks more than two and a half times smaller than the volume/area scaling model glacier. However, the flowline model in its “out-of-the-box” condition, i.e., without dedicated calibration of the ice creep parameter  $A$ , tends to overestimate ice volumes (cf. Maussion et al. 2019; Farinotti et al. 2019). A more detailed discussion on this topic is provided in Section 4.1. Interestingly enough, the yearly ice volume changes (i.e., specific mass balance times surface area) under any random climate scenario are again remarkably similar between both models. Looking at all climate scenarios the volume/area scaling estimates yearly absolute

<sup>1</sup>The fluctuations are computed as the relative difference between minimum and maximum value during that period. The relative difference between two values  $a$  and  $b$  refers to their absolute difference relative to the average between them  $\left| \frac{a-b}{(a+b)/2} \right|$ .

changes of  $(4.9 \pm 3.7) \cdot 10^6 \text{ km}^3$  (average  $\pm$  standard deviation) and the flowline model  $(5.0 \pm 3.5) \cdot 10^6 \text{ km}^3$ . Since both mass balance models are almost identical this was to be expected. Additionally, these values are also comparable to the observations presents in [Klug et al. \(2018\)](#). Using the RGI area of 2003 ( $8.04 \text{ km}^2$ ), the average specific mass balance of  $1.2 \text{ m we. yr}^{-1}$  between 2001/2002 and 2010/2011 can be converted into an average yearly volume change of  $9.6 \cdot 10^6 \text{ km}^3$ .

The changes in surface area are slightly closer between both models, with values of +12% and -11% for the volume/area scaling model and +33% and -23% for the flowline model. The glacier length of the volume/area scaling model does hardly change at all. The year-to-year changes of glacier length estimated by the volume/area scaling model range between -11 m and +8 m, corresponding to a maximal change of 2% of the initial values. This amounts to a total length change of  $\pm 7\%$  for the volume/area scaling model over the entire simulation period, which is roughly five to six times less than the changes of +44% and -39% for the flowline model. The continuous length records for Hintereisferner from 1939 to 2003 ([Leclercq et al. 2014](#)) show an average yearly absolute length change of  $26 \pm 21 \text{ m}$  (mean  $\pm$  standard deviation) and a maximum of over 100 m. This amounts to an maximum observed yearly length changes of 1.6% in relation to the glacier length of 6.9 km in 2003. It seems that the values of relative length change of the volume/area scaling are comparable to observations, the absolute values, however, are far too low. The model length must therefore be seen as model parameter rather then physical glacier length, which is an indication that the volume/area scaling model cannot resolve all the same processes as a dedicated ice physics models can.

The changes in glacier geometries produced by the volume/area scaling model are highly symmetrical. Absolute changes of ice volume, surface area and glacier length differ by a maximum of 7%, 3%, and 2%, respectively, between the run with positive and negative mass balance perturbation<sup>2</sup>. Again, this cannot be explained by the mass balance models. The climate scenarios used for this experiment are all based on an equilibrium climate. If the input climate is not altered by a temperature bias, the model glacier will stay in its equilibrium state under the constant climate scenario. Under a random climate scenario the model glacier will show some year-to-year variability, but still fluctuation around the same equilibrium values. This specific equilibrium mass balance can be approximated as a linear function of temperature bias (with  $r^2 > 99.9\%$ ), for small enough temperature biases between  $-1^\circ\text{C}$  and  $+1^\circ\text{C}$ . Thereby, the slopes of the linear functions and consequentially the initial specific mass balance are almost identical between the volume/area scaling and flowline model:  $+309 \text{ mm we. yr}^{-1}$  and  $-320 \text{ mm we. yr}^{-1}$  for the volume/area scaling model and  $+307 \text{ mm we. yr}^{-1}$  and  $-323 \text{ mm we. yr}^{-1}$  for the flowline model.

---

<sup>2</sup>The percentages correspond to the relative difference, as explained above

The initial mass balance values are quite symmetrical for both evolution models and can, therefore, not be the cause of the volume/area scaling model's symmetric equilibrium results.

However, since this study looks for benefits of a dedicated ice physics model rather than flaws of the volume/area scaling model, the question should be “What allows the flowline model to produce asymmetric results?”. And the answer is the mass-balance-elevation feedback. The flowline model continuously adjusts the surface elevation of each grid cell and passes the elevation information onto the mass balance model<sup>3</sup>. Suppressing the mass-balance-elevation feedback for the flowline model run results in a volume change of +38 % and -34 %. These results are symmetric and lower than with mass-balance-elevation feedback in place. The relative changes in ice volume are reduced to about twice the values produced by the volume/area scaling model. It has been shown, that the responses of the volume/area scaling model and the flowline model to a step change in climate are qualitatively similar but do not compare quantitatively. While the absolute equilibrium values are still in the same order of magnitude, they differ substantially. But what about the time domain? The following paragraphs look at temporal characteristics of the glacier model's response.

The implementation of the volume/area scaling model includes the corresponding response time scaling to estimate temporal changes (see Section 2.2.2). For a proper response time scaling, the length response time scale  $\tau_L$  and the area response time scale  $\tau_A$  must be estimated. The length response time scale can be estimated as ratio between ice volume and mass turnover (Jóhannesson et al. 1989), the area response time scale then follows from geometric considerations. The model-internal time scales computed for the Hintereisferner under a constant equilibrium climate amount to  $\tau_L \approx 38$  yr and  $\tau_L \approx 12.5$  yr. Those values are rather low compared to other findings of  $\tau_L \approx 100$  yr (Greuell 1992; Schuster 2020). However, it is possible that the used time scales are merely model parameters and do not correspond to the typically used e-folding time scales.

Processes evolving exponentially to an equilibrium can be characterized by their e-folding response time. The assumption that a glacier's geometry changes exponentially is valid for small enough perturbations in climate. The e-folding response time is computed as the time after which the initial difference between a glacier's geometric property (such as ice volume, surface area or glacier length) and its new equilibrium value has decreased by a factor of  $1 - e^{-1} \approx 63\%$ . For comparability, e-folding time scales are computed for both evolution models and all geometric properties. The values can be found in Table 3.2. As was to be expected, volume

---

<sup>3</sup>Implementation note: the mass balance feedback can be adjusted via the `mb_elev_feedback` parameter of the `FlowlineModel` class

response times  $\tau_V$  are smallest, followed by  $\tau_A$  and  $\tau_L$ . As already qualitatively estimated above, the volume/area scaling model adjust between two times and six times faster to the temperature perturbation of  $\pm 0.5^\circ\text{C}$  than the flowline model. This is especially visible for the growing glacier, where the flowline model takes almost 120 yr longer to reach a new equilibrium than the volume/area scaling model does ( $\tau_{V,\text{fl}} = 142$  yr vs.  $\tau_{V,\text{vas}} = 24$  yr).

**Table 3.2:** e-folding time scales for Hintereisferner (RGI60-11.00897) in response to a step change in climate of  $\Delta T = \pm 0.5^\circ\text{C}$  relative to the average climate between 1912 and 1942. Time scales are computed for changes in ice volume, surface area and glacier length, denoted as  $\tau_V$ ,  $\tau_A$  and  $\tau_L$ , respectively.

	$\tau_L$ [yr]	$\tau_A$ [yr]	$\tau_V$ [yr]
<b><math>\Delta T = -0.5^\circ\text{C}</math></b>			
V/A scaling	55	36	24
Flowline	184	160	142
<b><math>\Delta T = +0.5^\circ\text{C}</math></b>			
V/A scaling	52	33	22
Flowline	118	111	80

The results of the volume/area scaling model are again very symmetric between the positive and negative temperature perturbation. The volume/area scaling e-folding time scales range within 9 % of each other, while the flowline response time scales vary up to 55 %<sup>4</sup>. Suppressing the mass-balance-elevation feedback for the flowline model results in similarly symmetric result. It has to be noted, that the length e-folding response time for the volume/area scaling model  $\tau_{L,\text{vas}} \approx 55$  yr is over twenty years ( $\approx 30$  %) longer than the model-internal time scale. However, the volume/area scaling model does not show an asymptotic or exponential adjustment. The adjustment of glacier geometries looks like the signal of an underdamped oscillator, with a strongly discernible overshoot. The damping factor seems to be controlled by the model-internal time scale, which could allow for an additional tuning parameter. A closer look at this oscillatory behavior is provided in Section 3.4.2

While Hintereisferner is not representative for all Alpine glaciers, the same experiment performed on other single glaciers yields similar results (see Appendix A). For some glaciers (e.g., Mer de Glace, Glacier d'Argentière) the change in relative ice volume is comparable between the two evolution models. This must, however,

---

<sup>4</sup>The percentages correspond to the relative difference, as explained above.

be interpreted with great care. One one hand, this may be a mathematical artifact, since the initial ice volume estimated by the scaling relation is much smaller than the one from the numerical ice thickness inversion. On the other hand, the numerical thickness inversion is not calibrated and may therefore also be wrong. Unlike ice volume and glacier length, the initial surface area is equivalent for both models. This generally results in better agreement of estimated final equilibrium areas, even though the glacier areas simulated by the volume/area scaling model show far more and stronger fluctuations under random climates.

Anyway, all of those observations are not robust, since scaling relations are developed to work best on a global or at least a regional scale. The scaling constant  $c$  is a random variable which can vary drastically from glacier to glacier. It is possible that the global mean value of  $c = 0.034 \text{ km}^{3 - 2\gamma}$  is a bad fit for the characteristics of Hintereisferner (or any other single glacier). A detailed look at the model's sensitivity to the scaling constant is provided in Section 3.4.3.

## 3.2 Autocorrelation function and Power spectral density

The time series analysis presented in this section is inspired by Roe and Baker (2014). This is done by investigating the length signals of different glaciers, modeled as response to different constant climate scenarios with random year-to-year variabilities (Figure 3.2). The power spectral density (PSD, Figure 3.3), the autocorrelation function (ACF, Figure 3.4) and the partial autocorrelation function (PACF, Figure 3.5) give insight into the periodicity and dominant frequencies of a given signal.

### 3.2.1 Theoretical background

The correlation coefficient is a measure for the linear dependency between two (random) variables. A positive correlation coefficient close to +1 indicates a strong direct relationship between the two variables, a negative correlation coefficient close to -1 indicates a strong indirect relationship, while a correlation coefficient around zero indicates that the variables are independent. The autocorrelation function (ACF) computes the correlation coefficient between a signal and a lagged copy of itself, as a function of lag time  $k$ . The lagged copy of a signal simply refers to the signal shifted by the lag time  $k$ . The intuition behind the ACF is the relation between past and present values of a signal. It is used find possible periodicities hidden in noisy signals and gives an estimate on how strong neighboring data points influence each other. A high autocorrelation at lag time  $k$  indicates that data points at time  $t$

and  $t+k$  have similar values. The ACF at lag time  $k = 0$  is obviously one, since any signal correlates to 100 % with itself. The partial autocorrelation function (PACF) measures only the direct influence of values with lag time  $k$ , eliminating the effects of all shorter lag times ([Box et al. 2015](#)).

A simple model to describe a stationary random time series is an autoregressive-moving-average (ARMA) model. It predicts future values of a random variable, based on a linear combination of past values and past error terms of said variable. The number of included lag terms is defined by the order  $p$  of the autoregressive term and the order  $q$  of the moving-average term. The number of statistically significant non-zero terms of the ACF and PACF can be used to estimate the order of an ARMA( $p,q$ ) model, respectively ([Box et al. 2015](#)). The linear three stage model by [Roe and Baker \(2014\)](#) is an ARMA(3,3) model. While the goal of this work is not to define an ARMA glacier model, a brief analysis is provided in an attempt to quantify the autocorrelation.

The power spectral density (PSD) is the Fourier transform of the ACF. A Fourier transformation decomposes a signal into a spectrum of frequencies, or much rather into a collection of frequency bins for the discrete Fourier transformation (DFT) used hereafter. Hence, the PSD is as function of frequency. The signal's power describes its energy per unit time. Thereby, the power is of unit [X<sup>2</sup>] if the signal's unit is [X], and must not be actual physical power of unit [W]. The power density is the power normalized with the frequency bin width, hence the power density has the unit [X<sup>2</sup>/Hz] if the frequency is measured in [Hz]. The PSD is used to find dominant frequencies in noisy signals.

### 3.2.2 Experimental setup

The ACF, PACF and PSD are computed for the glacier length signal, in analogy to ([Roe and Baker 2014](#)). The behavior of the volume/area scaling model is compared to the flowline model for the following six Alpine glaciers:

- Hintereisferner (RGI60-11.00897), Ötztal Alps, Austria
- Pasterze (RGI60-11.00106), Hohe Tauern, Austria
- Mer de Glace (RGI60-11.03643), Mont Blanc massif, France
- Glacier d'Argentière (RGI60-11.03638), Mont Blanc massif, France
- Großer Aletschgletscher (RGI60-11.01450), Bernese Alps, Switzerland
- Rhonegletscher (RGI60-11.01238), Urner Alps, Switzerland

These glaciers are arbitrarily selected because of their size and notoriety. All glaciers are subjected to different white noise climate conditions for 23 000 years. The remaining settings are analogous to the single glacier test case. The `RandomMassBalance` model is initialized around the respective equilibrium year for each glacier ( $y_0 = t^*$ ), whereby both evolution model use the same  $t^*$  reference table (as before). The mass balance residual is omitted ( $\beta^* = 0$ ). The input climate shows no autocorrelation and a constant PSD curve, and can therefore be classified as white noise with non-zero mean. To increase the amount of available data, each glacier is again subjected to three different climate scenarios, specified by a temperature bias of  $-0.5^\circ\text{C}$ ,  $0^\circ\text{C}$  and  $+0.5^\circ\text{C}$ . The initial 3000 years during which the glaciers adjust to the changed climate are clipped, which leaves three different sizes of the same glacier, each in equilibrium.

An ARMA model can only be applied to stationary time series. Stationarity is given if the mean and the variance are time independent and the signal shows no seasonality (for a formal definition see, e.g., [Box et al. \(2015\)](#)). The stationarity of the glacier length signals could easily be determined manually. However, the formally more correct Augmented Dickey–Fuller test (`statsmodels.tsa.stattools.adfuller`, [Cheung and Lai \(1995\)](#)) is used to test for stationary. It results in  $p$ -values far below 1 % for all signals. Hence, all signals can be considered as stationary.

The ACF is computed using the python function `statsmodels.tsa.stattools.acf` via a fast Fourier transform. The PSD is estimated using Welch's method. Welch's method reduces the variance in estimated power density. This is done by time-averaging at the cost of frequency resolution (e.g., [Welch 1967](#); [Proakis and Manolakis 2007](#)). The remaining 20 000 data points (starting from year 3000) are divided into nineteen time windows with a window size of 2000 and a 50 % overlap. The windows are tapered using the Hann function. For details about additional parameters see the default values of the python function `scipy.signal.welch`, which is used for the PSD computation.

### Length anomalies under random climate

Figure 3.2 shows the length anomalies with respect to the equilibrium value for the arbitrarily chosen period between 8000 and 12 000 years. This allows to formulate some first qualitative conclusions. The overlaid length changes seem to be in good agreement between the volume/area scaling and the flowline model. While correlations may be high, the difference in absolute length fluctuations is already apparent by looking at the y-scales (left for the flowline model and right for the volume/area scaling model). While the length changes estimated by the volume/area scaling model are all in the order of  $\pm 200\text{ m}$  (except  $\pm 500\text{ m}$  for the Pasterze, see

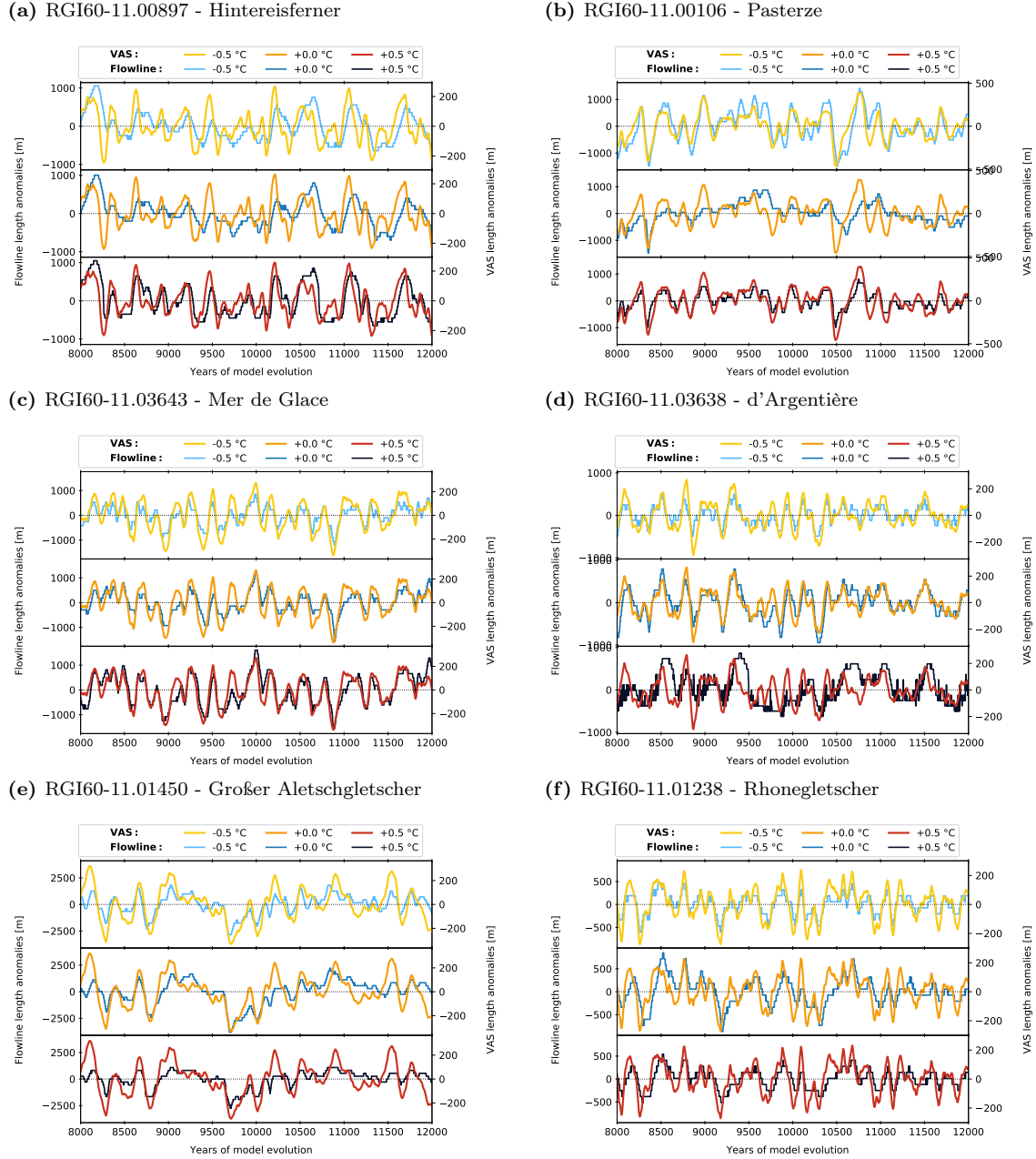


**Figure 3.2:** Length anomalies from to the respective average (equilibrium) value. The climate scenarios are based on a randomized equilibrium climate, with different temperature biases. Light blue, dark blue and ultramarine lines represent the flowline model, while yellow, orange and red lines represent the volume/area scaling model, with a temperature bias of  $-0.5^{\circ}\text{C}$ ,  $0^{\circ}\text{C}$  and  $+0.5^{\circ}\text{C}$ , respectively. Note the differences in y-axis scales.

Figure 3.2b), the flowline model predicts fluctuations between  $\pm 500$  m for the Rhonegletscher (Figure 3.2f) and  $\pm 2500$  m for the Aletschgletscher (Figure 3.2e). Furthermore, different sizes of the same glacier show similar but noticeable different length fluctuation under the flowline model, while there seems to be little to no differences under the volume/area scaling model. However, these first findings are only based on the visual inspection of a temporally limited subsample and are further investigated and quantified in the following sections.

### 3.2.3 Power spectral density

Glaciers act as low-pass filters for the natural climate variability. A low pass filter passes lower frequencies while attenuating higher frequencies, which results in a characteristic PSD curve. Figure 3.3 shows the PSD of glacier lengths for the six glaciers mentioned above. The power density stays in a constant range for frequencies up to  $3 \cdot 10^{-3} \text{ yr}^{-1}$  (corresponding to signals with a period of over 300 years) before decreasing with increasing frequency. This makes intuitive sense, since changes in glacier length are mainly driven by long term climatic trends and less by inter-annual variabilities in the climatic forcing. A single year with low temperatures and strong (cold season) precipitation has less impact on the glacier size than a decade of slightly above-average temperatures. While the overall shape of the PSDs are similar for the volume/area scaling model and the flowline model, there are some key differences. As seen before, the length changes estimated by the volume/area scaling model are smaller compared to the flowline model. Hence, the overall power of the flowline model is higher across all frequencies. In agreement with the symmetric behavior discussed before, the PSDs of the volume/area scaling model are practically identical for different sizes of the same glacier. The PSDs based on the flowline length are less coherent between different sizes of the same glacier, whereby there is no discernible relation between shape of PSD and glacier size. Additionally, the flowline model shows a rather constant power density for lower frequencies. This is due to the discrete changes in glacier length of the flowline model, whose resolution depends on the grid size (100 m in this case). The volume/area scaling model length is a continuous variable, resulting in a constantly decreasing power density. While the absolute values are different, the slope of the PSDs are almost identical between volume/area scaling and flowline model for medium frequencies up to about  $3 \cdot 10^{-2} \text{ yr}^{-1}$  (corresponding to signals with a period of over 30 years). This indicates that the breakdown of energy from larger to smaller scales happens at similar rates for both models (cf. the energy cascade for turbulent flows, e.g., Wyngaard (2010)).

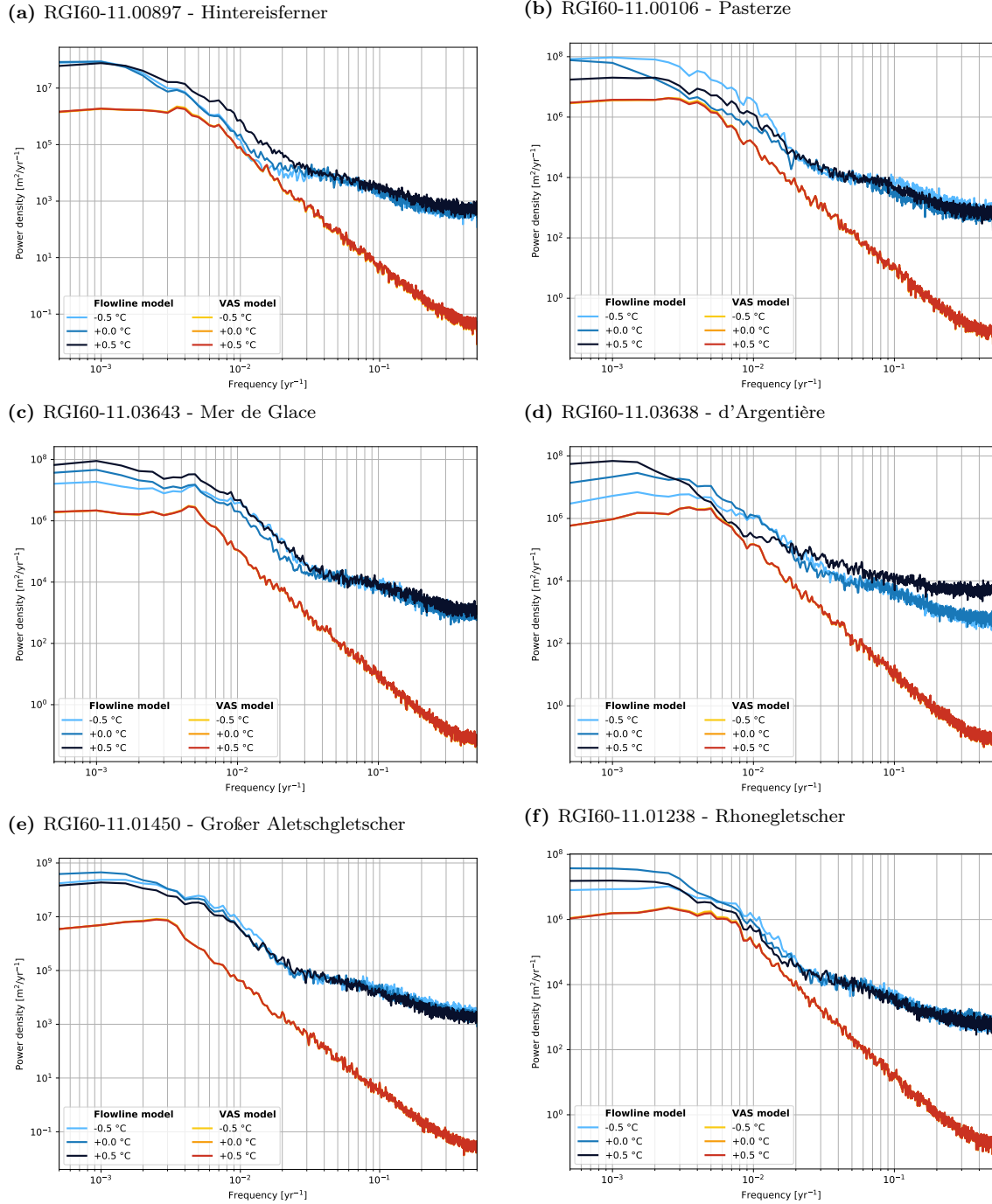


**Figure 3.3:** Power spectral density of modeled glacier length for different alpine glaciers. Different lines represent different combinations of evolution models and climate scenarios. The climate scenarios are based on a randomized equilibrium climate, with different temperature biases. Light blue, dark blue and ultramarine lines represent the flowline model, while yellow, orange and red lines represent the volume/area scaling model, with a temperature bias of  $-0.5^{\circ}\text{C}$ ,  $0^{\circ}\text{C}$  and  $+0.5^{\circ}\text{C}$ , respectively. Note the differences in y-axis scales.

### 3.2.4 Autocorrelation function

Figure 3.4 shows the autocorrelation function (ACF) of modeled glacier length for lag times up to 200 years. A general observation about the ACF can be made for both models, all glaciers and climate scenarios: the correlation is high for the first few lag times, before it decreases exponentially. This points at an autoregressive (AR) term and a moving-average (MA) term in the data. An autoregressive-moving-average model (ARMA) predicts future values of a random variable based on a linear combination of the past values and past error terms of said variable. This makes intuitive sense for glaciers, since the past and current glacier size and the difference to the equilibrium value have a direct influence on next years glacier size. A more detailed discussion of a potential ARMA model is provided at the end of this section.

Same as for the PSDs, the ACFs for the volume/area scaling length signals are almost identical between different sizes of the same glacier, indicating that the glacier size has little to no effect on the transient behavior of the model. The volume/area scaling model represents the glacier as a simple cuboid without any additional information about the glacier shape. The absolute dimensions of that cuboid seem to have less of an effect on the ACF than other parameters, which differ from glacier to glacier. Some glaciers, like the Glacier d'Argentière and the Aletschgletscher show statistically significant negative correlations for higher lag terms between 80 and 250 years, while the others show very little to no significant negative correlation for higher lag times. However, no apparent relation between the strength of negative correlations for later lag times and any other glacier parameter, like the average slope or the model-internal lag times, was found. The average slope is the only additional geometric information of the volume/area scaling model, even if it is implemented only indirectly. It is computed as the relation between elevation range (extracted from the DEM) and glacier length (scaled from the RGI area), and thereby somewhat independent of the other scaled glacier geometries. However, it affects the temporal evolution, since changes in terminus elevation—and thereby changes in specific mass balance—are linearly related to changes in glacier length. This can be seen in the ACF plots, which vary from glacier to glacier but not between different sizes of the same glacier. However, there is no obvious pattern when comparing the ACF to the average slope.

The flowline model is able to represent different glacier geometries and grasp individual responses under different equilibrium climates, which can be seen in the vastly different ACFs. They differ from glacier to glacier, but also for different sizes of the same glacier. However, there are again no discernible patterns, which confirms the notion that the flowline model is capable of simulating each glacier's individual response. The autocorrelation of the flowline model is generally stronger than for

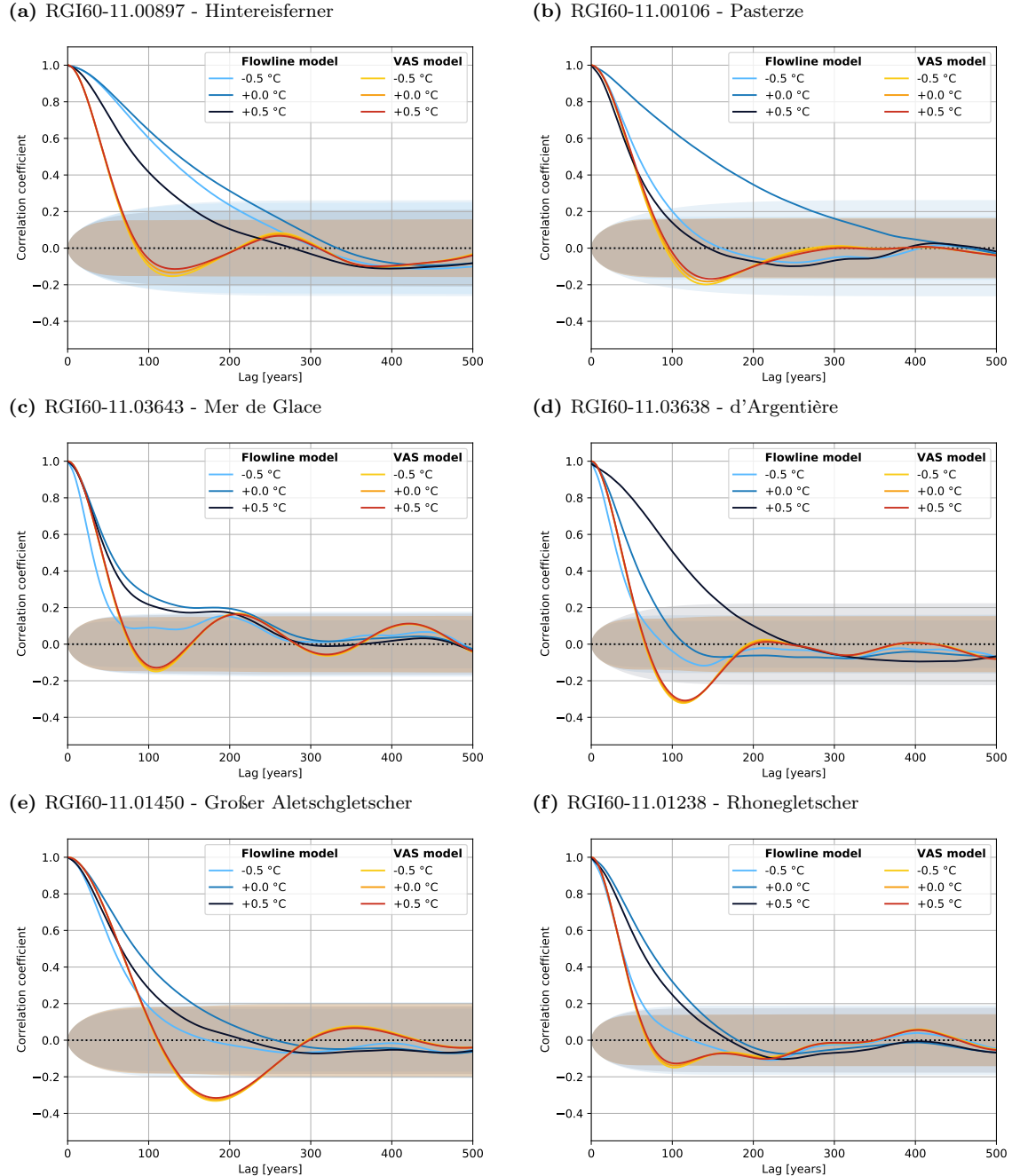


**Figure 3.4:** Autocorrelation function of modeled length for lag times between zero and 200 years. Different lines represent different combinations of evolution model and climate scenario. The random climate scenario is based on an equilibrium climate, with different temperature biases. Light blue, dark blue and ultramarine represent the flowline model, while yellow, orange and red lines represent the volume/area scaling model, with a temperature bias of  $-0.5^{\circ}\text{C}$ ,  $0^{\circ}\text{C}$  and  $+0.5^{\circ}\text{C}$ , respectively. The 99 % confidence intervals are shaded in the corresponding colors.

the volume/area scaling runs for most glaciers and most temperature biases, even though not for all. The following list points to some particular observations:

- for Hintereisferner (Figure 3.4a) the ACFs of the flowline model show higher correlations than for the volume/area scaling model, while for Mer de Glace (Figure 3.4c) and Großer Aletschgletscher (Figure 3.4e) the flowline model ACFs show equal or lower correlations for lag time up to around fifty years;
- the flowline model of the Pasterze (Figure 3.4b) shows a strong autocorrelation under the equilibrium climate, i.e., for its medium size, ( $r > 0.6$  for lags times up to one-hundred years and statistically significant up until a lag time of 243 years), while under a warmer and colder equilibrium climate ( $\pm 0.5^\circ\text{C}$ ) the autocorrelation of all lag times is comparable to the volume/area scaling model;
- similarly, the flowline model of the Glacier d'Argentière (Figure 3.4d) shows a strong autocorrelation under the warmer equilibrium climate ( $+0.5^\circ\text{C}$ ), while the autocorrelation under the other two climate scenarios is even lower than the ACF of the volume/area scaling model.

The only observation made for all glaciers, it that the volume/area scaling model shows a stronger or equal autocorrelation for shorter lag time (i.e., less than about twenty years) than the flowline model. This is true even for glaciers, where the autocorrelation of the flowline mode is generally stronger than for the volume/area scaling model (e.g., Hintereisferner).

Figure 3.5 shows the partial autocorrelation function (PACF) of modeled glacier length for lag times up to twenty years. The PACF measures only the direct influences from one point in time to the following, eliminating the effects of all shorter lag times. This is an important additional measure, since strong correlations for short lag times influences the correlation of all following lag terms. Consider, for example, an exponentially decaying signal, which halves its value with each time step  $\Phi(t) = 0.5\Phi(t - 1)$ , will have an autocorrelation of 0.5 for lag 1, 0.25 for lag 2, 0.125 for lag 3, and so on. Depending on the sample size these values will be statistically significant. However, in this example only the previous value  $\Phi(t - 1)$  has a direct effect on the current one  $\Phi(t)$ , since only one lag term is included in the definition of the signal. The PACF will only show a significant correlation at lag one, i.e., defining an AR(1) process.

All the PACFs of the volume/area scaling model lengths (left panels of Figure 3.5) show a strong positive correlation for lag times of 1 year, followed by a strong negative correlation which then slowly increases towards zero. Correlations for lag times ten and greater are not, or only marginally, significant. Again, there are

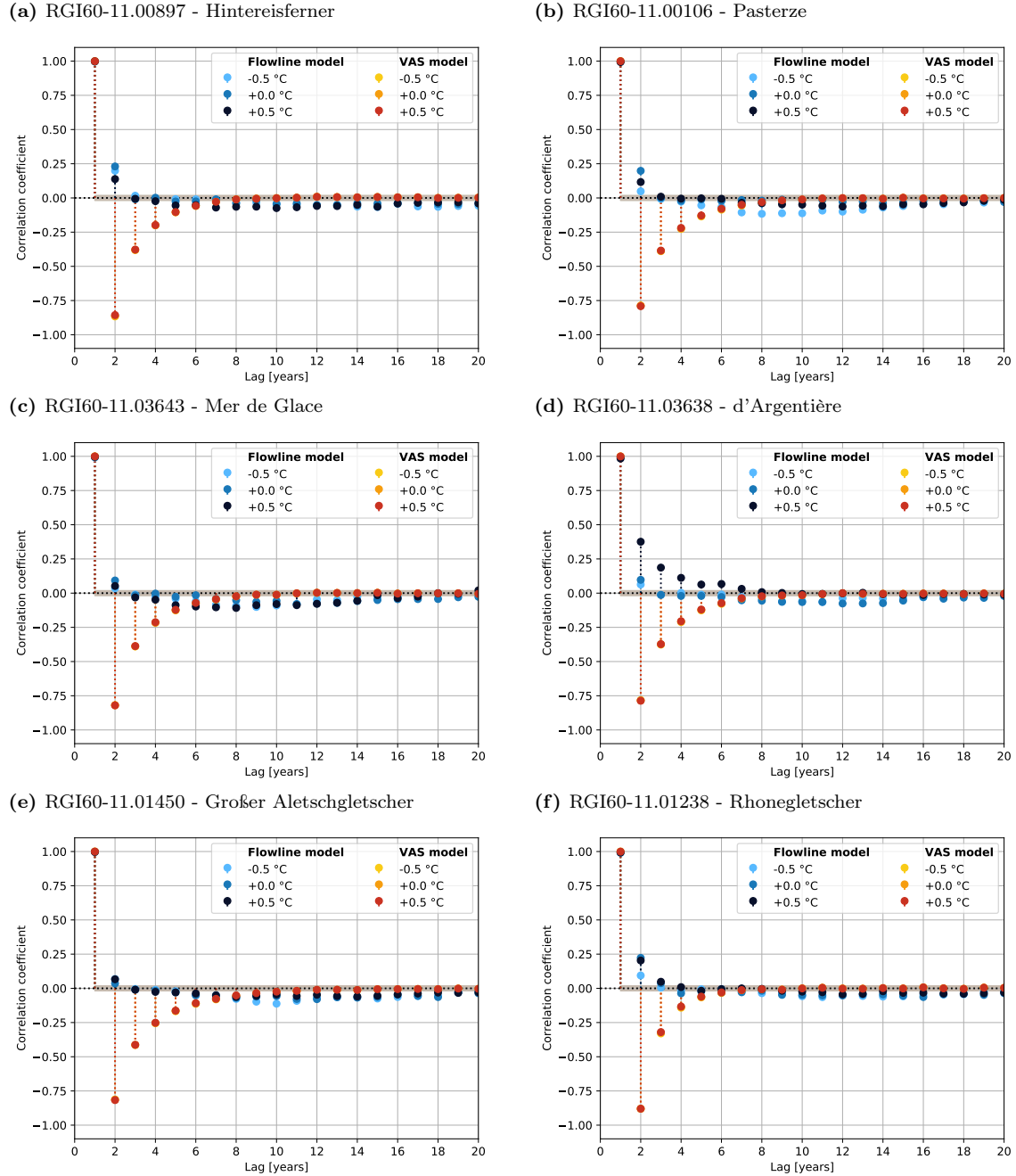


**Figure 3.5:** Partial autocorrelation function of modeled length for lag times between zero and 200 years. Different lines represent different combinations of evolution model and climate scenario. The random climate scenario is based on an equilibrium climate, with different temperature biases. Light blue, dark blue and ultramarine dots represent the flowline model, while yellow, orange and red dots represent the volume/area scaling model, with a temperature bias of  $-0.5^{\circ}\text{C}$ ,  $0^{\circ}\text{C}$  and  $+0.5^{\circ}\text{C}$ , respectively. The 99 % confidence intervals are shaded in the corresponding colors.

no discernible differences between different sizes of the same glacier and very little differences from one glacier to another. The PACFs for the flowline model lengths show the same high correlation for the lag time of one year, before decreasing towards zero. The decrease towards statistical insignificant correlations happens quite fast for most glaciers. Only Mer de Glace (Figure 3.5c) and Glacier d'Argentière (Figure 3.5d), both for the warmer climate, and Rhonegletscher (Figure 3.5f), for the equilibrium climate, show significant correlations for lag times greater than three years. For higher lag times between ten and twenty years there are some negative correlations, even though they are only marginally significant. This indicates that the length of the previous year has a strong direct influence on the current length (almost 1:1), while length of two or more years back has only a weak direct (for the flowline model) or even an inverse influence (for the volume/area scalingmodel). Those results mainly from the mathematical derivation of the PACF and has hence little physical meaning.

The number of statistically significant terms of the PACF informs on the order  $p$  for the AR( $p$ ) model. The order specifies the of number lag terms that are considered. Analogously, the order  $q$  for the MA( $q$ ) model can be estimated from the number of significant terms of the ACF. By this definition, the volume/area scaling model could be represented by an ARMA(9, 70) model, and the flowline model by an ARMA(3, 140). Hereby, the orders are taken as average over all glaciers and climate scenarios (see Appendix B for details). While an AR model with nine lag terms would be big but still feasible, a MA model with over one-hundred lag terms is neither practicable nor does it make sense. Especially, since [Roe and Baker \(2014\)](#) use an ARMA(3,3) model to produce comparable results to a flowline model. It is not the intent of this work to investigate the relation between a glacier's geometry and its ACF, neither to fit an ARMA model to the data. However, it is most notable that the flowline model behaves differently not only for different glaciers, but also for different sizes of the same glacier. The *one size fits all* approach of the volume/area scaling model produces more homogeneous results, the ACFs and PACFs are mostly independent of a glacier's size.

### 3.3 Regional runs with all Alpine glaciers

Volume/area scaling applied to single glaciers gives only an order of magnitude estimation, since the scaling constant  $c$  is a globally averaged value. A potential relative error in  $c$  will be directly transferred to any volume estimation ([Bahr et al. 2015](#)). Hence, volume/area scaling should not be applied to individual glaciers, but only to populations of glaciers, where the scaling approach shows its strength: the law of large number assures a reasonable estimation of the collective glacier ice

volume, since random errors will be canceled out by each other ([Bahr et al. 2015](#)). The first regional simulation over Alpine glaciers shown in this section, compares the behavior of the volume/area scaling model to the flowline model under different climate scenarios (analogous to the single glacier test case, see [Section 3.1](#)).

### 3.3.1 Experimental setup

The experimental setup is analogous to the single glacier test case, again comparing the volume/area scaling model to the flowline model, with some minor modifications. To best reflect the regional glacial evolution, the default OGGM [mass balance calibration](#) is used (see [Section 2.1.2](#)). This means, each evolution model uses its own  $t^*$  reference table (which may result in different  $t^*$  for the same glacier depending on the evolution model). The mass balance residual is again omitted ( $\beta^* = 0$ ), since this experiment intends to investigate the model behavior rather than absolute real-world values. Both evolution models run with the [ConstantMassBalance](#) model and the [RandomMassBalance](#) model, for 1000 years each. The mass balance models are initialized with  $y_0 = t^*$  and run with the same three different temperature biases as before ( $0^\circ\text{C}$ ,  $-0.5^\circ\text{C}$ ,  $+0.5^\circ\text{C}$ ).

### 3.3.2 Results

[Figure 3.6](#) shows the temporal evolution of aggregate glacier ice volume of all Alpine glaciers for the volume/area scaling model (left panel) and the flowline model (right panel) with three different equilibrium climates each. Both evolution models run for 1000 years with the [ConstantMassBalance](#) model and the [RandomMassBalance](#) model. The random climate with its year-to-year fluctuations is more physical than the completely constant climate. However, the resulting changes in glacier ice volume under both climate scenarios are almost identical. This makes intuitive sense, considering that glaciers act as natural low-pass filters for climatic variabilities (as established above, see [Section 3.2.3](#)). Short term climatic variabilities have little to no effect on the ice volume of a single glacier, much less on the aggregate ice volume of an entire region. Over the last 200 years of the simulations, the relative differences in aggregate ice volume between the constant and random climate scenario never exceed 0.6 % for the volume/area scaling model and 1.7 % for the flowline model. Only the  $0^\circ\text{C}$ -run of flowline model shows higher relative differences, with an average of 2.0 % over the last 200 years, up to a maximum of 2.7 %. While the total ice volume stays close to its initial value, it shows a slight increase over time. After an initially strong increase of 1.6 % over the first fifty years and another fifty years of constant values, the volume grows almost linearly with about  $0.53 \text{ km}^3$  per 100 years under the constant climate scenario. This results in a total volume change

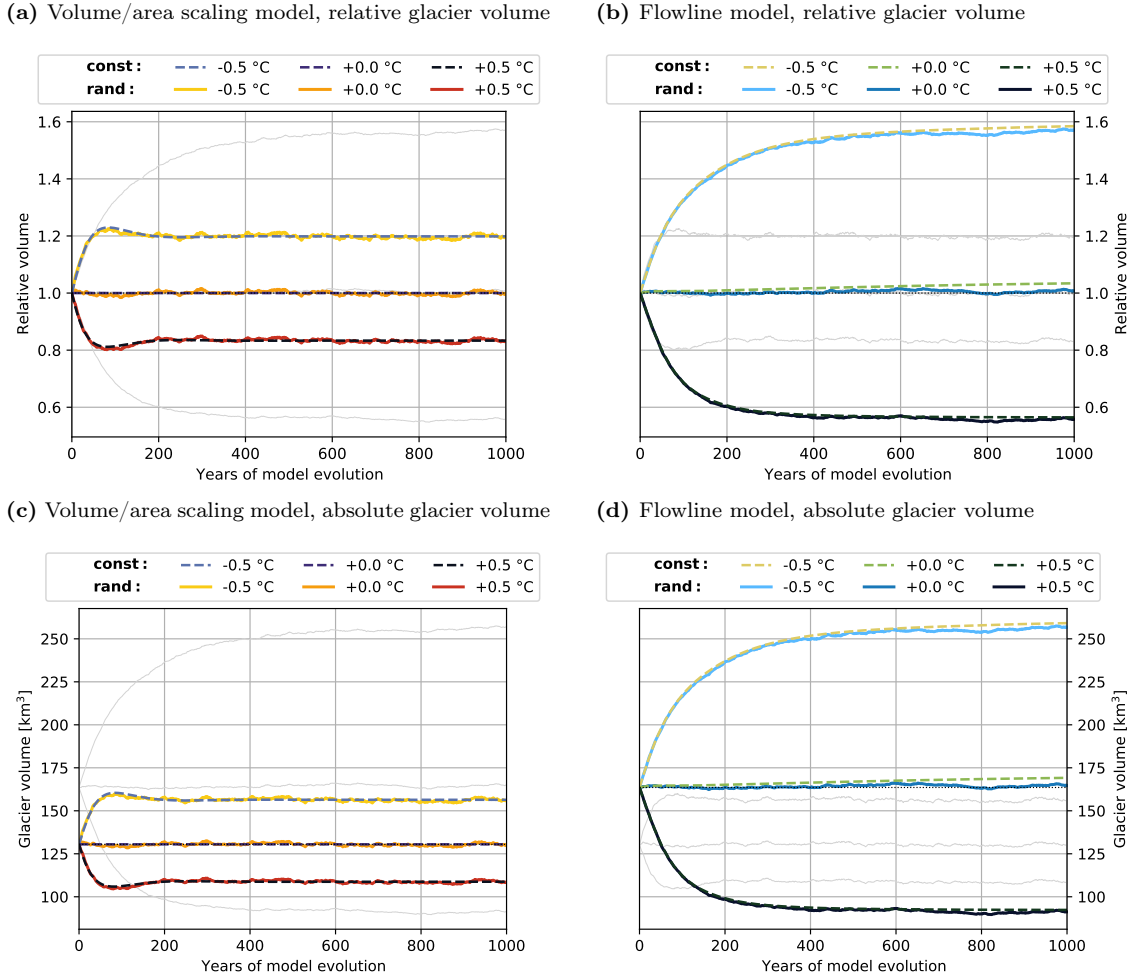


**Figure 3.6:** Time series of relative ice volume normalized with the initial values (upper panels) and absolute ice volume (lower panels), for all glaciers in the HISTALP domain. The left panels show the result of the volume/area scaling model, the right panels show the results of the flowline model. Solid lines represent the random climate scenarios, while dashed lines represent the constant climate scenarios. All climate scenarios are based on an equilibrium climate. The applied temperature biases of  $-0.5^{\circ}\text{C}$ ,  $0^{\circ}\text{C}$  and  $+0.5^{\circ}\text{C}$  are color coded, see legend for details. Light gray lines represent the volume evolutions of the other model, to facilitate comparisons.

of  $5.6 \text{ km}^3$  ( $+3.4\%$  of the initial value) after 1000 years of simulation. Under the random climate scenario, the total ice volume grows slower, most likely since the oscillations will reduce certain feedback loops. Hence, the following discussion is simplified by only considering the constant climate scenarios.

The volume/area scaling model estimates a total Alpine ice volume of  $156 \text{ km}^3$  ( $+20\%$ ),  $130 \text{ km}^3$  ( $\pm 0\%$ ) and  $109 \text{ km}^3$  ( $-17\%$ ), while the flowline model estimates a total Alpine ice volume of  $259 \text{ km}^3$  ( $+59\%$ ),  $169 \text{ km}^3$  ( $+3\%$ ) and  $92 \text{ km}^3$  ( $-44\%$ ), after 1000 years of simulation under a temperature bias of  $-0.5^{\circ}\text{C}$ ,  $0^{\circ}\text{C}$  and  $+0.5^{\circ}\text{C}$ , respectively. The volume/area scaling model estimate is much closer to the consensus estimate of Farinotti et al. (2019), a detailed discussion is provided in Section 4.1.

All the general characteristics of the volume/area scaling model found for the Hintereisferner test case turn up again for the regional. The changes in ice volume estimated by the volume/area scaling scaling model are much smaller when compared to the flowline model, by a factor of  $\approx 3.5$ . The oscillatory behavior of the volume/area scaling model is still visible. The volume/area scaling model's response time scales to the step changes in climate are shorter than for the flowline model. The volume e-folding time scales of both models are comparable to the single glacier test case:  $\tau_V = 23$  yr and  $\tau_V = 20$  yr for the volume/area scaling model and  $\tau_V = 125$  yr and  $\tau_V = 79$  yr for the flowline model, for the negative and positive temperature perturbation, respectively. These values are highly influenced by the larger glaciers and serve only as a guidance level. The symmetric behavior of the volume/area scaling model is still reflected in the response times, but less so in the new equilibrium values.

The next section explores the possibilities of tuning the volume/area scaling model via different parameters for the used scaling relations. This also provides a range of plausible results and serves as uncertainty estimation.

## 3.4 Sensitivity experiments

Before moving to the final experiments of projecting the future ice mass loss in the Alps and High Mountain Asia, it is necessary to determine the model's sensitivities. The following sensitivity analysis investigates the effects of the model-internal time scales and the scaling parameters on the model behavior. Both parameter sets are specific to the scaling model, since they determine the response time scaling as well as the volume/length and volume/area scaling. For consistency, the sensitivity experiments are performed on Hintereisferner (RGI60-11.00897) as a single glacier test case and on all Alpine glaciers inside the HISTALP domain. For simplicity, only the **ConstantMassBalance** model with a temperature bias of  $+0.5^\circ\text{C}$  is used for all runs.

### 3.4.1 Experimental setup

The scaling model estimates glacial evolution via the implemented response time scaling. Response time scaling adjusts the yearly changes in length and area, in relation to the total possible changes, using the model-internal response time scales for length and area,  $\tau_L$  and  $\tau_A$ , respectively. The estimate for the model-internal time scales loosely follows Jóhannesson et al. (1989) (see Section 2.1.3 and 2.2.2 for details). However, the model-internal time scales are good possible tuning parameters. The sensitivity experiments compare the model output for different time

### Take Home Message: Sensitivity experiments

- The model-internal time scales control the damping ratio of the oscillation, longer time scales correspond to stronger overshoots.
- Halving the model-internal time scales leads to an almost asymptotic change in aggregate ice volume of the HISTALP domain, showing only negligible oscillations.
- Different scaling constants lead to a different initial ice volume and a different initial glacier length, which in turn affect the e-folding time scales.
- Changing the scaling constants has little to no effect on the normalized volume change and normalized equilibrium volume.
- Custom scaling constants and exponents increase the change in ice volume ever so slightly, but the results are still not comparable to the flowline model.

scales, modified by a linear factor  $\tau_{\text{sens.}} = f \cdot \tau$ . Hereby, the factor  $f$  is only applied to  $\tau_L$ , since  $\tau_A$  is a just linear function of  $\tau_L$ . Starting from the default value ( $f = 1$ ) as baseline, the effects of halved ( $f = 0.5$ ) and doubled ( $f = 2$ ) model-internal time scales are investigated.

The other obvious choice for tuning parameters are the scaling exponents and scaling constants. The scaling constants for volume/length and volume/area scaling,  $c_L$  and  $c_A$ , respectively, can be seen as random variables. The randomness stems from the statistically similar, but not identical, dimensionless parameters for length, area and volume varying from glacier to glacier. Thanks to the law of large numbers, the global scaling constants  $c_L = 0.0180 \text{ km}^{3-q}$  and  $c_A = 0.0340 \text{ km}^{3-2\gamma}$  are a reasonable choice for a global ice volume estimation ([Bahr et al. 2015](#)). However, those parameters may be a bad fit for certain regions and therefore need calibration. While the scaling constants are not constant, the scaling exponents are. The volume/area scaling exponent was first derived as the slope of the linear regression of volume and area observations in log-log space (e.g., [Chen and Ohmura 1990](#)). [Bahr et al. \(1997\)](#) found that their values are fixed by the underlying physics and depend only on a single set of closure conditions. The closure conditions are in turn tightly bound by observations. Different common closures lead to the same results. Hence, it is strongly advised to use the global values of  $q = 2.2$  and  $\gamma = 1.375$  for the volume/length and volume/area scaling. Furthermore, even if different closure

conditions could be justified, the area scaling exponent is bound  $1.16 \leq \gamma \leq 1.5$  by simple geometric reasoning ([Bahr et al. 2015](#), Section 8.2).

As for the time scale sensitivity experiments, the global values of the scaling exponents serve as baseline. The next run uses custom scaling constant derived from a linear regression in log-log space but with a fixed slope corresponding to the global scaling exponents. The last run uses full custom scaling constants and exponents, again derived from a linear regression in log-log space. For reasons of simplicity, data points of volume, area and length are taken from the OGGM flowline model glaciers and not from observations. The inversion volume serves as glacier volume, the RGI area as surface area and the longest centerline as glacier length.

Since a linear regression can not be computed from a single data point, the Hintereisferner test case differentiates only between global and custom scaling constants (obtained by solving the scaling relations for  $c$ ) while using the global default scaling exponents in both cases. The following two sets of scaling parameters are used:

- (a) global (default) values of  $c_L = 4.551 \text{ m}^{3-q}$ ,  $q = 2.2$  for volume/length scaling and  $c_A = 0.191 \text{ m}^{3-2\gamma}$ ,  $\gamma = 1.375$  for volume/area scaling
- (b) custom scaling constants  $c_L = 1.555 \text{ m}^{3-q}$  and  $c_A = 0.252 \text{ m}^{3-2\gamma}$  with the global and physically based scaling exponents  $q = 2.2$  and  $\gamma = 1.375$

For comparability, the sensitivity runs on Hintereisferner (RGI60-11.00897) are setup exactly the same as the test case (see Section 3.1). This means a fixed *equilibrium year*  $t^* = 1927$  and no mass balance residual during the run. The regional Alpine runs are setup as before (see Section 3.3) and use the following three sets of scaling parameters:

- (a) global (default) values of  $c_L = 4.551 \text{ m}^{3-q}$ ,  $q = 2.2$  for volume/length scaling and  $c_A = 0.191 \text{ m}^{3-2\gamma}$ ,  $\gamma = 1.375$  for volume/area scaling
- (b) custom scaling constants  $c_L = 1.805 \text{ m}^{3-q}$  and  $c_A = 0.250 \text{ m}^{3-2\gamma}$  with the global and physically based scaling exponents  $q = 2.2$  and  $\gamma = 1.375$
- (c) custom scaling constants and scaling exponents  $c_L = 0.244 \text{ m}^{3-q}$ ,  $q = 2.517$  for volume/length scaling and  $c_A = 0.117 \text{ m}^{3-2\gamma}$ ,  $\gamma = 1.441$  for volume/area scaling

Disclaimer: While scaling constants and exponents based in observations would be preferable, the values of the custom scaling parameters are not as important for these sensitivity experiments, as long as they are different from the global values. In fact, the sensitivity experiment could easily be conducted with a set of fabricated exponents. For the same reason, it is also inconsequential that scaling exponents

derived from a numerical model depend on the model's closure conditions (Bahr et al. 2015, Section 8.9). This potential source for errors is acknowledged, but the flowline model is not tested for its closure conditions. While the custom scaling exponents lie within the range of physical sensible values, finding closure conditions supporting the computed values would go beyond the scope of this work.

### 3.4.2 Sensitivity to model-internal time scales

Let's again start with the Hintereisferner test case, before moving to the regional scale. As was to be expected, the model-internal time scales do not affect the absolute values, but control only the oscillatory behavior. The e-folding response time scales for length and area are directly proportional to the model-internal time scales. Halving and doubling the time scales results in a respective change of  $-4\text{ yr}$  and  $+7\text{ yr}$  for the area response time and  $-10\text{ yr}$  and  $+15\text{ yr}$  for the length response time<sup>5</sup>. The asymmetric responses hint at the non-linear effect of the time scales. Interestingly enough, the e-folding response time for volume is indirectly proportional to the model internal time scales, and changes only by  $\pm 1\text{ yr}$ . This means, while the glacier takes longer to reach its new equilibrium area and length, it takes less time to reach the new equilibrium volume (and vice versa). This is, however, most likely just a mathematical artifact, which stems from the oscillatory behavior and is discussed in the following.

The main change, however, is seen in the oscillation amplitude (Figure 3.7a). The damping ratio seems to be controlled by the model-internal time scales. Higher model-internal time scales lead to stronger oscillations and vice versa. But even with halved model-internal time scales, the modeled volume adjustment still shows some oscillations. With the default values, the volume/area scaling model overshoots the volume change estimate by 5 % of the final equilibrium value and it takes 371 years to reach an equilibrium. Hereby, an equilibrium state is (somewhat arbitrarily) defined as the range of  $\pm 0.1\%$  of the equilibrium value at year 1000. Halving and doubling the model-internal time scales changes the overshoot to 1 % and 11 % of the equilibrium value, respectively. The time span until a new equilibrium is reached seems to be almost linearly dependent on the model-internal time scales. By halving and doubling the model-internal time scales it takes 150 years and 688 years for the model to reach a new steady state, respectively.

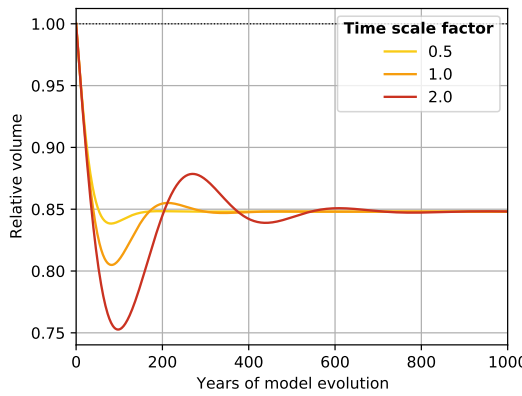
The same qualitative findings are made for the regional run with all Alpine glaciers (Figure 3.7c). The absolute values do not change for different model-internal time scales, only the oscillatory behavior does. While longer model-internal time scales result again in stronger overshoots, the oscillations seem generally more

---

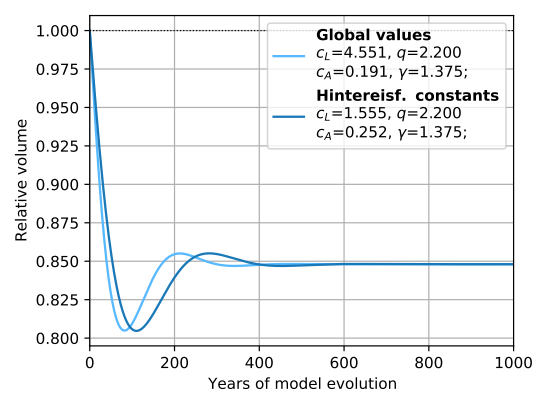
<sup>5</sup>The changes refer to the values shown in Section 3.1.

damped for the regional run. This is most likely a side effect of the summation over all Alpine glacier, whereby small scale oscillations can cancel each other out. The overshoots amount to 0.2 %, 3.0 % and 8.0 % of the equilibrium value for a time scale factor of 0.5, 1 and 2, respectively. Thereby it takes 133 years, 335 years and 642 years to reach a new steady state. When halving the model-internal time scales, the aggregate volume evolution shows almost no more discernible oscillations and is basically of exponential (asymptotic) nature.

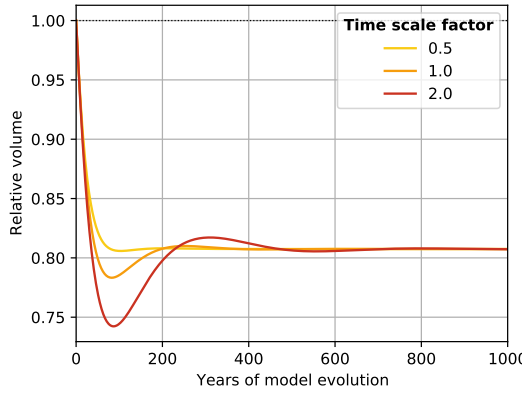
(a) Hintereisferner, different model-internal time scales



(b) Hintereisferner, different scaling constants



(c) HISTALP domain, different model-internal time scales



(d) HISTALP domain, different scaling constants and scaling exponents

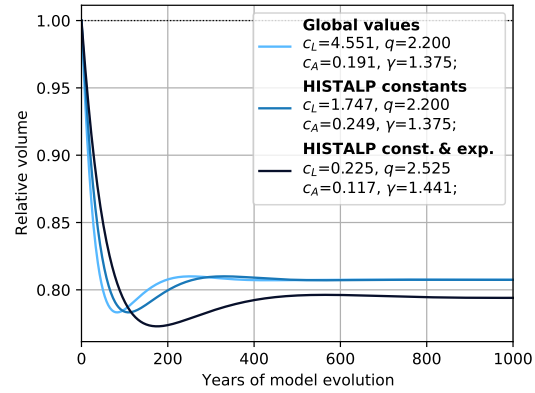


**Figure 3.7:** Temporal evolution of glacier ice volume under a positive temperature bias of  $+0.5^{\circ}\text{C}$  for the Hintereisferner (RGI60-11.00897) in the two upper panels (a) and (b) and for the entire HISTALP domain in the two lower panels (c) and (d). The right panels show results for different model-internal time scales, scaled by a linear factor (see legend for details). The left panels show results for different scaling constants and scaling exponents (see legend for details). Note the difference in y-axis scales.

### 3.4.3 Sensitivity to scaling parameters

As seen above, the model-internal time scale do not change the absolute values of any geometric glacier property. So what about the scaling parameters? The following

paragraph compares the model behavior between the custom Hintereisferner scaling constants and the global scaling constants (Figure 3.7b). The scaling exponents are held constant, since it is not possible to compute a linear regression from a single data point. Changing the scaling constants leads to different absolute values. As explained in Section 2.2.2, the volume/area scaling model starts by computing the initial glacier volume from the surface area via the volume/area scaling relation. Hence, the initial area stays the same while the initial ice volume increases with the custom scaling constants. The initial volume for the Hintereisferner increases to  $0.787 \text{ km}^3$  with custom scaling constants  $c_L = 1.555 \text{ m}^{3-q}$  and  $c_A = 0.252 \text{ m}^{3-2\gamma}$ , compared to the  $0.596 \text{ km}^3$  with the global values. While starting with a larger initial ice volume increases the absolute change in ice volume ( $-0.120 \text{ km}^3$  vs.  $-0.091 \text{ km}^3$ ), it still results in a larger equilibrium ice volume ( $0.667 \text{ km}^3$  vs.  $0.506 \text{ km}^3$ ). However, when normalized with the respective initial ice volumes, the changes in ice volume, the equilibrium values and the overshoots (i.e., minimum values due to the oscillatory behavior) are almost identical (the differences lie far below 0.1%). This comes as no surprise, since the scaling constants are canceled out during the normalization process. In fact, when estimating *changes* in regional or global ice volume the scaling constant  $c$  can be eliminated altogether (Bahr et al. 2015, Section 8.5). While the relative values do not change, the temporal evolution does. As already discussed, the bigger custom scaling constant  $c_A$  leads to a bigger initial ice volume. Increasing the glacier's ice volume in turn increases the glacier's response time, since larger glaciers generally react slower to climatic changes. The volume e-folding response time increases to 30 years with the custom scaling constants, compared to 23 years with the global values. The increased response time goes hand in hand with a stronger oscillation. While the amplitude stays the same, the frequency decreases. Hence, the peak of the overshoot shifts by 28 years (to year 100 after the initial climate perturbation) and it takes much longer to reach the new equilibrium state (493 years vs. 371 years). While the glacier length reacts analogously to the custom scaling constants, the surface area does not. This was to be expected, since the initial surface area does not depend on the scaling parameters. While the equilibrium value and the e-folding response time are practically not affected, the oscillation amplifies. In addition to the decreased frequency, as for ice volume and glacier length, the surface area overshoots by  $15\,761 \text{ m}^2$  more under the custom scaling constants (which corresponds to  $\approx 0.2\%$  of the equilibrium value).

Again, the results of the regional Alpine run (Figure 3.7d) are analogous to the Hintereisferner test case. While the Hintereisferner test case compares only the global and custom scaling constants, an additional run with custom scaling constants and scaling exponents is investigated. As seen above, changing the scaling constants results in different absolute values (for the initial volume as well as for

the final equilibrium volume). However, when normalized with the initial values only the run with custom scaling exponents shows a different (bigger) change in ice volume. The total modeled glacier ice volume shrinks from an initial  $229.7 \text{ km}^3$  to a final  $182.4 \text{ km}^3$ , subjected to a positive temperature bias of  $+0.5^\circ\text{C}$ . The change of  $-47.3 \text{ km}^3$  corresponds to  $-21\%$  of the initial value. However, the result does still not compare to the  $-47\%$  of the flowline model and is not significantly different from the  $-19\%$  for the other two volume/area scaling runs.

## 3.5 Projections for the 21st century

This last experiments provides a quantitative estimation of the ice volume change over the 21st century, again comparing the volume/area scaling model to the flowline model. In addition to the Alps (or much rather the entire RGI region 11, i.e., Central Europe), the experiment runs for all glacier of High Mountain Asia (RGI region 13, 14 and 15, i.e., Central Asia, South Asia West and South Asia East, respectively). The mass balance models are driven by climate data from fifteen different general circulation models<sup>6</sup> (GCMs) from the Coupled Model Intercomparison Project Phase 6 (CMIP6, [Eyring et al. 2016](#)), resulting in an ensemble prediction with fifteen members for four different Shared Socioeconomic Pathways (SSP).

### 3.5.1 Experimental setup

The inclusion of non Alpine glaciers makes necessitates the use of the global CRU climate dataset. As with the HISTALP dataset before, the volume/area scaling mass balance model must be calibrated (see Section 2.1.2), which is done using updated global parameters from [Malles and Marzeion \(2020\)](#) ( $a = 3, T^{\text{melt}} = 0^\circ\text{C}, T^{\text{solid precip}} = 4^\circ\text{C}$ ). The flowline model defaults to the standard OGGM values. To further increase the accuracy of the results, the mass balance residual  $\beta^*$  of both models is corrected via the `matchRegionalGeodetic_mb` task, to match the observations presented by [Davaze et al. \(2020\)](#).

The 21st century projections are modeled with climate data from fifteen GCMs from CMIP6 for the pathways SSP1-2.6, SSP2-4.5, SSP3-7.0 and SSP5-8.5. The new scenario framework brings together the social development pathways and the Representative Concentration Pathways (RCPS, indicated by the radiative forcing

---

<sup>6</sup>BCC-CSM2MR ([Xin et al. 2019](#)), CAMS-CSM1.0 ([Rong 2019](#)), CESM2 ([Danabasoglu 2019a](#)), CESM2-WACCM ([Danabasoglu 2019b](#)), CMCC-CM2-SR5 ([Lovato and Peano 2020](#)), EC-Earth3 ([EC-Earth](#)), EC-Earth3-Veg ([EC-Earth](#)), FGOALS-f3-L ([YU 2019](#)), GFDL-ESM4 ([John et al. 2018](#)), INM-CM4-8 ([Volodin et al. 2019a](#)), INM-CM5-0 ([Volodin et al. 2019b](#)), MPI-ESM1.2-HR ([Schupfner et al. 2019; Steger et al. 2019](#)), MRI-ESM2.0 ([Yukimoto et al. 2019](#)), NorESM2-MM ([Bentsen et al. 2019](#)), TaiESM1.0 ([Lee and Liang 2020](#))

in  $\text{W m}^{-2}$  in 2100), or details see O’Neill et al. (2016); Riahi et al. (2017). The GCM data from CMIP6 is prepared using the OGGM task `process_cmip_data`, which applies the anomalies to the CRU baseline climate.

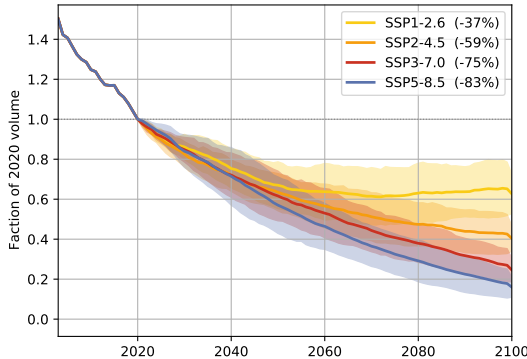
The projections start in 2003 (the observation date of most RGI outlines) and run until 2020 using CRU data, before continuing with the GCM data for the rest of the 21st century. The runs are invoked via the `run_from_climate_data`. The presented aggregate ice volumes are normalized with their respective value in 2020 for better comparability.

### 3.5.2 Results

Figure 3.8 shows the ice volume projections for Central Europe (RGI region 11) for the aforementioned SSPs, computed with the volume/area scaling model in the left panel and the flowline model in the right panel. All percentages are in relation to the 2020 ice volume. Again, both evolution models show qualitatively comparable results, while there are significant quantitative differences.

The volume/area scaling model predicts a strong and almost linear decrease in ice volume up to 2020, after which the mass loss attenuates. A new equilibrium is reached only under SSP1-2.6, after an estimated ice loss of  $-37\pm10\%$ . The ensemble average even shows a slight increase over the last 25 years, which most likely stems from the oscillatory behavior of the volume/area scaling model (cf. Section 3.1.2 and 3.3.2). Under all other SSPs the ice volume is still on a downward trajectory, with an estimated ice loss until 2020 of  $-59\pm6\%$ ,  $-75\pm6\%$ ,  $-83\pm5\%$  under SSP2-

(a) Volume/area scaling model projection for Central Europe (RGI region 11)



(b) Flowline model projection for Central Europe (RGI region 11)

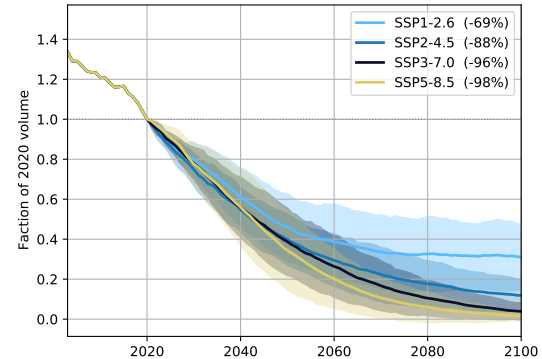


**Figure 3.8:** Ice volume projection for Central Europe (RGI region 11) using CMIP6 climate data over the 21st century, relative to the year 2020. The left panel shows the result of the volume/area scaling model, the right panel shows the results of the flowline model. Solid lines represent the ensemble average, while the shade represents the  $1\sigma$  band. All ensembles have fifteen members. Colors denote different Shared Socioeconomic Pathways, refer to the legend for details. Thereby, the percentage values in parentheses indicate the ice loss relative to 2020.

4.5, SSP3-7.0, SSP5-8.5 respectively. The ice loss predicted by the flowline model ramps up over the initial years, than continues with a rather constant rate before attenuation in the second half of the 21st century and approaching a new equilibrium. The total ice loss amounts to  $-68 \pm 16\%$  under SSP1-2.6 and  $-88 \pm 8\%$  under SSP2-4.5. For the two SSPs with high forcings the entire glacier ice melts within the margin of error:  $-96 \pm 4\%$  under SSP3-7.0 and  $-98 \pm 2\%$  under SSP5-8.5.

Comparing the full simulation period, the volume/area scaling model generally shows an asymptotic decrease in ice volume while the ice loss predicted by the flowline model follows a sigmoidal shape. Overall, the volume/area scaling predicts less ice melt than the flowline model, so much so that the final estimates of one model are outside the margin of error of the other. The volume/area scaling model still shows a downward trajectory for all but the lowest forcing, indicating that volume/area scaling model reacts slower than the flowline model and may therefore catch up once a new equilibrium is reached. This, however, contradicts all the equilibrium experiments, where the volume/area scaling model reached its new equilibrium always before the flowline model.

Focusing on the “historical” part from 2003 to 2020, the volume/area scaling model estimates a total ice volume loss of one third (from 150 % in 2003 to 100 % in 2020) while the flowline model estimates a loss of one fourth (from 135 % in 2003 to 100 % in 2020). The regional average geodetic surface mass balance observations for Central Europe between 2000 and 2020 is  $-874 \text{ mm we. yr}^{-1}$ , while volume/area scaling model estimates  $-1590 \text{ mm we. yr}^{-1}$  and the flowline model  $-1608 \text{ mm we. yr}^{-1}$ . Those rather large differences show that both models in their respective “out-of-the-box” state have difficulties reproducing the mass balance observations for the Alps. Hence, the last calibration step uses `matchRegionalGeodetic_mb` to shift the mass balance residual  $\beta^*$  accordingly. This assures that the boundary conditions of both models are as similar as possible and the results as physical as possible. Therefore, the difference between the two models are all the more interesting, showing once more that they do not resolve all the same processes.

Figure 3.9 shows the 21st century ice volume projections for High Mountain Asia: Central Asia (RGI region 13) in the upper panels, South Asia East (RGI region 14) in the middle panels, South Asia West (RGI region 15) in the lower panels. The overall results are comparable to the simulation for Central Europe. The ensemble averages show an asymptotic or even linear decrease in ice volume for the volume/area scaling model (with rather narrow uncertainty bands) and a more sigmoidal decrease for the flowline model (with much broader uncertainty bands). The final values of both models are in closer agreement with each other, and are mostly within each others uncertainty bands (see Table 3.3). However, the flowline model still predicts more ice loss than the volume/area scaling model. The differences in

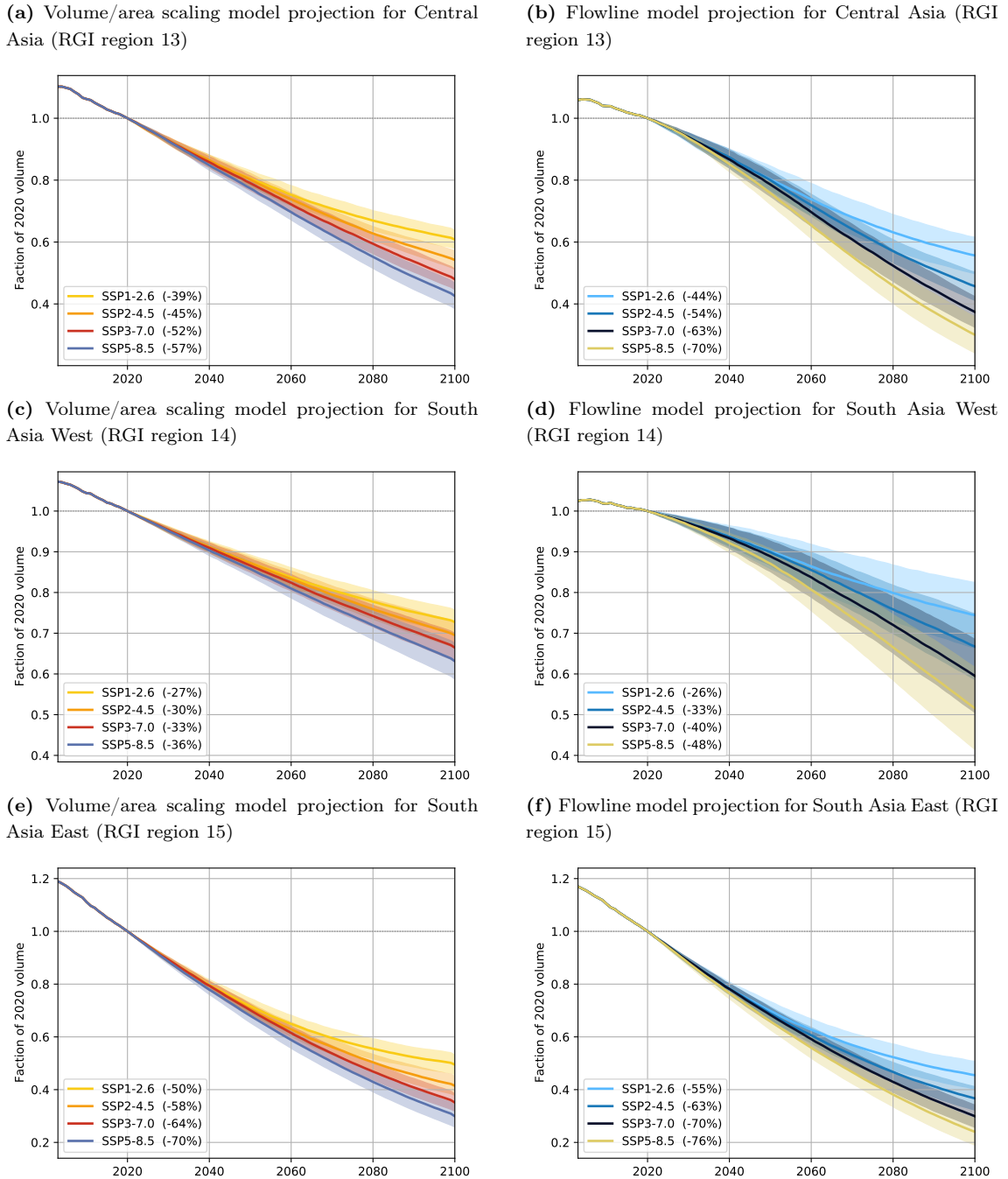


**Figure 3.9:** As Figure 3.8, but for Central Asia (RGI region 13) in the upper panels, South Asia West (RGI region 14) in the middle panels and South Asia East (RGI region 15) in the lower panels.

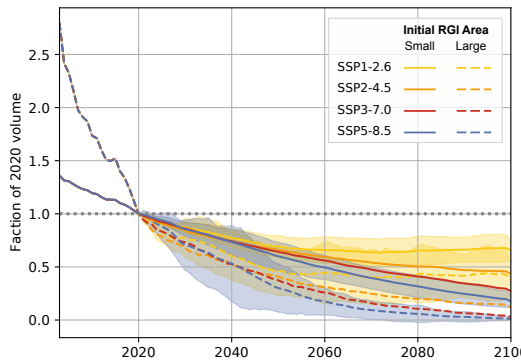
**Table 3.3:** Ensemble mean and standard deviation of projected ice volume loss in 2100, relative to the ice volume in 2020. Volume/area scaling model and flowline model are driven by climate data of fifteen GCMs from CMIP6.

	V/A scaling $\bar{\Delta V} \pm \sigma$ [%]	Flowline $\bar{\Delta V} \pm \sigma$ [%]
<b>Central Europe</b>		
SSP1-2.6	-37 ± 10	-69 ± 16
SSP2-4.5	-60 ± 6	-88 ± 8
SSP3-7.0	-75 ± 6	-96 ± 4
SSP5-8.5	-84 ± 5	-98 ± 2
<b>Central Asia</b>		
SSP1-2.6	-39 ± 3	-44 ± 6
SSP2-4.5	-46 ± 3	-54 ± 5
SSP3-7.0	-52 ± 3	-63 ± 5
SSP5-8.5	-57 ± 4	-70 ± 6
<b>South Asia East</b>		
SSP1-2.6	-27 ± 3	-26 ± 8
SSP2-4.5	-30 ± 3	-33 ± 8
SSP3-7.0	-34 ± 4	-40 ± 9
SSP5-8.5	-37 ± 4	-48 ± 10
<b>South Asia West</b>		
SSP1-2.6	-51 ± 4	-55 ± 5
SSP2-4.5	-59 ± 4	-63 ± 4
SSP3-7.0	-65 ± 3	-70 ± 4
SSP5-8.5	-70 ± 4	-76 ± 5

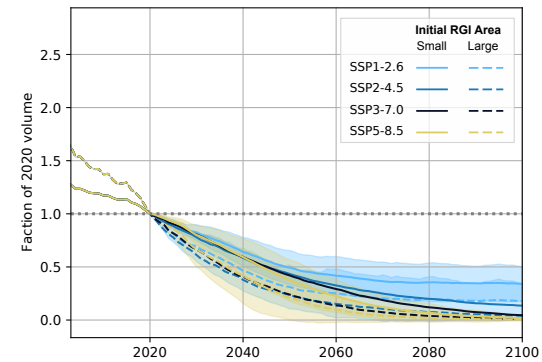
estimated ice loss up to 2020 between volume/area scaling and flowline model are also less pronounced, than for Central Europe. This can possibly be explained by the better agreement between observed and modeled mass balance, the computed differences and following shift of  $\beta^*$  range between 177 and 364 mm we. yr $^{-1}$ . Furthermore, given the empirical nature of the scaling relations the model performance increases with increasing glacier population size.

Finally, the model response is investigated as a function of initial glacier surface area. The glaciers of each region are divided in two size classes, above and below the 95th percentiles in RGI area (see Table 3.4 for details). While the regions have different distributions of glacier sizes, the area thresholds for all regions are in the same order of magnitude ( $\approx 3 \text{ km}^2$ ) and the aggregate area of the upper 5 % of glaciers amounts to more than half of the total area (between 52 % and 66 %).

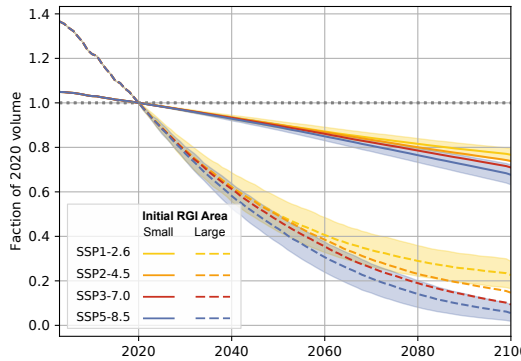
(a) Volume/area scaling model projection for Central Europe (RGI region 11)



(b) Flowline model projection for Central Europe (RGI region 11)



(c) Volume/area scaling model projection for South Asia West (RGI region 14)



(d) Flowline model projection for South Asia West (RGI region 14)

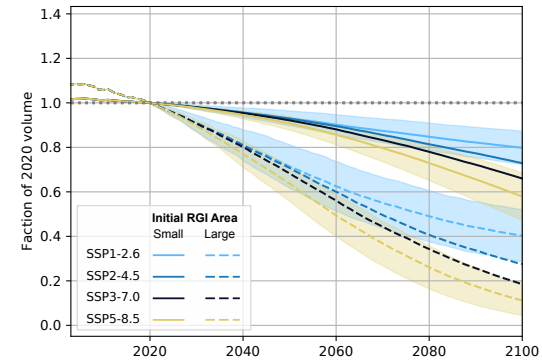


**Figure 3.10:** As Figure 3.3 for Central Europe (upper panels) and South Asia West (lower panels), but distinguishing between small glaciers (dashed lines) and large glaciers (solid lines). Small glaciers are all glaciers below the 95th percentile in RGI start area, large glacier all glaciers above. Uncertainty bands are only shown for SSP1 and SSP5.

Figure 3.10 shows the 21st century volume projections distinguishing between small and large glaciers for Central Europe and South Asia West. There are no unexpected results: the smaller glacier loose more ice volume relative to 2020 in less time; the flowline model shows less differences in ice loss between the two size classes than the volume/area scaling model. The same holds true for Central Asia and South Asia East (not shown). The differences in ice volume evolution between the two size classes are much larger for High Mountain Asia than for Central Europe. This indicates that glacier size does matter, however mostly for very large glaciers. South Asia West has about seven times more glaciers than Central Europe, but almost eighteen times the surface area in the larger size class (in addition to an already higher 95th percentile, see Table 3.4).

The small glaciers modeled by the volume/area scaling model loose considerably more ice volume before 2020, than the large ones. For example, the estimated ice loss for Central Europe between 2003 and 2020 amounts to 64% (i.e., from 280% to 100%) for the small glaciers, while under SSP1-2.6 and SSP2-4.5 some ice persists throughout the rest of the 21st century. However, since the glaciers in Central Europe are overall smaller, there is generally less difference in projected ice volume between the two size classes compared to High Mountain Asia (true for the volume/area scaling model and flowline model.)

**Table 3.4:** Number of glaciers and total surface area of the lower 95 % and upper 95 % of RGI area, additional the threshold area, i.e. the 95th percentile, is given.

	Lower 95 %		Threshold $A [\text{km}^2]$	Upper 5 %	
	$n_{\text{Glaciers}}$	$\sum A [\text{km}^2]$		$n_{\text{Glaciers}}$	$\sum A [\text{km}^2]$
<b>Central Europe</b>	3730	831	2.15	197	1261
<b>Central Asia</b>	51707	21460	2.96	2722	27844
<b>South Asia West</b>	26588	11490	3.46	1400	22079
<b>South Asia East</b>	12463	7066	4.10	656	7668

# Chapter 4

## Discussion

The volume/area scaling model is able to simulated glaciers under various climate inputs with conceptually correct results. The ice volume projections for the Alps and High Mountain Asia over the 21st century show that the volume/area scaling model produces results in agreement with recent studies (e.g., [Marzeion et al. 2020](#)). Despite the lack of a dedicated ice physics module, the projected changes in relative ice volume are comparable to the flowline model—even if not always within its uncertainty bounds. More precisely, the changes in glacier geometries estimated by the volume/area scaling model are generally smaller than those of the flowline model. The limitations of the volume/area scaling model responsible for the differences are identified with idealized equilibrium experiments: the missing mass-balance-elevation feedback causes symmetric results for positive and negative mass balance perturbations; the response time scaling results in an oscillating behavior, paradoxically caused by too long model-internal time scales, while the resulting response time scales are rather short. This chapter discusses strength and limitations of the volume/area scaling model and frames its performance in relation to other models and recent studies.

### 4.1 Values of ice volume (change)

Using the volume/area scaling relation to estimate initial glacier ice volumes results in much lower values compared to the numerical ice thickness inversion (cf. [Farinotti et al. 2009](#)) used by the OGGM flowline model. However, comparing the initial ice volumes for the Alps (see Section 3.3) to the consensus estimate of  $130 \pm 30 \text{ km}^3$  for Central Europe (RGI region 11) by [Farinotti et al. \(2019\)](#), the volume/area scaling model estimate of  $130 \text{ km}^3$  is much closer than the flowline model estimate of  $164 \text{ km}^3$ . This overestimation of the flowline model is mainly a result of the fixed default values for the ice creep parameter  $A$  and the sliding parameter  $f_s$ . The

effect of  $A$  on the ice volume estimation on the example of Hintereisferner is shown in [Maussion et al. \(2019\)](#), Figure 6), with similar results as presented in Table 3.1. Calibration of  $A$  with ice thickness observations suggest a correction of  $A$  with a factor of 1.1 to 1.5 on the global scale, and even more on a regional scale, e.g., a factor 3 for the Alps ([OGGM Developers 2021](#)). Since these parameters are also used for the forward dynamical model run, they do not only affect the initial volume estimations but also ice volume change estimations.

Stepping away from the idealized equilibrium experiments, how do the ice volume projections over the 21st century for Central Europe (Section 3.5) compare to the literature? [Marzeion et al. \(2012\)](#), cf. Figure 21 estimate a total ice loss of  $-48\%$  for RCP2.6,  $-65\%$  for RCP4.5,  $-69\%$  for RCP6.0,  $-85\%$  for RCP8.5 relative to 2020 (reconstructed from supplementary material). These values are slightly higher than estimated by the volume/area scaling model under comparable SSPs. Possible explanations include the following: the use of CMIP5 data for the entire run, i.e., also for the historical part up to 2012, instead of CRU data; the different mass balance calibration parameters, and the usage of the precipitation gradient. However, the results of [Marzeion et al. \(2012\)](#) could not fully be reproduced by the new implementation of the volume/area scaling model. This would warrant further investigations and a direct comparison using the original code.

All other recent studies using different models to run global projections under CMIP5 present generally higher values of ice loss for Central Europe than the volume/area scaling model: [Radić et al. \(2014\)](#) estimate  $-84\%$  for RCP4.5 and  $-96\%$  for RCP8.5 (relative to 2006); [Huss and Hock \(2015\)](#) estimate  $-77\%$  for RCP2.6,  $-89\%$  for RCP4.5 and  $-98\%$  for RCP8.5 (relative to 2010); [Zekollari et al. \(2019\)](#) estimate  $-63\%$  for RCP2.6,  $-78\%$  for RCP4.5 and  $-94\%$  for RCP8.5 (relative to 2017). Hereby, all values refer to the respective ensemble means. The results from the flowline model are somewhere in between these values. The same general remarks hold true for the projections for High Mountain Asia. A complete comparison of 21st century projection results for all RGI regions and eleven global models is shown in [Marzeion et al. \(2020\)](#), Figures S1–S20 in the supporting informations).

As a final note, for the volume/area scaling model it is possible to adjust the absolute values of initial ice volume by using regionally calibrated scaling parameters. However, the sensitivity analysis (Section 3.4.3) shows that the relative volume change is not affected by different parameters (in agreement with [Radić et al. \(2007, 2008\)](#)). The missing processes that were identified in this study are discussed in the following section.

## 4.2 Missing physical processes

The positive feedback loop between surface mass balance and surface elevation has a non-negligible effect on glacier mass change ([Huss et al. 2012](#); [Schäfer et al. 2015](#)). If the surface elevation decreases as a result of a negative mass balance, the air temperature above the ice surface will subsequently increase, according to the negative temperature gradient. Higher temperatures, in turn, lead to increased melt, which further decreases the surface elevation (this feedback loop works analogously for increasing surface elevations due to positive mass balance). However, the only direct feedback between glacier geometry and specific mass balance of the volume/area scaling model happens at the glacier terminus. Changes in glacier length are linearly relayed to changes in terminus elevation, depending on the average surface slope. This is aggravated with the fact that the modeled changes in glacier length are strongly underestimated, which results in a general underestimation of glacier mass change and a symmetric response to positive and negative step changes in temperature. The symmetric response can be reproduced by the flowline model, if the implemented mass-balance-elevation feedback is turned off (see Section [3.1](#), [3.3](#)).

The missing implementation of explicit thickness changes additionally influences the change of glacier length. [Roe and Baker \(2014\)](#) show that glaciers respond to step changes in climate in three overlapping stages: (1) changes in interior thickness cause (2) changes in terminus flux, which in turn drive (3) changes in glacier length. Subsequently, the glacier length does not change exponentially, but much rather sigmoidally. The length change rate needs some time to ramp up to its maximum value, before it slowly drops again and the glacier length approaches its new equilibrium value. The third-order linear ARMA(3,3) model proposed by [Roe and Baker \(2014\)](#) is able to adequately simulate all three stages. It produces a sigmoidal change of glacier length, and performs comparably to a flowline model.

Using this three-stage model, [Roe et al. \(2020\)](#) attribute all of the observed glacier mass loss over the industrial era to anthropogenic forcings. This disputes the findings of [Marzeion et al. \(2014\)](#), who estimated an anthropogenic contribution of only  $25 \pm 35\%$  during the period from 1851 to 2010 increasing to  $69 \pm 24\%$  over the last twenty years (1991–2000) using the volume/area scaling model. A possible explanation can be found in the model-internal time scales. The model-internal time scale for length changes used by [Marzeion et al. \(2012\)](#) is based on the mass turnover  $\tau_L \propto 1/P_{\text{clim}}^{\text{solid}}(t^*)$  (see Section [2.1.3](#) for details), rather than using the geometric timescale  $\tau_L \propto -1/\dot{b}_{\text{terminus}}$  proposed by [Jóhannesson et al. \(1989\)](#). [Roe et al. \(2020\)](#) argue that the computed response times are too large, since the average precipitation is mostly lower than the corresponding terminus ablation rate. This corroborates the findings presented in Section [3.4.2](#). The oscillatory behavior of

the geometry response can be reduced by lowering the model internal time scales. However, the volume/area scaling already shows strong short term variability under natural year-to-year climate variability. Lowering the model-internal time scales may result in even stronger fluctuations and make the model react even quicker to changes in climate.

The widely used e-folding response time scale can not be linked directly to any glacier characteristic and should be seen as a relative measure much rather than an absolute number ([Schuster 2020](#)). The ACF could possibly add information, or even supersede, to the concept of e-folding response times as glacier characteristics. Possible future work could include a in-depth investigation on how glacier characteristics influence its ACF.

### 4.3 Mass balance calibration

[Roe et al. \(2020\)](#) additionally argue that the mass balance calibration is another source of uncertainty. By assuming that neighboring glaciers are likely in equilibrium around the same time only climatic factors are considered, while other factors, like the glacier size, are neglected. Small glaciers (or more precisely, glaciers with a short response time) are never far from equilibrium due to their fast geometry adjustments, while large glaciers (or more precisely, glaciers with a long response time) may take many years before they even start reacting to a trend in climate. This potential source of uncertainty is already acknowledged by [Maussion et al. \(2019\)](#), reasoning that even potentially large errors in  $t^*$  will result in comparably small errors in  $\mu^*$ , due to the equilibrium constraint. However, an investigation of this problem is not possible within this study, since the volume/area scaling model and the OGGM both rely on the same calibration method and are therefore equally affected by it.

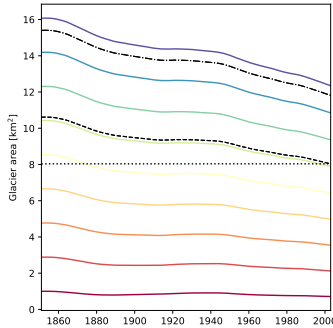
A different problem with the mass balance calibration presents by [Marzeion et al. \(2012\)](#) concerns the difference between summing over monthly averages versus the averaging over yearly sums for the climatological value of melting temperature. Using monthly climatological values (as in the average temperature in January) has a potential pitfall. Imagine a hypothetical time series of average January temperatures over 31 years, with an average monthly temperature around  $-10^\circ\text{C}$  for each year except one particularly warm year with  $+10^\circ\text{C}$ . The climatological temperature average for January will therefore be close to  $-10^\circ\text{C}$ . Hence, using this monthly average for the mass balance calibration no melt occurs in January. But that one warm January with a highly positive temperature has definitely caused some ice melt, which is not accounted for by the climatological value. Therefore the use of yearly sums of positive melting temperature and solid precipitation, so the mass loss

and mass gain of each month is accounted for. However, this problem was already identified and implemented in the OGGM.

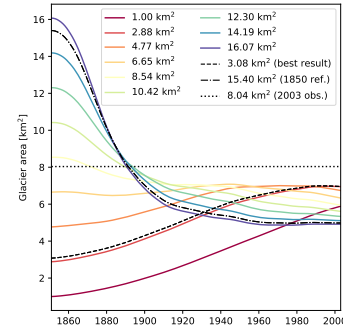
## 4.4 Initializing historic glacier states

The initialization of past glacier states proposed by Marzeion et al. (2012), or much rather the implementation thereof, has a conceptual error. Response time scaling introduces a “glacier memory”, which inhibits the model to run backwards in time. Hence, the value for the initial glacier surface area in 1850 (the year in which the original historic simulations started) is estimated via a trial-and-error process: iterating over a range of possible values for the 1850 area and choosing the one which results in the area closest to the RGI observation at the year of measurement<sup>1</sup>.

(a) Original implementation with constant (i.e., not adjusted) initial terminus elevation



(b) Physical consistent implementation with adjusted initial terminus elevation



(c) Physical consistent implementation with added instant geometry changes, i.e.,  $\tau_L = \tau_A = 1$  yr

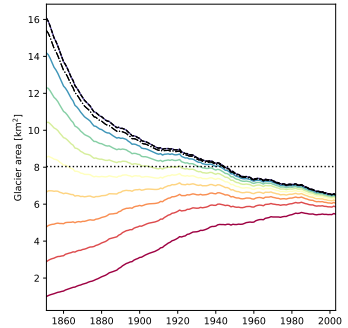


**Figure 4.1:** Evolution of Hintereisferner (RGI60-11.00897) surface area for different initial values, from 1851 to 2003, forced by HISTALP climate data.

Figure 4.1a shows the result of this process, i.e., the temporal evolution of glacier surface area from 1850 to 2003 for different start values on the example of Hintereisferner. For each iteration, the initial volume  $V_0$  and initial length  $L_0$  are estimated from the initial area  $A_0$  using the scaling relations (see Section 2.1.3 and Figure 2.1). The terminus elevation, however, is not adjusted to the new glacier length, but kept constant at the RGI reference value. Thereby, the new and now larger (or smaller) glacier is confined to the same elevation band as the RGI reference glacier, which implies a lower (or higher) average slope. This may make intuitive sense, given the Alpine topography of steep mountains and flatter valleys, and also the results do not look suspicious (which is probably why the bug was not noticed). However, keeping

<sup>1</sup>Implementation note: the task `find_start_area()` uses a minimization function rather the originally described and used iterative process and it allows to decide whether to update the terminus elevation or not.

the initial terminus elevation constant results in equal initial specific mass balance for different sized glaciers, which makes little physical sense.

This problem is easily fixed by adjusting the terminus elevation to the new glacier length, in the same way as during all the other time steps (see Section 2.1.3 and Figure 2.1). This results in higher and mostly positive values of initial specific mass balance for smaller initial glaciers (given that they retreat into higher elevations), and lower and possibly negative values for larger initial glaciers (given that they reach further into the ablation zone). However, by doing so, the model is not able to reproduce a surface area close to the observed area in 2003 for some glaciers, regardless of the initial area in 1850 (see Figure 4.1b). Furthermore, the larger initial glaciers end up with a lower surface area than the smaller initial glaciers. This “turn over” is also seen for ice volume and glacier length (not shown), and reinforces the notion that the model internal time scales are too long, i.e., past glacier states have too much of an influence.

The hypothesis of too long time scales is tested by allowing for instant geometry updates, i.e., setting the time scales to  $\tau_L = \tau_A = 1\text{ yr}$ . As can be seen Figure 4.1c, the “overturning” vanishes. However, the areas still converge to a similar range as for the physically consistent model, which may in some cases be far off the observed value.

When comparing the original and physical consistent implementation, the same initial areas, even if only slightly different from the RGI reference value, result in drastically different glacier evolutions (look at  $A_0 = 6.65\text{ km}^2$  and  $A_0 = 10.42\text{ km}^2$  in Figure 4.1a and b). It hints on a dependency of the time scales to the average slope. This additionally supports the argument that the terminus mass balance is a better suited to estimate glacier time scales than precipitation, since terminus mass balance also depends on the average surface slope, or much rather the terminus elevation.

# Chapter 5

## Conclusions

Glaciers are controlled by their mass balance and the resulting ice flow. Hence, a glacier model has to incorporate a mass balance model, to account for accumulation and ablation, and a dynamic model, to update glacier geometries in response to mass balance changes. A dynamic model based on scaling relations, such as the here presented combination of volume/area, volume/length and response time scaling, can produce qualitatively comparable results to a state-of-the-art flowline model. Thereby, the results of real world applications like projections of regional glacial evolution forced by GCM models are mostly within the uncertainty bounds of each other, while idealized equilibrium experiments expose the limitations and shortcomings of the volume/area scaling model.

The overall behavior of the volume/area scaling model is as expected, i.e., the model correctly simulates advances and retreats in response to step changes in climate as well as to natural climate variability, it has the ability to reach a new equilibrium, and it shows characteristics of a low-pass filter. However, changes in ice volume, surface area and glacier length are generally underestimated when compared to the flowline model. The model-internal representation of time scales has been identified as the main source of those differences and other unexpected and unwanted behaviors. The conducted sensitivity analysis, backed by [Roe et al. \(2020\)](#), concludes that the used time scale parameterization results in too high values. The timescales could be exploited as future tuning parameter. Using the geometric timescales based on the terminus ablation rate ([Jóhannesson et al. 1989](#)) rather than the turnover may improve the results.

Additional errors are introduced by missing physically relevant processes, which are not resolved by the volume/area scaling model. Those include but are not limited to, a missing mass-balance-elevation feedback, a constant average slope, and no awareness of the surrounding topography. While these processes may be secondary on a global scale, estimates for regions with many small glaciers like the Alps vary significantly between scaling and flowline model. The usage of more

complex models is advisable for future projections of glacier mass changes, especially given the nowadays available computational power.

This study detailed the underlying principles and implementation process of a simple global glacier model based on glacier scaling relations ([Marzeion et al. 2012](#)) in the OGGM framework. The implementation of the volume/area scaling model in the OGGM framework is a success on its own. As suggested by [Maussion et al. \(2019\)](#), the implementation of simpler approaches, such as the one presented here, allows to test the benefits of the increased model complexity. Such extension of the OGGM are obviously not limited to simple model, but may as well add more complex processes (e.g., an improved calving parametrization, [Recinos et al. 2019](#)). It shows the benefits of an open source, modular, community driven glacier model. Comparing different parametrization and estimating uncertainties are imperative to improve projections of future glacier mass loss and its consequences. The global implementation of the scaling model and the implementation of additional geometry parameterizations (e.g., GloGEM by [Huss and Hock 2015](#)) could give further insights into the benefits and limitations of explicit glacier dynamics.

# Appendix A

## Single glacier test cases

The first experiment was performend as a single glacier test case on the example of Hintereisferner (RGI60-11.00897), see Section 3.1.1 for details on the experimental setup. The test case was intended to get a first qualitative impression, drawing conclusions from a single data point is, however, still questionable. Therefore, the exact same experiment was performend on five more single glaciers (Pasterze, Mer de Glace, Glacier d'Argentière, Großer Aletschgletscher, Rhonegletscher) and the results are shown here below. While there are differences between the different glaciers, all general findings presented in Section 3.1.2 hold true.

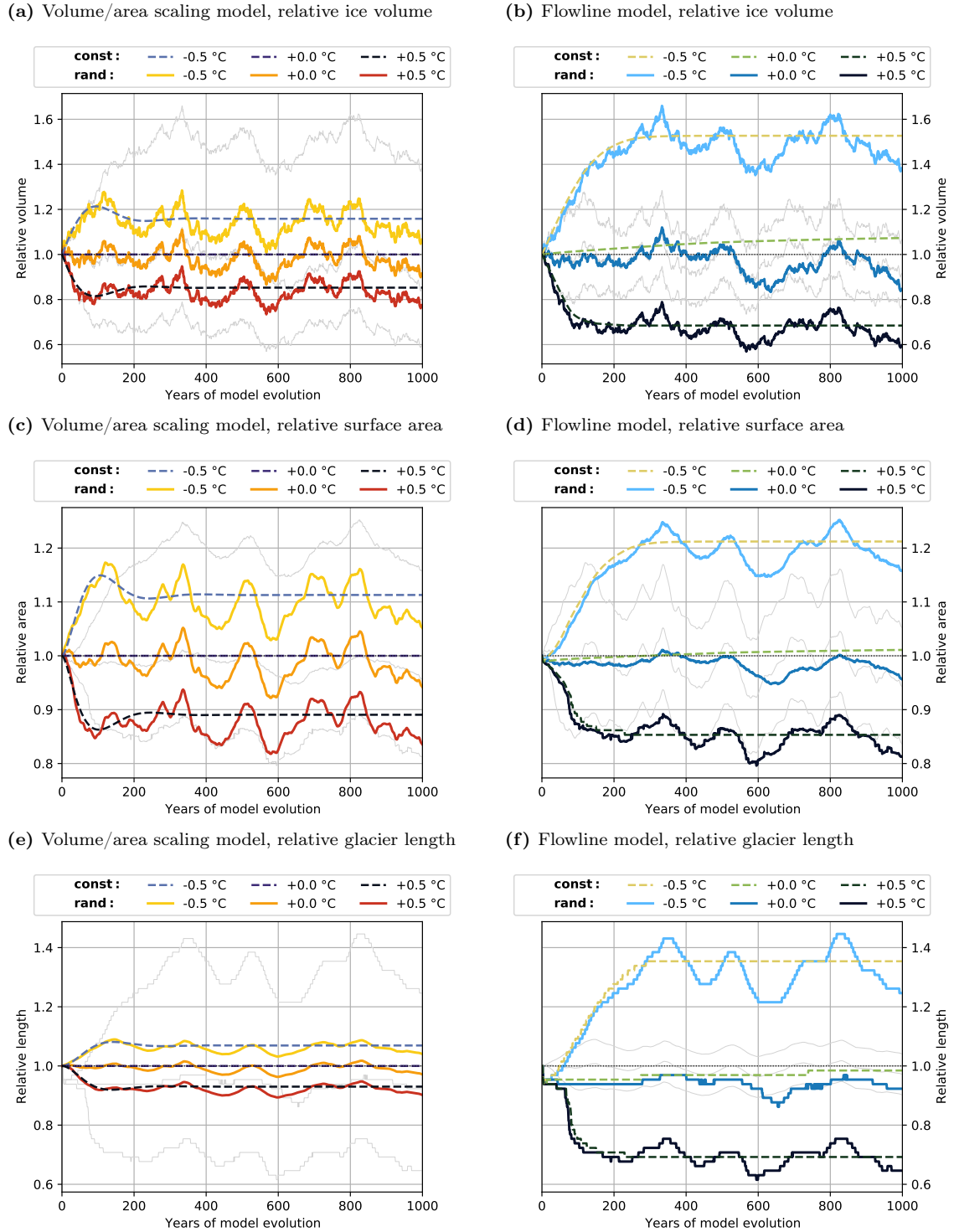


**Figure A.1:** Temporal evolution of ice volume in (a) and (b), surface area in (c) and (d) and glacier length in (e) and (f) for Pasterze (RGI60-11.00106). The shown values are normalized with their respective initial values. The left panels show the result of the volume/area scaling model, the right panels show the results of the flowline model. Solid lines represent the random climate scenarios, while dashed lines represent the constant climate scenarios. All climate scenarios are based on an equilibrium climate. The applied temperature biases of  $-0.5^{\circ}\text{C}$ ,  $0^{\circ}\text{C}$  and  $+0.5^{\circ}\text{C}$  are color coded, see legend for details. The dotted line indicates the initial volume. The light gray lines represent the volume evolutions of the other model, to facilitate comparisons.

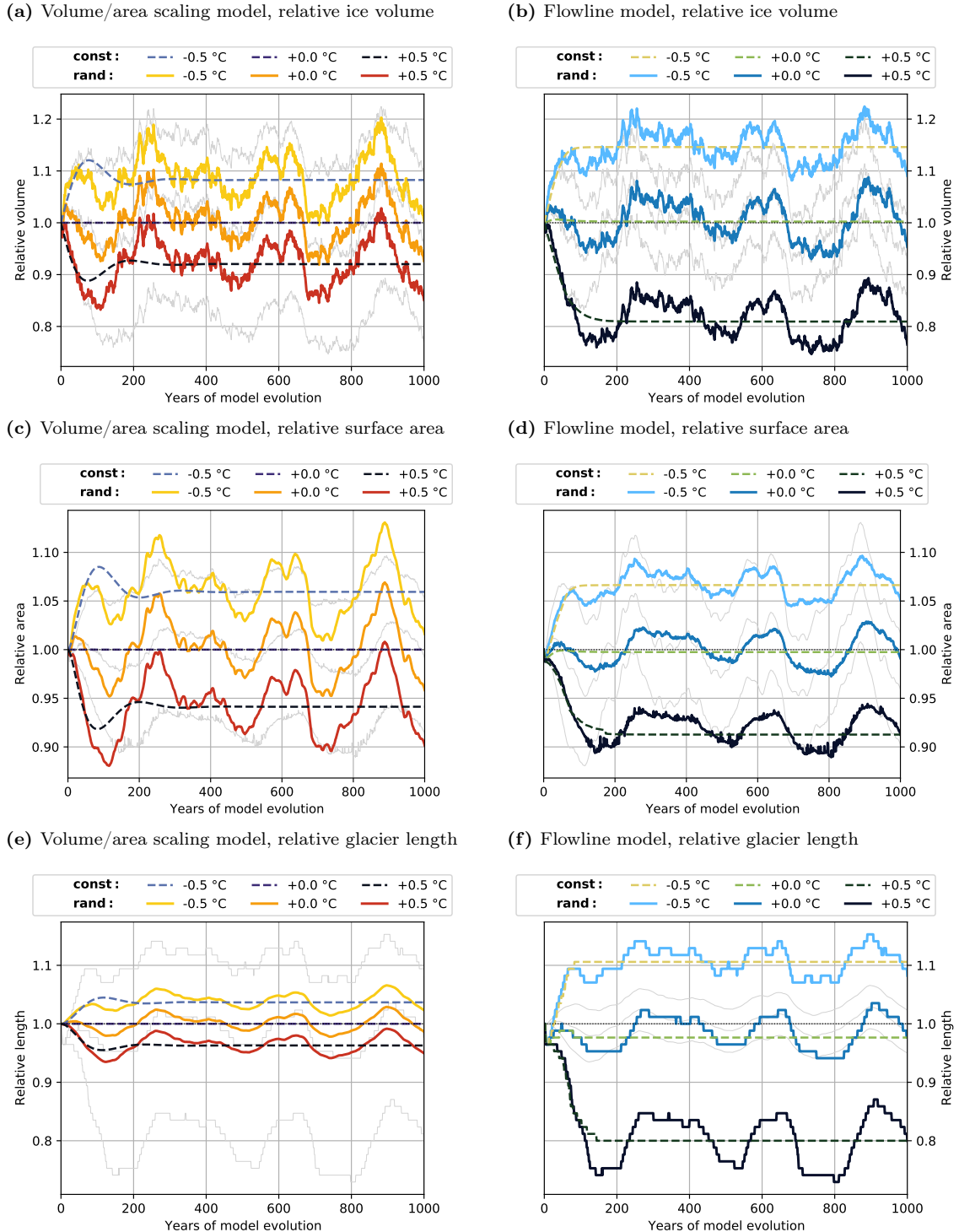


**Figure A.2:** Temporal evolution of ice volume in (a) and (b), surface area in (c) and (d) and glacier length in (e) and (f) for Mer de Glace (RGI60-11.03643). The shown values area normalized with their respective initial values. The left panels show the result of the volume/area scaling model, the right panels show the results of the flowline model. Solid lines represent the random climate scenarios, while dashed lines represent the constant climate scenarios. All climate scenarios are based on an equilibrium climate. The applied temperature biases of  $-0.5\text{ }^{\circ}\text{C}$ ,  $0\text{ }^{\circ}\text{C}$  and  $+0.5\text{ }^{\circ}\text{C}$  are color coded, see legend for details. The dotted line indicates the initial volume. The light gray lines represent the volume evolutions of the other model, to facilitate comparisons.

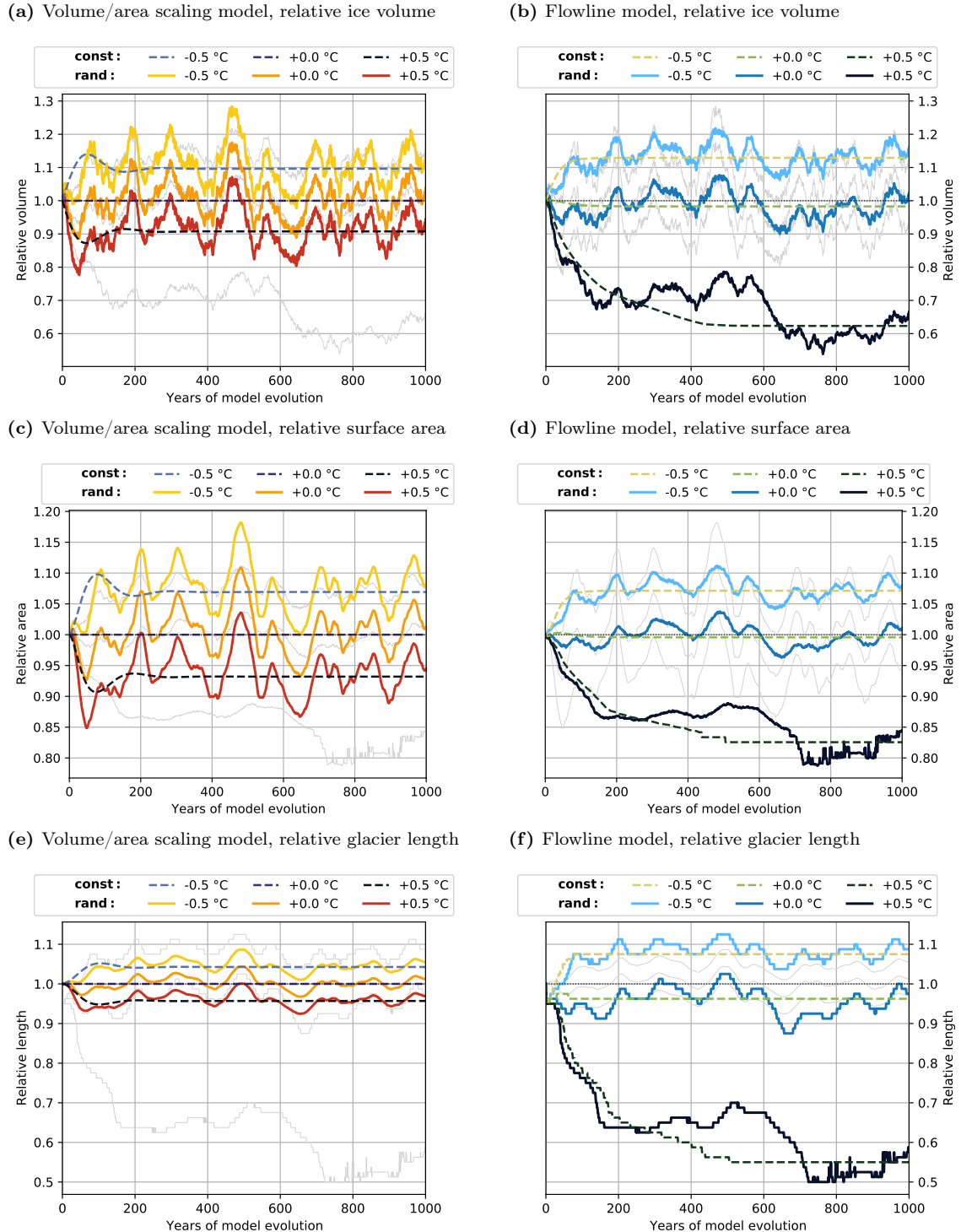


**Figure A.3:** Temporal evolution of ice volume in (a) and (b), surface area in (c) and (d) and glacier length in (e) and (f) for **Glacier d'Argentière (RGI60-11.03638)**. The shown values area normalized with their respective initial values. The left panels show the result of the volume/area scaling model, the right panels show the results of the flowline model. Solid lines represent the random climate scenarios, while dashed lines represent the constant climate scenarios. All climate scenarios are based on an equilibrium climate. The applied temperature biases of  $-0.5\text{ }^{\circ}\text{C}$ ,  $0\text{ }^{\circ}\text{C}$  and  $+0.5\text{ }^{\circ}\text{C}$  are color coded, see legend for details. The dotted line indicates the initial volume. The light gray lines represent the volume evolutions of the other model, to facilitate comparisons.

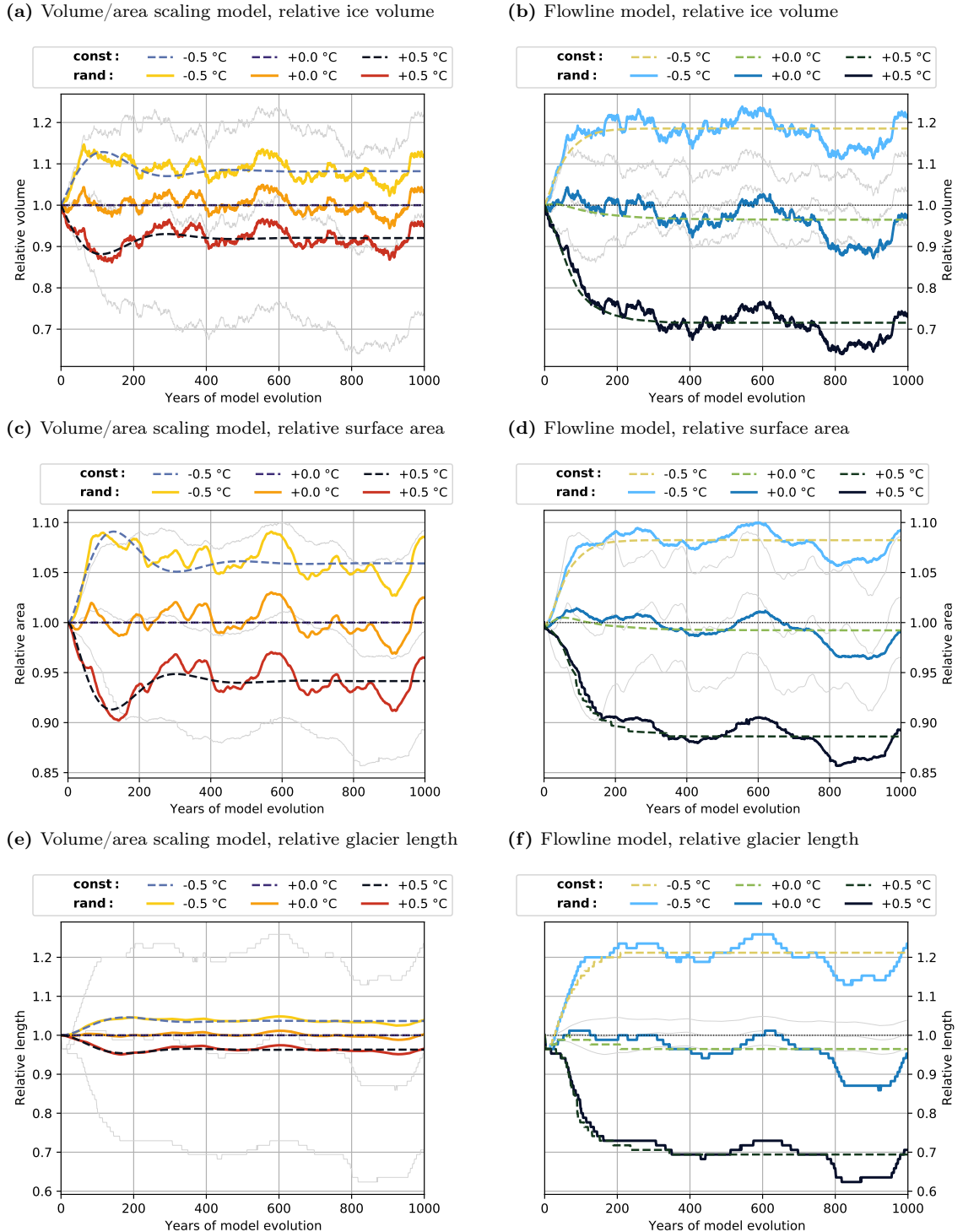


**Figure A.4:** Temporal evolution of ice volume in (a) and (b), surface area in (c) and (d) and glacier length in (e) and (f) for **Großer Aletschgletscher (RGI60-11.01450)**. The shown values are normalized with their respective initial values. The left panels show the result of the volume/area scaling model, the right panels show the results of the flowline model. Solid lines represent the random climate scenarios, while dashed lines represent the constant climate scenarios. All climate scenarios are based on an equilibrium climate. The applied temperature biases of  $-0.5\text{ }^{\circ}\text{C}$ ,  $0\text{ }^{\circ}\text{C}$  and  $+0.5\text{ }^{\circ}\text{C}$  are color coded, see legend for details. The dotted line indicates the initial volume. The light gray lines represent the volume evolutions of the other model, to facilitate comparisons.

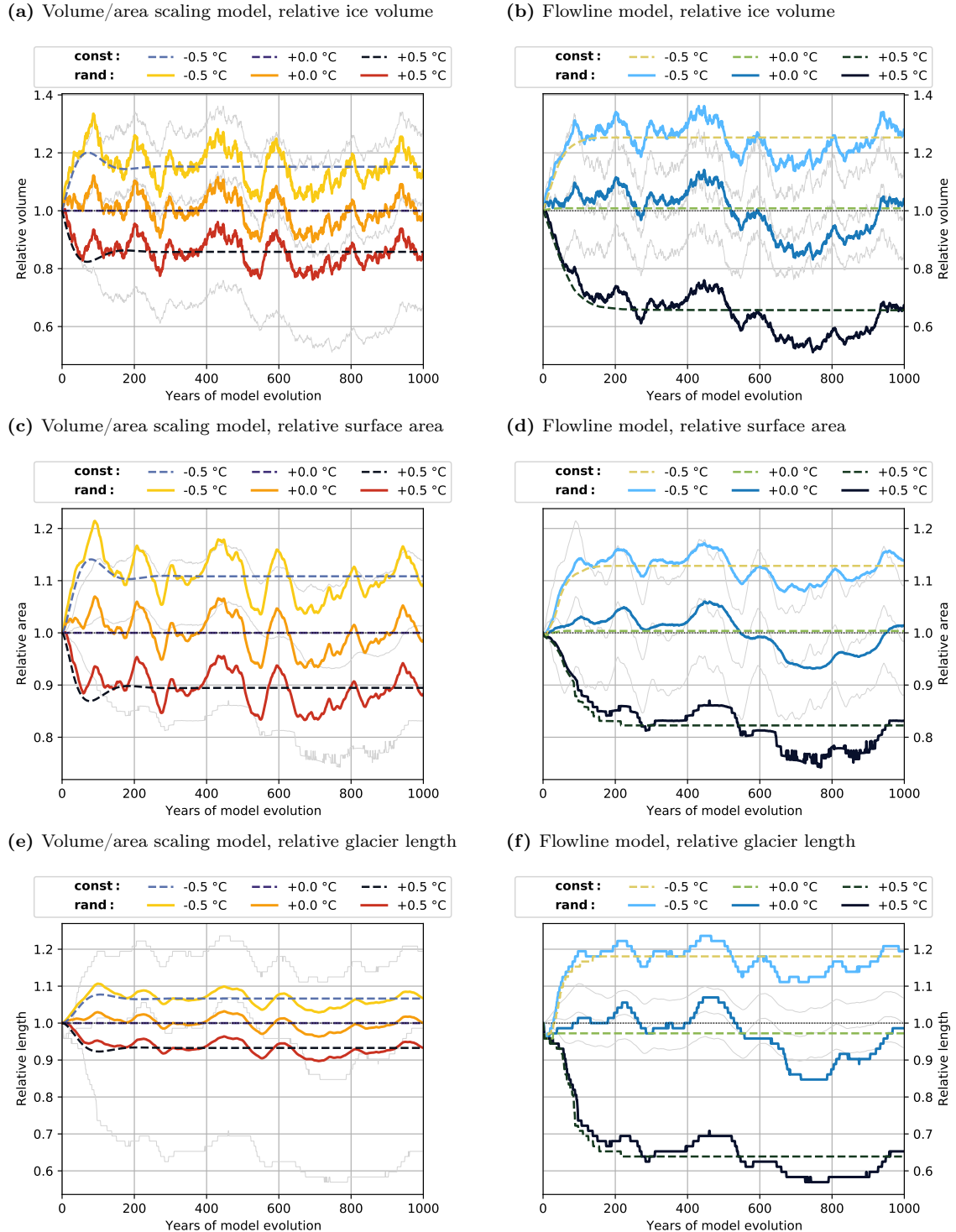
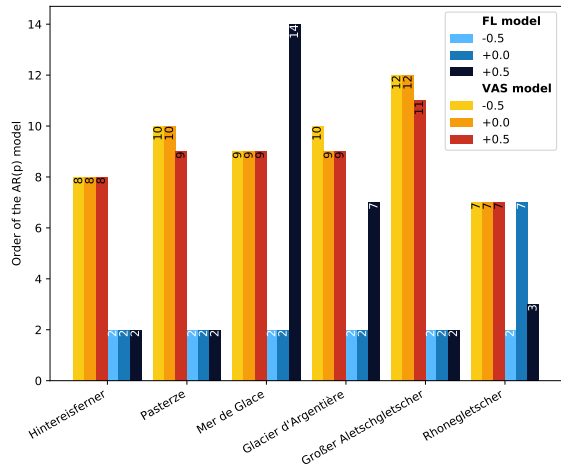


**Figure A.5:** Temporal evolution of ice volume in (a) and (b), surface area in (c) and (d) and glacier length in (e) and (f) for Rhonegletscher (RGI60-11.01238). The shown values are normalized with their respective initial values. The left panels show the result of the volume/area scaling model, the right panels show the results of the flowline model. Solid lines represent the random climate scenarios, while dashed lines represent the constant climate scenarios. All climate scenarios are based on an equilibrium climate. The applied temperature biases of  $-0.5^{\circ}\text{C}$ ,  $0^{\circ}\text{C}$  and  $+0.5^{\circ}\text{C}$  are color coded, see legend for details. The dotted line indicates the initial volume. The light gray lines represent the volume evolutions of the other model, to facilitate comparisons.

# Appendix B

## ARMA model order

(a) Order  $p$  for the autoregressive term



(b) Order  $q$  for the moving-average term

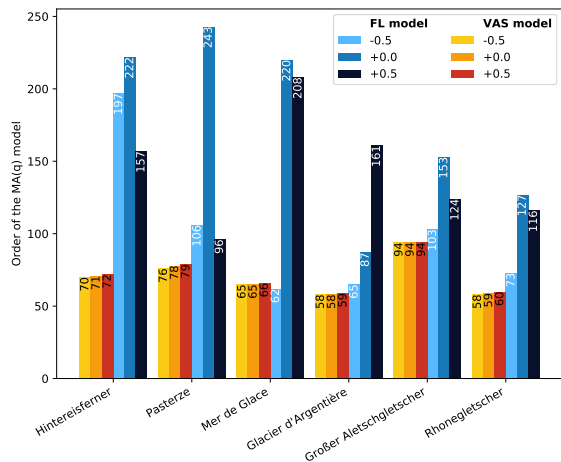


**Figure B.1:** Orders  $p$  and  $q$  for a potential ARMA( $p,q$ ) model, estimated from the ACFs and PACFs of the length change signal in response to a white noise climate (see Section 3.2.4)



# Bibliography

- Adhikari, S. and S. J. Marshall, 2012: Glacier volume-area relation for high-order mechanics and transient glacier states. *Geophysical Research Letters*, **39** (16), 1–6, doi:10.1029/2012GL052712.
- Ali, S. A., S. Aadhar, H. L. Shah, and V. Mishra, 2018: Projected Increase in Hydropower Production in India under Climate Change. *Scientific Reports*, **8** (1), 12450, doi:10.1038/s41598-018-30489-4, URL <https://doi.org/10.1038/s41598-018-30489-4>.
- Allen, M., et al., 2018: Chapter 1: Framing and Context. *Global Warming of 1.5°C. An IPCC Special Report on the impacts of global warming of 1.5°C above pre-industrial levels and related global greenhouse gas emission pathways, in the context of strengthening the global response to the threat of climate change*,, Masson-Delmotte, P. Z. V., H.-O. Pörtner, D. Roberts, J. Skea, P. Shukla, A. Pirani, W. Moufouma-Okia, C. Péan, R. Pidcock, S. Connors, J. Matthews, Y. Chen, X. Zhou, M. Gomis, E. Lonnoy, T. Maycock, M. Tignor, and T. Waterfield, Eds., 49–92, URL <https://www.ipcc.ch/sr15/chapter/chapter-1/>.
- Arendt, A., et al., 2012: Randolph glacier inventory [v1. 0]: A dataset of global glacier outlines. global land ice measurements from space, boulder colorado, usa.
- Auer, I. and R. Böhm, 2007: HISTALP – historical instrumental climatological surface time series of the Greater Alpine Region. *INTERNATIONAL JOURNAL OF CLIMATOLOGY*, **27**, doi:10.1002/joc.1377.
- Bahr, D. B., 1997a: Global distributions of glacier properties: A stochastic scaling paradigm. *Water Resources Research*, **33** (7), 1669–1679, doi:10.1029/97WR00824, URL <http://dx.doi.org/10.1029/97WR00824>.
- Bahr, D. B., 1997b: Width and length scaling of glaciers. *Journal of Glaciology*, **43** (145), 557–562, doi:10.3189/s0022143000035164.
- Bahr, D. B., M. Dyurgerov, and M. F. Meier, 2009: Sea-level rise from glaciers and ice caps: A lower bound. *Geophysical Research Letters*, **36** (3), 2–5, doi:10.1029/2008GL036309.

- Bahr, D. B., M. F. Meier, and S. D. Peckham, 1997: The physical basis of glacier volume-area scaling. *Journal of Geophysical Research: Solid Earth*, **102** (B9), 20 355–20 362, doi:10.1029/97jb01696.
- Bahr, D. B., W. T. Pfeffer, and G. Kaser, 2014: Glacier volume estimation as an ill-posed inversion. *Journal of Glaciology*, **60** (223), 922–934, doi:10.3189/2014JoG14J062.
- Bahr, D. B., W. T. Pfeffer, and G. Kaser, 2015: A review of volume-area scaling of glaciers. *Reviews of Geophysics*, **53** (1), 95–140, doi:10.1002/2014RG000470, URL <http://doi.org/10.1002/2014RG000470>.
- Bamber, J. L., R. M. Westaway, B. Marzeion, and B. Wouters, 2018: The land ice contribution to sea level during the satellite era. *Environmental Research Letters*, **13** (6), 063 008, doi:10.1088/1748-9326/aac2f0, URL <https://doi.org/10.1088%2F1748-9326%2Faac2f0>.
- Bentsen, M., et al., 2019: Ncc noresm2-mm model output prepared for cmip6 scenarioip. Earth System Grid Federation, URL <https://doi.org/10.22033/ESGF/CMIP6.608>, doi:10.22033/ESGF/CMIP6.608, URL <https://doi.org/10.22033/ESGF/CMIP6.608>.
- Bindschadler, R., 1982: A numerical model of temperate glacier flow applied to the quiescent phase of a surge-type glacier. *Journal of Glaciology*, **28** (99), 239–265, doi:10.3189/S0022143000011618.
- Bliss, A., R. Hock, and V. Radić, 2014: Global response of glacier runoff to twenty-first century climate change. *Journal of Geophysical Research: Earth Surface*, **119** (4), 717–730, doi:10.1002/2013JF002931, URL <http://doi.wiley.com/10.1002/2013JF002931>.
- Box, G. E. P., G. M. Jenkins, G. C. Reinsel, and G. M. Ljung, 2015: *Time Series Analysis: Forecasting and Control (Wiley Series in Probability and Statistics)*. Wiley, URL <https://www.xarg.org/ref/a/1118675029/>.
- Braithwaite, R., Y. Zhang, and S. Raper, 2003: Temperature sensitivity of the mass balance of mountain glaciers and ice caps as a climatological characteristic. *Zeitschrift für Gletscherkunde und Glazialgeologie*, **38** (1), 35–61.
- Budd, W. F. and D. Jenssen, 1975: Numerical modelling of glacier systems W. F. Budd and D. Jenssen. *Snow and Ice-Symposium*, **(104)**, 257–291.

- Chen, J. and A. Ohmura, 1990: Estimation of Alpine glacier water resources and their change since the 1870s. *Hydrology in mountainous regions I*, **V** (193), 127–135.
- Cheung, Y.-W. and K. S. Lai, 1995: Lag order and critical values of the augmented dickey–fuller test. *Journal of Business & Economic Statistics*, **13** (3), 277–280.
- Church, J. A., et al., 2013: Chapter 13: Sea Level Change. *Climate Change 2013: The Physical Science Basis. Contribution of Working Group I to the Fifth Assessment Report of the Intergovernmental Panel on Climate Change*, T. Stocker, D. Qin, G.-K. Plattner, M. Tignor, S. Allen, J. Boschung, A. Nauels, Y. Xia, V. Bex, and P. Midgley, Eds., Cambridge University Press, Cambridge, United Kingdom and New York, NY, USA, 1137–1216.
- Côté, J., C. Jablonowski, P. Bauer, and N. Wedi, 2015: Numerical methods of the atmosphere and ocean. *Seamless prediction of the Earth system: From minutes to months*, 101–124.
- Cuffey, K. and W. Paterson, 2010: *The Physics of Glaciers*. Elsevier Science, URL <https://books.google.at/books?id=Jca2v1u1EKEC>.
- Danabasoglu, G., 2019a: Ncar cesm2 model output prepared for cmip6 scenariomip. Earth System Grid Federation, URL <https://doi.org/10.22033/ESGF/CMIP6.2201>, doi:10.22033/ESGF/CMIP6.2201, URL <https://doi.org/10.22033/ESGF/CMIP6.2201>.
- Danabasoglu, G., 2019b: Ncar cesm2-waccm model output prepared for cmip6 scenariomip. Earth System Grid Federation, URL <https://doi.org/10.22033/ESGF/CMIP6.10026>, doi:10.22033/ESGF/CMIP6.10026, URL <https://doi.org/10.22033/ESGF/CMIP6.10026>.
- Davaze, L., A. Rabatel, A. Dufour, R. Hugonet, and Y. Arnaud, 2020: Region-Wide Annual Glacier Surface Mass Balance for the European Alps From 2000 to 2016. *Frontiers in Earth Science*, **8** (May), 1–14, doi:10.3389/feart.2020.00149.
- Deline, P., et al., 2015: Chapter 15 - ice loss and slope stability in high-mountain regions. *Snow and Ice-Related Hazards, Risks and Disasters*, J. F. Shroder, W. Haeberli, and C. Whiteman, Eds., Academic Press, Boston, 521 – 561, doi:<https://doi.org/10.1016/B978-0-12-394849-6.00015-9>, URL <http://www.sciencedirect.com/science/article/pii/B9780123948496000159>.
- Dusch, M., 2018: Mass-balance model calibration for the alps. OGGM Blog, URL "<https://oggm.org/2018/08/10/histalp-parameters/>", posted on August 10,

- 2018, URL "<https://oggm.org/2018/08/10/histalp-parameters/>", posted on August 10, 2018.
- (EC-Earth), E.-E. C., 2019a: Ec-earth-consortium ec-earth3 model output prepared for cmip6 scenariomip. Earth System Grid Federation, URL <https://doi.org/10.22033/ESGF/CMIP6.251>, doi:10.22033/ESGF/CMIP6.251, URL <https://doi.org/10.22033/ESGF/CMIP6.251>.
- (EC-Earth), E.-E. C., 2019b: Ec-earth-consortium ec-earth3-veg model output prepared for cmip6 scenariomip. Earth System Grid Federation, URL <https://doi.org/10.22033/ESGF/CMIP6.727>, doi:10.22033/ESGF/CMIP6.727, URL <https://doi.org/10.22033/ESGF/CMIP6.727>.
- Evans, J. H., 1972: Dimensional analysis and the buckingham pi theorem. *American Journal of Physics*, **40**, 1815, doi:10.1119/1.1987069, URL <http://doi.org/10.1119/1.1987069>.
- Eyring, V., S. Bony, G. A. Meehl, C. A. Senior, B. Stevens, R. J. Stouffer, and K. E. Taylor, 2016: Overview of the coupled model intercomparison project phase 6 (cmip6) experimental design and organization. *Geoscientific Model Development*, **9** (5), 1937–1958, doi:10.5194/gmd-9-1937-2016, URL <https://gmd.copernicus.org/articles/9/1937/2016/>.
- Farinotti, D. and M. Huss, 2013: An upper-bound estimate for the accuracy of glacier volume-area scaling. *Cryosphere*, **7** (6), 1707–1720, doi:10.5194/tc-7-1707-2013.
- Farinotti, D., M. Huss, A. Bauder, M. Funk, and M. Truffer, 2009: A method to estimate the ice volume and ice-thickness distribution of alpine glaciers. *Journal of Glaciology*, **55** (191), 422–430, doi:10.3189/002214309788816759, URL <https://doi.org/10.3189/002214309788816759>.
- Farinotti, D., M. Huss, J. J. Fürst, J. Landmann, H. Machguth, F. Maussion, and A. Pandit, 2019: A consensus estimate for the ice thickness distribution of all glaciers on Earth. *Nature Geoscience*, **12** (3), 168–173, doi:10.1038/s41561-019-0300-3.
- Farinotti, D., A. Pistocchi, and M. Huss, 2016: From dwindling ice to headwater lakes: could dams replace glaciers in the european alps? *Environmental Research Letters*, **11** (5), 054022, doi:10.1088/1748-9326/11/5/054022, URL <https://doi.org/10.1088%2F1748-9326%2F11%2F5%2F054022>.

- Farinotti, D., et al., 2017: How accurate are estimates of glacier ice thickness? Results from ITMIX, the Ice Thickness Models Intercomparison eXperiment. *Cryosphere*, **11** (2), 949–970, doi:10.5194/tc-11-949-2017.
- Farinotti, D., et al., 2020: Results from the Ice Thickness Models Intercomparison eXperiment phase 2 (ITMIX2), doi:10.3389/feart.2020.571923.
- Gardner, A. S., et al., 2013: A reconciled estimate of glacier contributions to sea level rise: 2003 to 2009. *Science*, **340** (6134), 852–857, doi:10.1126/science.1234532.
- Giesen, R. H. and J. Oerlemans, 2013: Climate-model induced differences in the 21st century global and regional glacier contributions to sea-level rise. *Climate Dynamics*, **41** (11-12), 3283–3300, doi:10.1007/s00382-013-1743-7.
- Gregory, J. M. and J. Oerlemans, 1998: Simulated future sea-level rise due to glacier melt based on regionally and seasonally resolved temperature changes. *Nature*, **391** (6666), 474–476, doi:10.1038/35119, URL <http://www.nature.com/articles/35119>.
- Greuell, W., 1992: Hintereisferner, austria: mass-balance reconstruction and numerical modelling of the historical length variations. *Journal of Glaciology*, **38** (129), 233–244, doi:10.3189/S0022143000003646.
- Haeberli, W., Y. Schaub, and C. Huggel, 2017: Increasing risks related to landslides from degrading permafrost into new lakes in de-glaciating mountain ranges. *Geomorphology*, **293**, 405 – 417, doi:<https://doi.org/10.1016/j.geomorph.2016.02.009>, URL <http://www.sciencedirect.com/science/article/pii/S0169555X16300381>, permafrost and periglacial research from coasts to mountains.
- Harris, I., P. Jones, T. Osborn, and D. Lister, 2014: Updated high-resolution grids of monthly climatic observations – the cru ts3.10 dataset. *International Journal of Climatology*, **34** (3), 623–642, doi:<https://doi.org/10.1002/joc.3711>, URL <https://rmets.onlinelibrary.wiley.com/doi/abs/10.1002/joc.3711>, <https://rmets.onlinelibrary.wiley.com/doi/pdf/10.1002/joc.3711>.
- Hirabayashi, Y., Y. Zang, S. Watanabe, S. Koirala, and S. Kanae, 2013: Projection of glacier mass changes under a high-emission climate scenario using the global glacier model HYOGA2. *Hydrological Research Letters*, **7** (1), 6–11, doi:10.3178/hrl.7.6.
- Hock, R., A. Bliss, B. E. Marzeion, R. H. Giesen, Y. Hirabayashi, M. Huss, V. Radic, and A. B. Slanger, 2019: GlacierMIP-A model intercomparison of global-scale

- glacier mass-balance models and projections. *Journal of Glaciology*, **65** (251), 453–467, doi:10.1017/jog.2019.22.
- Huss, M. and D. Farinotti, 2012: Distributed ice thickness and volume of all glaciers around the globe. *Journal of Geophysical Research: Earth Surface*, **117** (4), 1–10, doi:10.1029/2012JF002523, URL <https://doi.org/10.1029/2012JF002523>.
- Huss, M. and R. Hock, 2015: A new model for global glacier change and sea-level rise. *Frontiers in Earth Science*, **3** (September), 1–22, doi:10.3389/feart.2015.00054.
- Huss, M. and R. Hock, 2018: Global-scale hydrological response to future glacier mass loss. *Nature Climate Change*, **8** (2), 135–140, doi:10.1038/s41558-017-0049-x, URL <https://doi.org/10.1038/s41558-017-0049-x>.
- Huss, M., R. Hock, A. Bauder, and M. Funk, 2012: Conventional versus reference-surface mass balance. *Journal of Glaciology*, **58** (208), 278–286, doi:10.3189/2012JoG11J216.
- Huss, M., G. Jouvet, D. Farinotti, and A. Bauder, 2010: Future high-mountain hydrology: A new parameterization of glacier retreat. *Hydrology and Earth System Sciences*, **14** (5), 815–829, doi:10.5194/hess-14-815-2010.
- Hutter, K., 1983: *Theoretical Glaciology*. 1st ed., Springer Netherlands, Dordrecht, doi:10.1007/978-94-015-1167-4, URL <http://link.springer.com/10.1007/978-94-015-1167-4>.
- Immerzeel, W. W., et al., 2020: Importance and vulnerability of the world's water towers. *Nature*, **577** (7790), 364–369, doi:10.1038/s41586-019-1822-y, URL <https://doi.org/10.1038/s41586-019-1822-y>.
- IPCC, 2007: *Climate Change 2007: The Physical Science Basis. Contribution of Working Group I to the Fourth Assessment Report of the Intergovernmental Panel on Climate Change*. Cambridge University Press, Cambridge, United Kingdom and New York, NY, USA, 996 pp.
- IPCC, 2013: *Climate Change 2013: The Physical Science Basis. Contribution of Working Group I to the Fifth Assessment Report of the Intergovernmental Panel on Climate Change*. Cambridge University Press, Cambridge, United Kingdom and New York, NY, USA, 1535 pp.
- IPCC, 2019: Technical summary. *IPCC Special Report on the Ocean and Cryosphere in a Changing Climate*, H.-O. Pörtner, D. Roberts, V. Masson-Delmotte, M. T. P. Zhai, E. Poloczanska, K. Mintenbeck, A. Alegría, M. Nicolai, A. Okem, J. Petzold, B. Rama, and N. Weyer, Eds., 37–70.

- Jarvis, A., E. Guevara, H. Reuter, and A. Nelson, 2008: Hole-filled srtm for the globe, version 4. CGIAR Consortium for Spatial Information, University of Twente, published by CGIAR-CSI on 19 August 2008., published by CGIAR-CSI on 19 August 2008.
- Jóhannesson, T., C. Rymond, and E. Waddington, 1989: Time-scale for adjustment of glaciers to changes in mass balance. **35** (1).
- John, J. G., et al., 2018: Noaa-gfdl gfdl-esm4 model output prepared for cmip6 scenariomip. Earth System Grid Federation, URL <https://doi.org/10.22033/ESGF/CMIP6.1414>, doi:10.22033/ESGF/CMIP6.1414, URL <https://doi.org/10.22033/ESGF/CMIP6.1414>.
- Kaser, G., J. G. Cogley, M. B. Dyurgerov, M. F. Meier, and A. Ohmura, 2006: Mass balance of glaciers and ice caps: Consensus estimates for 1961–2004. *Geophysical Research Letters*, **33** (19), doi:10.1029/2006GL027511, URL <https://agupubs.onlinelibrary.wiley.com/doi/abs/10.1029/2006GL027511>, <https://agupubs.onlinelibrary.wiley.com/doi/pdf/10.1029/2006GL027511>.
- Klug, C., et al., 2018: Geodetic reanalysis of annual glaciological mass balances (2001–2011) of hintereisferner, austria. *The Cryosphere*, **12** (3), 833–849, doi: 10.5194/tc-12-833-2018, URL <https://tc.copernicus.org/articles/12/833/2018/>.
- Lauritzen, P. H., C. Jablonowski, M. A. Taylor, and R. D. Nair, 2011: *Numerical techniques for global atmospheric models*, Vol. 80. Springer Science & Business Media.
- Leclercq, P. W., J. Oerlemans, H. J. Basagic, I. Bushueva, A. Cook, and R. Le Bris, 2014: A data set of worldwide glacier fluctuations. *The Cryosphere*, **8**, 659–672.
- Lee, W.-L. and H.-C. Liang, 2020: As-rcec taiesm1.0 model output prepared for cmip6 scenariomip. Earth System Grid Federation, URL <https://doi.org/10.22033/ESGF/CMIP6.9688>, doi:10.22033/ESGF/CMIP6.9688, URL <https://doi.org/10.22033/ESGF/CMIP6.9688>.
- Lemieux, C. J., M. Groulx, E. Halpenny, H. Stager, J. Dawson, E. J. Stewart, and G. T. Hvenegaard, 2018: “the end of the ice age?”: Disappearing world heritage and the climate change communication imperative. *Environmental Communication*, **12** (5), 653–671, doi:10.1080/17524032.2017.1400454, URL <https://doi.org/10.1080/17524032.2017.1400454>, <https://doi.org/10.1080/17524032.2017.1400454>.

- Lovato, T. and D. Peano, 2020: Cmcc cmcc-cm2-sr5 model output prepared for cmip6 scenariomip. Earth System Grid Federation, URL <https://doi.org/10.22033/ESGF/CMIP6.1365>, doi:10.22033/ESGF/CMIP6.1365, URL <https://doi.org/10.22033/ESGF/CMIP6.1365>.
- Malles, J.-H. and B. Marzeion, 2020: 20th century global glacier mass change: an ensemble-based model reconstruction. *The Cryosphere Discussions*, **2020**, 1–30, doi:10.5194/tc-2020-320, URL <https://tc.copernicus.org/preprints/tc-2020-320/>.
- Marzeion, B., J. G. Cogley, K. Richter, and D. Parkes, 2014: Attribution of global glacier mass loss to anthropogenic and natural causes. *Science*, **345** (6199), 919–921, doi:10.1126/science.1254702, URL <https://www.scienmag.org/lookup/doi/10.1126/science.1254702>.
- Marzeion, B., A. H. Jarosch, and M. Hofer, 2012: Past and future sea-level change from the surface mass balance of glaciers. *The Cryosphere*, **6** (6), 1295–1322, doi:10.5194/tc-6-1295-2012.
- Marzeion, B., P. W. Leclercq, J. G. Cogley, and A. H. Jarosch, 2015: Brief Communication: Global reconstructions of glacier mass change during the 20th century are consistent. *Cryosphere*, **9** (6), 2399–2404, doi:10.5194/tc-9-2399-2015.
- Marzeion, B., et al., 2020: Partitioning the Uncertainty of Ensemble Projections of Global Glacier Mass Change. *Earth's Future*, **8** (7), 1–25, doi:10.1029/2019EF001470.
- Maussion, F., et al., 2019: The Open Global Glacier Model (OGGM) v1.1. *Geoscientific Model Development*, **12** (3), 909–931, doi:10.5194/gmd-12-909-2019, URL <https://doi.org/10.5194/gmd-12-909-2019>.
- Meier, M. F., M. B. Dyurgerov, U. K. Rick, S. O'Neel, W. T. Pfeffer, R. S. Anderson, S. P. Anderson, and A. F. Glazovsky, 2007: Glaciers dominate eustatic sea-level rise in the 21st century. *Science*, **317** (5841), 1064–1067, doi:10.1126/science.1143906.
- Milner, A. M., et al., 2017: Glacier shrinkage driving global changes in downstream systems. *Proceedings of the National Academy of Sciences*, **114** (37), 9770–9778, doi:10.1073/pnas.1619807114, URL <https://www.pnas.org/content/114/37/9770>, <https://www.pnas.org/content/114/37/9770.full.pdf>.
- Mourey, J., M. Marcuzzi, L. Ravanel, and F. Pallandre, 2019: Effects of climate change on high Alpine mountain environments: Evolution of mountaineering

- routes in the Mont Blanc massif (Western Alps) over half a century. *Arctic, Antarctic, and Alpine Research*, **51** (1), 176–189, doi:10.1080/15230430.2019.1612216, URL <https://doi.org/10.1080/15230430.2019.1612216>.
- Nowicki, S. M., et al., 2016: Ice sheet model intercomparison project (ismip6) contribution to cmip6. *Geoscientific model development*, **9** (12), 4521.
- Oerlemans, J., 1997: A flowline model for Nigardsbreen, Norway: Projection of future glacier length based on dynamic calibration with the historic record. *Annals of Glaciology*, **24** (iv), 382–389, doi:10.3189/S0260305500012489, URL <https://doi.org/10.3189/S0260305500012489>.
- OGGM Developers, 2021: Pitfalls and limitations. OGGM Documentations, URL "<https://docs.oggm.org/en/latest/pitfalls.html#the-default-ice-dynamics-parameter-glen-a-is-roughly-calibrated>", posted on Februar 9, 2021, URL "<https://docs.oggm.org/en/latest/pitfalls.html#the-default-ice-dynamics-parameter-glen-a-is-roughly-calibrated>", posted on Februar 9, 2021.
- O'Neill, B. C., et al., 2016: The Scenario Model Intercomparison Project (ScenarioMIP) for CMIP6. *Geoscientific Model Development*, **9** (9), 3461–3482, doi: 10.5194/gmd-9-3461-2016.
- Pattyn, F., et al., 2012: Results of the marine ice sheet model intercomparison project, mismip. *The Cryosphere*, **6** (3), 573–588.
- Pfeffer, W. T., J. T. Harper, and S. O'Neal, 2008: Kinematic constraints on glacier contributions to 21st-century sea-level rise. *Science*, **321** (5894), 1340–1343, doi: 10.1126/science.1159099.
- Pfeffer, W. T., et al., 2014: The randolph glacier inventory: a globally complete inventory of glaciers. *Journal of Glaciology*, **60** (221), 537–552, doi: 10.3189/2014JoG13J176.
- Proakis, J. and D. Manolakis, 2007: *Digital Signal Processing*. Prentice Hall international editions, Pearson Prentice Hall, URL [https://books.google.at/books?id=H\\_5SAAAAMAAJ](https://books.google.at/books?id=H_5SAAAAMAAJ).
- Radić, V., A. Bliss, A. C. Beedlow, R. Hock, E. Miles, and J. G. Cogley, 2014: Regional and global projections of twenty-first century glacier mass changes in response to climate scenarios from global climate models. *Climate Dynamics*, **42** (1-2), 37–58, doi:10.1007/s00382-013-1719-7.

- Radić, V. and R. Hock, 2011: Regionally differentiated contribution of mountain glaciers and ice caps to future sea-level rise. *Nature Geoscience*, **4** (2), 91–94, doi:10.1038/ngeo1052.
- Radić, V. and R. Hock, 2014: Glaciers in the Earth’s Hydrological Cycle: Assessments of Glacier Mass and Runoff Changes on Global and Regional Scales. *Surveys in Geophysics*, **35** (3), 813–837, doi:10.1007/s10712-013-9262-y, URL <http://link.springer.com/10.1007/s10712-013-9262-y>.
- Radić, V., R. Hock, and J. Oerlemans, 2007: Volume-area scaling vs flow-line modelling in glacier volume projections. *Annals of Glaciology*, **46**, 234–240, doi:10.3189/172756407782871288, URL <http://doi.org/10.3189/172756407782871288>.
- Radić, V., R. Hock, and J. Oerlemans, 2008: Analysis of scaling methods in deriving future volume evolutions of valley glaciers. *Journal of Glaciology*, **54** (187), 601–612, doi:10.3189/002214308786570809, URL <https://doi.org/10.3189/002214308786570809>.
- Raper, S. C. and R. J. Braithwaite, 2006: Low sea level rise projections from mountain glaciers and icecaps under global warming. *Nature*, **439** (7074), 311–313, doi:10.1038/nature04448.
- Raper, S. C., O. Brown, and R. J. Braithwaite, 2000: A geometric glacier model for sea-level change calculations. *Journal of Glaciology*, **46** (154), 357–368, doi:10.3189/172756500781833034.
- Recinos, B., F. Maussion, T. Rothenpieler, and B. Marzeion, 2019: Impact of frontal ablation on the ice thickness estimation of marine-terminating glaciers in alaska. *The Cryosphere*, **13** (10), 2657–2672.
- Riahi, K., et al., 2017: The Shared Socioeconomic Pathways and their energy, land use, and greenhouse gas emissions implications: An overview. *Global Environmental Change*, **42**, 153–168, doi:10.1016/j.gloenvcha.2016.05.009.
- Richardson, S. D. and J. M. Reynolds, 2000: An overview of glacial hazards in the himalayas. *Quaternary International*, **65–66**, 31 – 47, doi:[https://doi.org/10.1016/S1040-6182\(99\)00035-X](https://doi.org/10.1016/S1040-6182(99)00035-X), URL <http://www.sciencedirect.com/science/article/pii/S104061829900035X>.
- Roe, G. H. and M. B. Baker, 2014: Glacier response to climate perturbations: an accurate linear geometric model. *Journal of Glaciology*, **60** (222), 670–684, doi: <https://doi.org/10.3189/2014jog14j016>.

- Roe, G. H., J. E. Christian, and B. Marzeion, 2020: On the attribution of industrial-era glacier mass loss to anthropogenic climate change. *The Cryosphere Discussions*, **(October)**, 1–27.
- Rong, X., 2019: Cams cams-csm1.0 model output prepared for cmip6 scenariomip. Earth System Grid Federation, URL <https://doi.org/10.22033/ESGF/CMIP6.11004>, doi:10.22033/ESGF/CMIP6.11004, URL <https://doi.org/10.22033/ESGF/CMIP6.11004>.
- Sakai, A. and K. Fujita, 2017: Contrasting glacier responses to recent climate change in high-mountain Asia. *Scientific Reports*, **7** (1), 1–8, doi:10.1038/s41598-017-14256-5, URL <http://dx.doi.org/10.1038/s41598-017-14256-5>.
- Schäfer, M., M. Möller, T. Zwinger, and J. Moore, 2015: Dynamic modelling of future glacier changes: mass-balance/elevation feedback in projections for the Vestfonna ice cap, Nordaustlandet, Svalbard. *Journal of Glaciology*, **61** (230), 1121–1136, doi:10.3189/2015JoG14J184, URL [https://www.cambridge.org/core/product/identifier/S0022143000200300/type/journal\\_article](https://www.cambridge.org/core/product/identifier/S0022143000200300/type/journal_article).
- Schupfner, M., et al., 2019: Dkrz mpi-esm1.2-hr model output prepared for cmip6 scenariomip. Earth System Grid Federation, URL <https://doi.org/10.22033/ESGF/CMIP6.2450>, doi:10.22033/ESGF/CMIP6.2450, URL <https://doi.org/10.22033/ESGF/CMIP6.2450>.
- Schuster, L., 2020: Response time of glaciers using the Open Global Glacier Model : from simple idealized experiments to an estimate for Alpine glaciers. Ph.D. thesis.
- Shannon, S., et al., 2019: Global glacier volume projections under high-end climate change scenarios. *The Cryosphere*, **13** (1), 325–350, doi:10.5194/tc-13-325-2019, URL <https://tc.copernicus.org/articles/13/325/2019/>.
- Slangen, A. B., F. Adloff, S. Jevrejeva, P. W. Leclercq, B. Marzeion, Y. Wada, and R. Winkelmann, 2017: A Review of Recent Updates of Sea-Level Projections at Global and Regional Scales. *Surveys in Geophysics*, **38** (1), 385–406, doi: 10.1007/s10712-016-9374-2.
- Slangen, A. B., C. A. Katsman, R. S. van de Wal, L. L. Vermeersen, and R. E. Riva, 2012: Towards regional projections of twenty-first century sea-level change based on IPCC SRES scenarios. *Climate Dynamics*, **38** (5-6), 1191–1209, doi: 10.1007/s00382-011-1057-6.
- Slangen, A. B. and R. S. Van De Wal, 2011: An assessment of uncertainties in using volume-area modelling for computing the twenty-first century glacier contribution to sea-level change. *Cryosphere*, **5** (3), 673–686, doi:10.5194/tc-5-673-2011.

- Steger, C., et al., 2019: Dwd mpi-esm1.2-hr model output prepared for cmip6 scenariomip. Earth System Grid Federation, URL <https://doi.org/10.22033/ESGF/CMIP6.1869>, doi:10.22033/ESGF/CMIP6.1869, URL <https://doi.org/10.22033/ESGF/CMIP6.1869>.
- Stewart, E. J., J. Wilson, S. Espiner, H. Purdie, C. Lemieux, and J. Dawson, 2016: Implications of climate change for glacier tourism. *Tourism Geographies*, **18** (4), 377–398, doi:10.1080/14616688.2016.1198416, URL <https://doi.org/10.1080/14616688.2016.1198416>, <https://doi.org/10.1080/14616688.2016.1198416>.
- Van De Wal, R. S. and M. Wild, 2001: Modelling the response of glaciers to climate change by applying volume-area scaling in combination with a high resolution GCM. *Climate Dynamics*, **18** (3-4), 359–366, doi:10.1007/s003820100184.
- Vaughan, D., et al., 2013: Chapter 4: Observations: Cryosphere. *Climate Change 2013: The Physical Science Basis. Contribution of Working Group I to the Fifth Assessment Report of the Intergovernmental Panel on Climate Change*, T. Stocker, D. Qin, G.-K. Plattner, M. Tignor, S. Allen, J. Boschung, A. Nauels, Y. Xia, V. Bex, and P. Midgley, Eds., Cambridge University Press, Cambridge, United Kingdom and New York, NY, USA, 1137–1216.
- Volodin, E., et al., 2019a: Inm inm-cm4-8 model output prepared for cmip6 scenariomip. Earth System Grid Federation, URL <https://doi.org/10.22033/ESGF/CMIP6.12321>, doi:10.22033/ESGF/CMIP6.12321, URL <https://doi.org/10.22033/ESGF/CMIP6.12321>.
- Volodin, E., et al., 2019b: Inm inm-cm5-0 model output prepared for cmip6 scenariomip. Earth System Grid Federation, URL <https://doi.org/10.22033/ESGF/CMIP6.12322>, doi:10.22033/ESGF/CMIP6.12322, URL <https://doi.org/10.22033/ESGF/CMIP6.12322>.
- Welch, P., 1967: The use of fast fourier transform for the estimation of power spectra: A method based on time averaging over short, modified periodograms. *IEEE Transactions on Audio and Electroacoustics*, **15** (2), 70–73.
- Williamson, D. L., 2007: The evolution of dynamical cores for global atmospheric models. *Journal of the Meteorological Society of Japan. Ser. II*, **85**, 241–269.
- World Glacier Monitoring Service, Zürich, Switzerland, 2017: Wgms: Fluctuations of glaciers database. doi:10.5904/wgms-fog-2017-10.
- Wyngaard, J. C., 2010: *Turbulence in the Atmosphere*. Cambridge University Press.

- Xin, X., et al., 2019: Bcc bcc-csm2mr model output prepared for cmip6 scenarioip. Earth System Grid Federation, URL <https://doi.org/10.22033/ESGF/CMIP6.1732>, doi:10.22033/ESGF/CMIP6.1732, URL <https://doi.org/10.22033/ESGF/CMIP6.1732>.
- Yarin, L., 2012: *The Pi-Theorem: Applications to Fluid Mechanics and Heat and Mass Transfer*. 1st ed., Experimental Fluid Mechanics 1, Springer-Verlag Berlin Heidelberg, URL <http://gen.lib.rus.ec/book/index.php?md5=bb5d37bae370f38d174c7ef66f5f5ad8>.
- YU, Y., 2019: Cas fgoals-f3-l model output prepared for cmip6 scenarioip. Earth System Grid Federation, URL <https://doi.org/10.22033/ESGF/CMIP6.2046>, doi:10.22033/ESGF/CMIP6.2046, URL <https://doi.org/10.22033/ESGF/CMIP6.2046>.
- Yukimoto, S., et al., 2019: Mri mri-esm2.0 model output prepared for cmip6 scenarioip. Earth System Grid Federation, URL <https://doi.org/10.22033/ESGF/CMIP6.638>, doi:10.22033/ESGF/CMIP6.638, URL <https://doi.org/10.22033/ESGF/CMIP6.638>.
- Zekollari, H., M. Huss, and D. Farinotti, 2019: Modelling the future evolution of glaciers in the European Alps under the EURO-CORDEX RCM ensemble. *Cryosphere*, **13** (4), 1125–1146, doi:10.5194/tc-13-1125-2019.
- Zemp, M., et al., 2019: Global glacier mass changes and their contributions to sea-level rise from 1961 to 2016. *Nature*, **568** (7752), 382–386, doi:10.1038/s41586-019-1071-0.



# Acknowledgments

...